

Preliminary studies on the influence of ultrasounds on the heat transfer rate in a crossflow heat exchanger

Bruna Filipa Faria da Silva Oliveira

Masters Dissertation

Supervisor: Carlos Manuel Coutinho Tavares de Pinho

Co-supervisor: Marta Sofia Ramos de Oliveira Santos



Mestrado Integrado de Engenharia Mecânica

June 2021

“Have no fear of perfection;

You’ll never reach it.”

Marie Curie

Acknowledgements

The development of this work would not have been possible without the help of a number of people, to whom I would like to acknowledge.

First of all, I would like to thank my advisor, Professor Carlos Pinho for the endless support and time shown throughout the semester in teaching and motivating me. Secondly, I would like to thank my co-adviser Eng.^a Marta Santos for all the availability and suggestions made in this work. Without their combined encouragement, this work would not have been possible.

I would like to express my gratitude towards INEGI for providing me with the installation needed for this project. A special thanks to Eng.^o Vítor Ferreira for always helping me concerning the installation and also all the suggestions made for this dissertation.

To all my friends that have accompanied me throughout this semester and all my academic career keeping me sane and motivated, all that support is appreciated. Also, to my boyfriend a special thanks for the unconditional support.

Last but not least, I would like to express my gratitude towards my family, mainly my parents and sisters, for always encouraging me to never give up, even in the direst situations.

Abstract

The present dissertation was developed within the Mechanical Engineer curriculum in the Thermal Energy masters option of the same course, for the 5th grade discipline Dissertation, taught at the Faculdade de Engenharia da Universidade do Porto (FEUP).

The main goal of this project was to study the influence of the ultrasounds in the heat transfer rate in the heat exchanger present at INEGI. The influence of the bubbling, tank insulation and entry cold fluid position were also studied. The hot/cold fluid pairs used were water/water and an aqueous LiBr solution/water and the type of heat exchanger used was a crossflow heat exchanger with the cold fluid mixed the hot fluid unmixed. There was also the intention of comparing the resulting values of the water as the hot fluid with the aqueous LiBr solution, but it was not entirely possible due to installation limitations.

With the provided setup, the first experiments done were with water/water. In these experiments, the hot fluid was heated to 60 °C and the cold fluid was at ambient temperature. By varying the mass flow rates of both fluids and measuring the inlet and exit temperatures of the hot and cold fluids in the heat exchanger tank, it was possible to obtain the overall heat transfer coefficient. For various tests this process was done while applying some test conditions like the use of ultrasounds, bubbling, ultrasounds and bubbling together, and tank insulation. The resulting values of the overall heat transfer coefficient were obtained and compared with each other along with the variation of the Reynolds number of the hot fluid. The convective heat transfer coefficients were also calculated. Some conclusions were drawn as to what test conditions provided bigger heat transfer enhancement and for which mass flow rate values.

Still in the experiments using water only, the entry cold water position was altered from a low position in the heat exchanger tank to a high position to study the influence that this change had in the heat transfer rate.

Afterwards, the hot fluid was switched from water to an aqueous LiBr solution with 55% concentration, while maintaining water as the cold fluid. The experiments were done in a similar way to the ones with water only performed previously, except the tank insulation was no longer applied. The overall heat transfer coefficient, Reynolds and convective heat transfer coefficients were all calculated as well to help draw a few conclusions about the heat transfer enhancement provided by the test conditions.

Lastly, the resulting values of the overall heat transfer coefficient of the tests with water/water and LiBr solution/water were compared for the base condition (no ultrasounds or bubbling) and for the ultrasounds condition. Due to different bubbling air injection rate, the experiments with the bubbling condition could not be compared between the two hot fluids.

It was concluded that the use of ultrasounds did not influence the heat transfer rate in this heat exchanger tank, while the bubbling effect increases it significantly.

Resumo

A presente dissertação foi elaborada no âmbito da disciplina “Dissertação”, que se enquadra no quinto ano lectivo do Mestrado Integrado em Engenharia Mecânica, na opção de mestrado Energia Térmica, lecionada na FEUP (Faculdade de Engenharia da Universidade do Porto).

O objetivo principal deste projeto era estudar a influência que os ultrasounds têm na taxa de transferência de calor no permutador de calor presente no INEGI. A influência do borbulhamento, isolamento do tanque e ponto de entrada do fluido quente também foram estudados. Os pares de fluidos quente/frio usados foram água/água e uma solução aquosa de LiBr/água e o tipo de permutador de calor usado era um tanque de troca de calor de escoamento cruzado com um fluido misturado e um não misturado. Havia também a intenção de comparar os valores resultantes da água como fluido quente com a solução aquosa de LiBr, mas não foi completamente possível devido a limitações da instalação.

Com a instalação proporcionada, as primeiras experiências feitas foram com água/água. Nestas experiências, o fluido quente era aquecido até 60 °C e o fluido frio estava à temperatura ambiente. Variando o caudal mássico de ambos os fluidos quente e frio e medindo as temperaturas de entrada e saída do fluido quente e do fluido frio no tanque de troca de calor, foi possível obter o coeficiente global de transferência de calor. Para vários testes este procedimento foi feito enquanto se aplicava algumas condições de testes como o uso de ultrasounds, borbulhamento, ultrasounds e borbulhamento em conjunto, e isolamento do tanque. Os valores resultantes do coeficiente global de transferência de calor foram obtidos e comparados uns com os outros juntamente com a variação do número de Reynolds do fluido quente. Os coeficientes de convecção também foram calculados. Algumas conclusões foram tiradas quanto a que testes providenciavam maiores aumentos na taxa de transferência de calor e para que valores de caudal mássico.

Ainda nas experiências usando apenas água, a posição de entrada da água fria foi alterada de uma posição em baixo no tanque de troca de calor para uma posição em cima para se estudar a influência que esta alteração tinha na taxa de transferência de calor.

Posteriormente, o fluido quente foi trocado de água para uma solução aquosa de LiBr com uma concentração de 55%, mantendo-se a água como fluido frio. As experiências foram executadas de uma maneira semelhante às feitas previamente com água como fluido quente, exceto que o isolamento do tanque deixou de ser aplicado. O coeficiente global de transferência de calor, o número de Reynolds e os coeficientes de convecção foram todos calculados também de maneira a se poder tirar conclusões quanto ao aumento da taxa de transferência de calor proporcionado pelas condições de testes.

Por fim, os resultados dos coeficientes globais de transferência de calor dos testes com água/água e solução de LiBr/água foram comparados para a condição base (sem ultrasounds ou borbulhamento) e para a condição dos ultrasounds. Por se terem usado diferentes taxas de borbulhamento, as experiências com o borbulhamento não se puderam comparar entre os dois fluidos quentes.

Preliminary studies on the influence of ultrasounds on the heat transfer rate in a crossflow heat exchanger

Foi concluído que o uso dos ultrassons não influenciava a taxa de transferência de calor no permutador de calor, enquanto que o borbulhamento aumentava-a significativamente.

Table of Contents

Abstract	v
Resumo.....	vii
List of figures	xi
List of Tables.....	xiii
1. Introduction	1
1.1. Project background and motivation.....	1
1.2. INEGI.....	2
1.3. Objectives of the project.....	2
1.4. Work methodology	2
1.5. Thesis structure	2
2. State of the Art.....	5
2.1. Ultrasounds applications.....	5
2.1.1. Acoustic Streaming.....	6
2.1.2. Acoustic Cavitation.....	6
2.1.3. Fouling factor	7
2.2. – Lithium Bromide	7
3. Lab Installation	9
3.1 Pump	10
3.2 Working fluids	12
3.3 Heating process.....	12
3.4 Regulating valves and piping.....	13
3.5 Bubbling.....	14
3.6 Ultrasounds	16
3.7 Heat exchanger tank	16
3.8 Data acquisition system	17
4. Tests with water	19
4.1 - Test conditions	19

4.1.1.	Mass flow rates	19
4.1.2.	Other test variables.....	20
4.2.	Data analysis.....	20
4.2.1.	The Logarithmic Mean Temperature Difference (LMTD) method	21
4.2.2.	The variation of UA with the test conditions.....	21
4.2.3.	The convective heat transfer coefficient	33
4.3.	Tests with water II.....	40
4.3.1.	Influence of the cold water entrance position.....	40
5.	Tests with LiBr solution	45
5.1.	Tests conditions.....	45
5.1.1.	Mass flow rates	45
5.1.2.	Test variables.....	45
5.2.	Data analysis.....	45
5.2.1.	The variation of UA with the test conditions.....	46
5.2.2.	Comparison of the LiBr tests with the water tests.....	51
5.2.3.	Convective heat transfer coefficient.....	54
6.	Conclusions	61
7.	Future works	63
	References.....	65
A.	Appendix A – Data acquisition software “DASYLab”	67
B.	Appendix B – Calibration of the mass flow meters (Water)	70
C.	Appendix C – Experimental results of the tests with water.....	75
D.	Appendix D – Experimental results of the tests with LiBr solution.....	83
E.	Appendix E – Calibration of the mass flow meter for the LiBr solution.....	86
F.	Appendix F – Obtaining of the LiBr solution physical properties.....	88

List of figures

Figure 2.1 - Classification of ultrasounds [2].	5
Figure 2.2- Effects of ultrasound propagation in liquids [4].	6
Figure 2.3 - Acoustic cavitation effect on a boundary layer [4].	7
Figure 3.1 - Overall installation.	9
Figure 3.2 – Simplified scheme of the installation (In blue, cold fluid. In red, hot fluid).	10
Figure 3.3 – Pump characteristics.	11
Figure 3.4 – Pump with the cooling fan.	11
Figure 3.5 – Heating process. A – Probe; B – The three resistances; C – Watt meter.	12
Figure 3.6 – PID controller.	13
Figure 3.7 – Valves present in the installation. A – Gate valve; B – Ball valve.	13
Figure 3.8 – Insulant applied in the hot fluid circuit.	14
Figure 3.9 – Bubbling effect.	15
Figure 3.10 – Pressure regulator and corresponding manometer attached to the air pipe supply.	15
Figure 3.11 – Ultrasound generator applied onto the heat exchanger tank.	16
Figure 3.12– Heat exchanger tank. A – copper coil; B – height mark; C – bubbling tube.	17
Figure 3.13 – Data acquisition board TC-32 [19].	18
Figure 3.14 – Data acquisition board USB-2416 [19].	18
Figure 4.1 – Correction factor plot for single pass crossflow heat exchanger, one fluid mixed, other unmixed [20].	22
Figure 4.2 – Evolution of the UA with the increase of Re_i for the “base” condition.	26
Figure 4.3 – Evolution of the UA with the increase of Re_i for the “bubbling” condition.	26
Figure 4.4 – Evolution of the UA with the increase of Re_i for the “ultrasounds, bubbling” condition.	27
Figure 4.5 – Evolution of the UA with the increase of Re_i for the “ultrasounds” condition.	27
Figure 4.6 – Evolution of the UA with the increase of Re_i for the “base” condition with insulation.	28
Figure 4.7 – Evolution of the UA with the increase of Re_i for the “bubbling” condition with insulation.	28
Figure 4.8 – Evolution of the UA with the increase of Re_i for the “ultrasounds” condition with insulation.	29
Figure 4.9 – Evolution of the UA with the increase of Re_i for the “ultrasounds, bubbling” condition with insulation.	29
Figure 4.10 – Evolution of the UA with the increase of Re_i : “base” vs “ultrasounds”.	30
Figure 4.11 – Evolution of the UA with the increase of Re_i : “base” vs “bubbling”.	30
Figure 4.12 – Evolution of the UA with the increase of Re_i : “bubbling” vs “ultrasounds”.	31
Figure 4.13 – Evolution of the UA with the increase of Re_i : “base” vs “insulation”.	31
Figure 4.14 – Evolution of the UA with the increase of Re_i : “ultrasounds” vs “ultrasounds, bubbling”.	32
Figure 4.15 – Evolution of the UA with the increase of Re_i : “bubbling” vs “ultrasounds, bubbling”.	32

Figure 4.16 – Evolution of the enhancement factor with the increase in cold water mass flow rate.	39
Figure 4.17 – Evolution of the enhancement factor with the increase in hot water mass flow rate.	39
Figure 4.18 – Different cold water entry positions. A – Below; B – Top.	40
Figure 5.1 - Evolution of the UA with the increase of Re_i for the “base” condition.....	47
Figure 5.2 - Evolution of the UA with the increase of Re_i for the “bubbling” condition.	48
Figure 5.3 - Evolution of the UA with the increase of Re_i for the “ultrasounds” condition.	48
Figure 5.4 - Evolution of the UA with the increase of Re_i for the “ultrasounds, bubbling” condition.	49
Figure 5.5 - Evolution of the UA with the increase of Re_i : “base” vs “ultrasounds”.	49
Figure 5.6 - Evolution of the UA with the increase of Re_i : “base” vs “bubbling”.	50
Figure 5.7 - Evolution of the UA with the increase of Re_i : “base” vs “ultrasounds, bubbling”.	50
Figure 5.8 - Evolution of the UA with the increase of Re_i : “bubbling” vs “ultrasounds, bubbling”.	51
Figure 5.9 - Evolution of the UA with the increase of Re_i in “base” condition: “water” vs “LiBr”. .	52
Figure 5.10 - Evolution of the UA with the increase of Re_i in “bubbling” condition: “water” vs “LiBr”.	52
Figure 5.11 - Evolution of the UA with the increase of Re_i in “ultrasounds” condition: “water” vs “LiBr”.	53
Figure 5.12 - Evolution of the UA with the increase of Re_i in “ultrasounds + bubbling” condition: “water” vs “LiBr”.	53
Figure 5.13 – Entry length solution for laminar flow in circular tubes [23].	58
Figure A.1 – “DASYLab” worksheet for the tests.	67
Figure A.2 – Calibration formula of the $C2$ flow meter in the “DASYLab” worksheet.....	68
Figure A.3 – Polynomial used for the c of the water, using the mean hot temperature in °C.	69
Figure B.1 – Weighting scale used in the calibration of the flow meters.	70
Figure B.2 – Trend line obtained through the calibration process of flow meter $C1$	71
Figure B.3 – $C1$ Trend line inserted in the worksheet of “DASYLab”.	71
Figure B.4 – Hot water calibration setup; A – Flow meter $C2$; B – Pump; C – Needle valve; D – Shut- off valve in T.	72
Figure B.5 – Graphic of the values obtained in the calibration process.	73
Figure B.6 – Comparison of the actual mass flow rate with the one calculated using equation B.3.	74
Figure E.1 – Trend line obtained through the LiBr solution calibration process.	86
Figure F.1 – Variation of the specific heat with the temperature in an EES Table.	88

List of Tables

Table 3.1– Dimensions of the heat exchanger tank.....	16
Table 4.1 – Test points with water arranged by cold and hot mass flow rates	19
Table 4.2 – New test points with water arranged by cold and hot mass flow rates.....	19
Table 4.3 – Dimensions of the copper coil of the installation.....	21
Table 4.4 – Reynolds and other properties of point “1.a” ($mc=2$ kg/min; $mh=2$ kg/min)	23
Table 4.5 – Reynolds and other properties of test point “1.b” ($mc=2$ kg/min; $mh=5$ kg/min)	23
Table 4.6 – Reynolds and other properties of test point “1.c” ($mc=2$ kg/min; $mh=8$ kg/min)	24
Table 4.7 – Reynolds and other properties of test point “2.a” ($mc=5$ kg/min; $mh=2$ kg/min)	24
Table 4.8 – Reynolds and other properties of test point “2.b” ($mc=5$ kg/min; $mh=5$ kg/min).....	24
Table 4.9 – Reynolds and other properties of test point “2.c” ($mc=5$ kg/min; $mh=8$ kg/min)	25
Table 4.10 – Reynolds and other properties of test point “3.d” ($mc=1.5$ kg/min; $mh=1.5$ kg/min) 25	25
Table 4.11 – Reynolds and other properties of test point “3.e” ($mc=1.5$ kg/min; $mh=3$ kg/min) ...	25
Table 4.12 – Reynolds and other properties of test point “3.f” ($mc=1.5$ kg/min; $mh=4$ kg/min)....	25
Table 4.13 – Figure marks representing each set of conditions	26
Table 4.14 – Reynolds, Prandtl and Nusselt numbers and convective heat transfer coefficients for test point “1.a” ($mc=2$ kg/min; $mh=2$ kg/min)	34
Table 4.15 – Reynolds, Prandtl and Nusselt numbers and convective heat transfer coefficients for test point “1.b” ($mc=2$ kg/min; $mh=5$ kg/min).....	35
Table 4.16 – Reynolds, Prandtl and Nusselt numbers and convective heat transfer coefficients for test point “1.c” ($mc=2$ kg/min; $mh=8$ kg/min)	35
Table 4.17 – Reynolds, Prandtl and Nusselt numbers and convective heat transfer coefficients for test point “2.a” ($mc=5$ kg/min; $mh=2$ kg/min)	35
Table 4.18 – Reynolds, Prandtl and Nusselt numbers and convective heat transfer coefficients for test point “2.b” ($mc=5$ kg/min; $mh=5$ kg/min).....	36
Table 4.19 – Reynolds, Prandtl and Nusselt numbers and convective heat transfer coefficients for test point “2.c” ($mc=5$ kg/min; $mh=8$ kg/min)	36
Table 4.20 – Reynolds, Prandtl and Nusselt numbers and convective heat transfer coefficients for test point “3.d” ($mc=1.5$ kg/min; $mh=1.5$ kg/min).....	36
Table 4.21 – Reynolds, Prandtl and Nusselt numbers and convective heat transfer coefficients for test point “3.e” ($mc=1.5$ kg/min; $mh=3$ kg/min).....	36
Table 4.22 – Reynolds, Prandtl and Nusselt numbers and convective heat transfer coefficients for test point “3.f” ($mc=1.5$ kg/min; $mh=4$ kg/min).....	37
Table 4.23 – Enhancement factors obtained in point “1.a” ($mc=2$ kg/min; $mh=2$ kg/min).....	37
Table 4.24 – Enhancement factors obtained in point “1.b” ($mc=2$ kg/min; $mh=5$ kg/min).....	37
Table 4.25 – Enhancement factors obtained in point “1.c” ($mc=2$ kg/min; $mh=8$ kg/min)	37
Table 4.26 – Enhancement factors obtained in point “2.a” ($mc=5$ kg/min; $mh=2$ kg/min).....	38
Table 4.27 – Enhancement factors obtained in point “2.b” ($mc=5$ kg/min; $mh=5$ kg/min).....	38
Table 4.28 – Enhancement factors obtained in point “2.c” ($mc=5$ kg/min; $mh=8$ kg/min)	38
Table 4.29 – Enhancement factors obtained in point “3.d” ($mc=1.5$ kg/min; $mh=1.5$ kg/min).....	38
Table 4.30 – Enhancement factors obtained in point “3.e” ($mc=1.5$ kg/min; $mh=3$ kg/min).....	38
Table 4.31 – Enhancement factors obtained in point “3.f” ($mc=1.5$ kg/min; $mh=4$ kg/min)	38

Table 4.32 - UA and Re_i for each test point in “base” condition for the new entry point.	41
Table 4.33 - UA and Re_i for each test point in “bubbling” condition for the new entry point.	41
Table 5.1 – Test points for the LiBr experiments	45
Table 5.2 - Reynolds and other properties of test point “11.a” ($mc=2$ kg/min; $mh=2$ kg/min).....	46
Table 5.3 - Reynolds and other properties of test point “11.b” ($mc=2$ kg/min; $mh=5$ kg/min).....	46
Table 5.4 - Reynolds and other properties of test point “13.d” ($mc=1.5$ kg/min; $mh=1.5$ kg/min). 46	
Table 5.5 - Reynolds and other properties of test point “13.e” ($mc=1.5$ kg/min; $mh=3$ kg/min)....	47
Table 5.6 - Reynolds and other properties of test point “11.z (10)” ($mc=2$ kg/min; $mh=10$ kg/min)	47
Table 5.7 - Reynolds and other properties of test point “11.z (12.5)” ($mc=2$ kg/min; $mh=12.5$ kg/min)	47
Table 5.8 - Reynolds, Prandtl, Nusselt numbers and convective heat transfer coefficients of point “11.z(10)” ($mc=2$ kg/min; $mh=10$ kg/min)	54
Table 5.9 - Reynolds, Prandtl, Nusselt numbers and convective heat transfer coefficients of point “11.z(12.5)” ($mc=2$ kg/min; $mh=12.5$ kg/min)	54
Table 5.10 – Enhancement factor of the bubbling effect for test point “11.z(10)” and “11.z(12.5)”	55
Table 5.11 - h_e values for the base condition in test points “1.a”, “1.b” and “1.c”	55
Table 5.12 – Shared values of h_e for both tests	56
Table 5.13 - Reynolds, Prandtl, Nusselt numbers and convective heat transfer coefficients of point “11.a” ($mc=2$ kg/min; $mh=2$ kg/min).....	56
Table 5.14 - Reynolds, Prandtl, Nusselt numbers and convective heat transfer coefficients of point “11.b” ($mc=2$ kg/min; $mh=5$ kg/min)	56
Table 5.15 - Reynolds, Prandtl, Nusselt numbers and convective heat transfer coefficients of point “13.d” ($mc=1.5$ kg/min; $mh=1.5$ kg/min)	56
Table 5.16 - Reynolds, Prandtl, Nusselt numbers and convective heat transfer coefficients of point “13.e” ($mc=1.5$ kg/min; $mh=3$ kg/min)	57
Table 5.17 – The inverse of Graetz number for test point “11.a” ($mc=2$ kg/min; $mh=2$ kg/min)....	58
Table 5.18 - The inverse of Graetz number for test point “11.b” ($mc=2$ kg/min; $mh=5$ kg/min)	58
Table 5.19 - The inverse of Graetz number for test point “11.b” ($mc=1.5$ kg/min; $mh=1.5$ kg/min)	58
Table 5.20 - The inverse of Graetz number for test point “11.b” ($mc=1.5$ kg/min; $mh=3$ kg/min) .	59
Table C.1 – Values obtained for test point “1.a” ($mc = 2$ kg/min; $mh = 2$ kg/min)	75
Table C.2 - Values obtained for test point “1.b” ($mc = 2$ kg/min; $mh = 5$ kg/min).....	76
Table C.3 – Values obtained for test point “1.c” ($mc = 2$ kg/min; $mh = 8$ kg/min)	77
Table C.4 – Values obtained for test point “2.a” ($mc = 5$ kg/min; $mh = 2$ kg/min)	78
Table C.5 – Values obtained for test point “2.b” ($mc = 5$ kg/min; $mh = 5$ kg/min).....	79
Table C.6 – Values obtained for test point “2.c” ($mc = 5$ kg/min; $mh = 8$ kg/min)	80
Table C.7 – Values obtained for test point “3.d” ($mc = 1.5$ kg/min; $mh = 1.5$ kg/min).....	81
Table C.8 – Values obtained for test point “3.e” ($mc = 1.5$ kg/min; $mh = 3$ kg/min).....	81
Table C.9 – Values obtained for test point “3.f” ($mc = 1.5$ kg/min; $mh = 4$ kg/min).....	82
Table D.1 - Values obtained for test point “11.a” ($mc = 2$ kg/min; $mh = 2$ kg/min)	83
Table D.2 - Values obtained for test point “11.b” ($mc = 2$ kg/min; $mh = 5$ kg/min)	84
Table D.3 - Values obtained for test point “13.d” ($mc = 1.5$ kg/min; $mh = 1.5$ kg/min)	84

Table D.4 - Values obtained for test point "13.e" ($mc = 1.5$ kg/min; $mh = 3$ kg/min) 85
Table D.5 - Values obtained for test point "11.z10" ($mc = 2$ kg/min; $mh = 10$ kg/min)..... 85
Table D.6 - Values obtained for test point "11.z10" ($mc = 2$ kg/min; $mh = 12.5$ kg/min)..... 85

Nomenclature

Designation	Definition	Units
Latin symbols		
A_i	Area of element i	[m ²]
A_{int}	Inner are of the coil	[m ²]
$A_{coil.int}$	Inner area of the coil	[m ²]
$A_{coil.ext}$	Outer area of the coil	[m ²]
C_1, C_2	Mass flow meters	[-]
c	Specific heat	[J/(kg.K)]
d	Specific gravity	[-]
D_i	Diameter of the element i	[m]
F	Correction factor of the LMTD method	[-]
h	Convective heat transfer coefficient	[W/(m ² .K)]
h_e	Convective heat transfer coefficient of coil's outer wall	[W/(m ² .K)]
h_i	Convective heat transfer coefficient of coil's inner wall	[W/(m ² .K)]
k_{copper}	Conductivity coefficient of copper	[W/(m.K)]
k_{hf}	Conductivity coefficient of hot fluid	[W/(m.K)]
k_{water}	Conductivity coefficient of water	[W/(m.K)]
k_{LiBr}	Conductivity coefficient of LiBr solution	[W/(m.K)]
L_{coil}	Length of the coil in serpentine	[m]
L_{total}	Total length of the coil	[m]
$L_{remaining}$	Length of the coil that is not in serpentine	[m]
$L_{h,turb}$	Hydrodynamic entry length of a turbulent flow	[m]
$L_{t,laminar}$	Hydrodynamic entry length of a laminar flow	[m]
\dot{m}_h	Mass flow rate of the hot fluid	[kg/s; kg/min]
\dot{m}_c	Mass flow rate of the cold fluid	[kg/s; kg/min]
Nu	Number of Nusselt	[-]
P	Parameter of the LMTD method	[-]

Pr	Number of Prandtl	[-]
Q_c	Calorific Power of the cold fluid	[W; kW]
Q_h	Calorific Power of the hot fluid	[W; kW]
R	Parameter of the LMTD method	[-]
Re_i	Number of Reynolds of the hot fluid	[-]
$R_{w_{cond}}$	Resistance of conduction of the coil's wall	[K/W]
R_{fi}	Fouling factor of the coil's inner wall	[K/W]
R_{fe}	Fouling factor of the coil's outer wall	[K/W]
T_1, T_2, \dots, T_5	Thermocouples	[-]
T_{hi}	Hot stream inlet temperature	[°C; K]
T_{ho}	Hot stream exit temperature	[°C; K]
T_{ci}	Cold stream inlet temperature	[°C; K]
T_{co}	Cold stream exit temperature	[°C; K]
T_{mh}	Mean temperature of the hot fluid	[°C; K]
UA	Overall heat transfer coefficient	[W/K]
v	Velocity of the hot flow	[m/s]
V	Voltage	[V]
V_{total}	Total volume of the heat exchanger tank	[m ³ ; cm ³]
V_{test}	Used volume of the heat exchanger tank for tests	[m ³ ; cm ³]
x	Mean value of the coil's total length	[m]

Greek symbols

α	Enhancement factor	[-]
μ	Dynamic viscosity	[N.s/m ²]
ρ	Mass volume/ density	[kg/m ³]
v	Specific volume	[m ³ /kg]
ΔT_{ml}	Logarithmic mean temperature	[°C; K]
$\Delta T_1; \Delta T_2$	Temperature differential in equation (4.4)	[°C; K]

Acronyms

<i>LMTD</i>	Logarithmic Mean Temperature Method
PID	Proportional Integral Derivative
PPR	Polypropylene
AHT	Absorption Heat Transformer

1. Introduction

Nowadays it is impossible to live by without energy. Its importance is undeniable and every day one uses energy in many formats such as electricity, heat, chemistry and work. However, apart from renewable energy which use renewable sources, the resources used to produce energy such as fossil fuels not only are limited but also bring terrible consequences when releasing carbon dioxide to the atmosphere aggravating global warming. Therefore, when using energy, one must save as much as possible not only for economical purposes but also for the protection of the world.

In that regard, the search for energy-saving methods is getting more demanding from the industry as they try to be more energy efficient in their industrial processes. Energy can be transferred between two systems through work and heat, the latter being designated heat transfer – energy is transferred from one system to another due to a difference in temperature [1]. Heat transfer devices are very diverse and can be used for climatization purposes, such as air-conditioning systems and refrigeration systems.

When it comes to energy transfer systems, heat transfer equipment such as the heat exchangers are often used. They enable heat transfer from a hotter fluid to a colder fluid without mixing them. This heat transfer consists in both convection and conduction. These devices are commonly used for different purposes (condensers, boilers, chemical processing, power production) but come with a few drawbacks, one of them being the fouling effect that takes place in their heat transfer area which with time reduces their efficiency [1,2].

For that matter, a few studies have been done regarding the use of ultrasounds to enhance the heat transfer rate and prevent the fouling effect that takes place in heat exchangers [3–7]. With the usage of ultrasonic vibrations, heat transfer between the two fluids is optimized in all kinds of heat exchangers, saving some energy while getting better overall results.

This project will study the influence of ultrasounds in a crossflow heat exchanger in a heat exchanger tank in two similar situations where the working fluids will vary. One in which both working fluids (hot and cold fluids) are water and the other where the working fluids are water as the cold fluid and an aqueous lithium bromide solution as the hot fluid.

1.1. Project background and motivation

This dissertation was proposed by the energy department of INEGI in order to better the heat transfer rate in heat exchangers with the purpose of possibly integrating it in a working PhD project which involves an Absorption Heat Transformer. According to the literature, the use of ultrasounds seems beneficial to the heat transfer rate, but studies on this subject are still limited, especially studies using LiBr/water as the heat transfer fluids. The purpose of this dissertation was to run some preliminary tests on a novel experimental setup, with the purpose of studying the effect of ultrasounds on heat transfer, particularly with LiBr/water as the heat transfer fluids. The aqueous LiBr solution was used since it is the solution used in the AHT of the PhD project,

Preliminary studies on the influence of ultrasounds on the heat transfer rate in a crossflow heat exchanger

and a possible way of improving the heat transfer rate in the AHT was the use of ultrasounds. Another effect that was studied was the importance of cold bubbling agitation on the heat transfer rate.

1.2. INEGI

The experimental work of the present dissertation was developed at the energy department of INEGI (“Instituto de Ciência e Inovação em Engenharia Mecânica e Engenharia”) in its “Laboratório de Combustão” (Combustion Laboratory). INEGI is a Research and Technology Organization (RTO), founded in 1986, focused on research and technology-based innovation activities, technology transfer, consulting and technological services, oriented to the development of industry and economy in general. It is a non-profit, private and recognized as a public utility entity.

1.3. Objectives of the project

The main goals of this project were:

- Analysis of the heat transfer rate of the installation provided at INEGI.
- Analysis of the heat transfer rate of two different hot fluids with and without the presence of ultrasounds and/or bubbling.
- Comparison of the results between the water and the lithium bromide solution, with and without the bubbling.

1.4. Work methodology

The dissertation will follow the subsequent method:

- Literature review of the effects ultrasounds have on heat exchange efficiency.
- Literature review of the aqueous solution of lithium bromide.
- Calibration of the system.
- Execution of tests with water, with and without ultrasounds or bubbling, for various hot and cold water mass flow rates.
- Execution of tests with the conditions mentioned above, this time using lithium bromide as the hot fluid.

1.5. Thesis structure

This dissertation is divided into seven sections, starting with a brief introduction of the subject at hand as well as the project background already in this section.

The following section concerns the information already existent about experiments using ultrasounds in the heat transfer field as well as the theory behind it. Supplementary information about the lithium bromide is also discussed in this section.

The third section depicts the present installation at INEGI with detail, describing each component and their roles in the setup. The procedure of the experiments is also explained in this section.

Preliminary studies on the influence of ultrasounds on the heat transfer rate in a crossflow heat exchanger

The next section explains the tests with water only, describing the variables and test conditions. Its data analysis is also present in this section, presenting the calculations done alongside its results, in the form of tables and graphics.

The section after portrays the tests done with the aqueous LiBr solution as the hot fluid, once more explaining its procedure and test conditions used. The data analysis of these experiments is presented, showing the resulting values. A comparison between the water/water tests and LiBr solution/water tests is made as well in this section.

In the sixth section some conclusions are made concerning all the tests done and the installation itself. Some results are presented as well as a brief summary of all the experiments done, pointing out some installation flaws.

Finally, the last section suggests some improvements to be made to the installation along with other ideas for future works in this field of experiments.

Preliminary studies on the influence of ultrasounds on the heat transfer rate in a crossflow heat exchanger

2. State of the Art

2.1. Ultrasounds applications

The human hearing range goes between 20 Hz and 20 kHz. Sound waves above the upper limit of the hearing range are classified as ultrasounds [4]. The use of ultrasonic waves has been studied roughly since World War I and so far has been shown useful for many applications in several fields like chemistry, food industry, medicine, physics, oceanography, biology and non-destructive testing [2,8]. Ultrasonic waves can be ordered into three categories according to their range of frequencies, as shown in figure 2.1:

- “Low frequency ultrasound” or “power ultrasound” – for frequencies between 20 and 100 kHz, these waves produce mainly physical effects on the matter submitted to it [9]. Acoustic streaming and cavitation are two phenomena that happen in fluids caused by it that have great value for heat transfer enhancement [4,10].
- “High frequency ultrasound” – for frequencies between 100 kHz and 1 MHz.
- “Low power ultrasound” – for frequencies above 1 MHz. These are commonly used for medical diagnoses and for nondestructive material control. So far, not many studies involving “Low power ultrasound” in heat transfer enhancement have been reported [4,11,12].

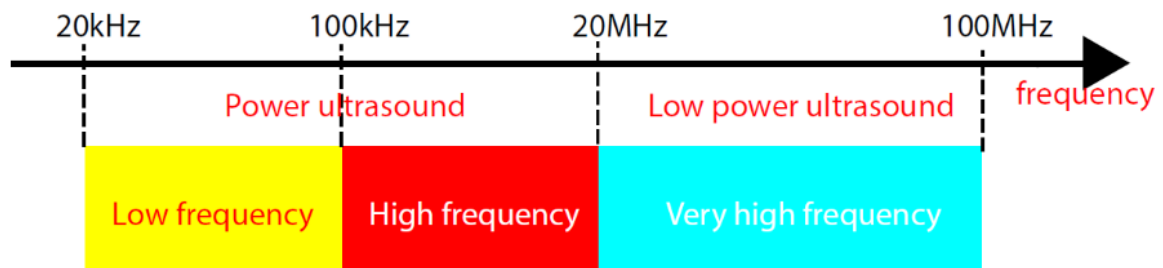


Figure 2.1 - Classification of ultrasounds [2].

Ultrasounds studies have been made in the heat transfer field for a few decades and its increasing popularity and well received results are due to its effects observed in the liquids. When an ultrasound passes through a liquid medium, it causes mechanical vibrations in it, which brings forth four known effects, figure 2.2. Among them, acoustic streaming and acoustic cavitation are the most relevant when it comes to heat transfer.

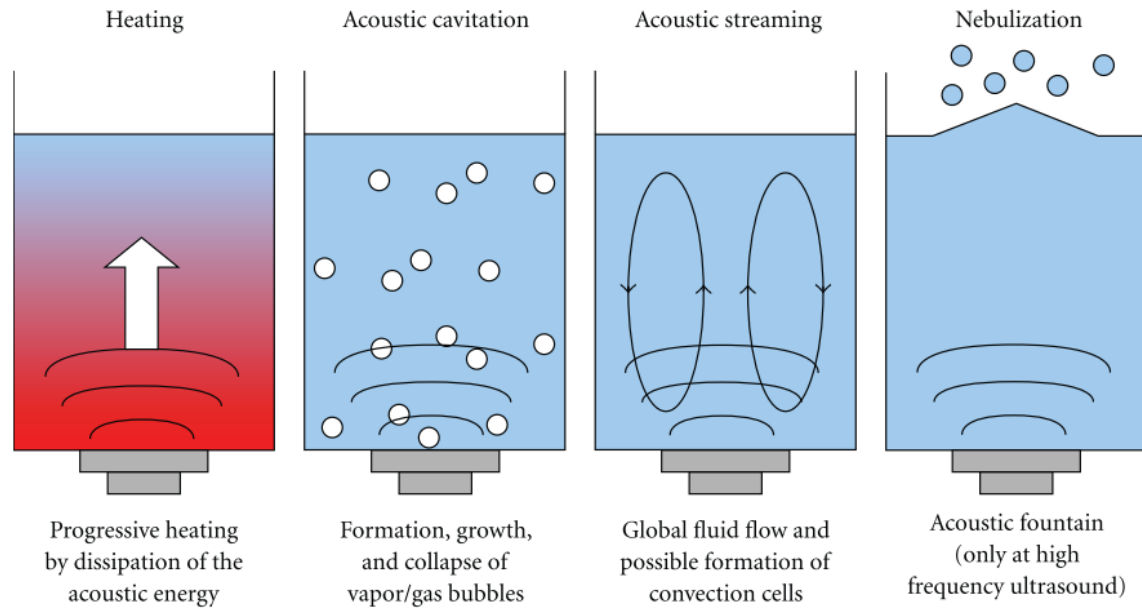


Figure 2.2- Effects of ultrasound propagation in liquids [4].

2.1.1. Acoustic Streaming

Acoustic streaming can be defined as circular flows in gas or liquids generated by acoustic waves. As sound waves propagate in the fluid, they are attenuated by absorption and scattered, and in the presence of high-intensity sound waves, this attenuation of pressure creates a steady bulk flow [13]. The speed gained by the fluid can lead to turbulence which promotes heat transfer rate. It also allows a better convection heat transfer coefficient near the solid boundaries [4].

2.1.2. Acoustic Cavitation

The acoustic cavitation can be defined as the formation, growth, oscillation and then collapse of gas bubbles within a liquid created from the propagation of ultrasonic waves in it [4,10]. The act of collapse of these gas bubbles generates physical effects (shock waves, turbulence, micro jets, shear forces, etc.) and even generates high temperatures for a short period of time within the bubbles. Its applications are varied. For example, cavitation is found to be useful in diagnostic and therapeutic medicine [14]. It can also be used in food processing applications like emulsification, filtration and tenderization [15].

For a few reasons it is believed that acoustic cavitation is the major factor in heat transfer enhancement by ultrasound. For example, bubble implosions near the solid-liquid interface reduces thermal resistance and creates micro turbulence by disrupting the thermal and velocity boundary as exemplified by figure 2.3 [4]. It is this phenomenon that allows the desired fouling reduction in heat exchangers. When the cavities and bubbles generated by ultrasonic propagating in liquid break out, some high pressure peaks form and make suspending solid, i.e. fouling crystals, smash into granules which may suspend in liquid, thus reducing the sedimentation of crystals on the heated wall [7].

Preliminary studies on the influence of ultrasounds on the heat transfer rate in a crossflow heat exchanger

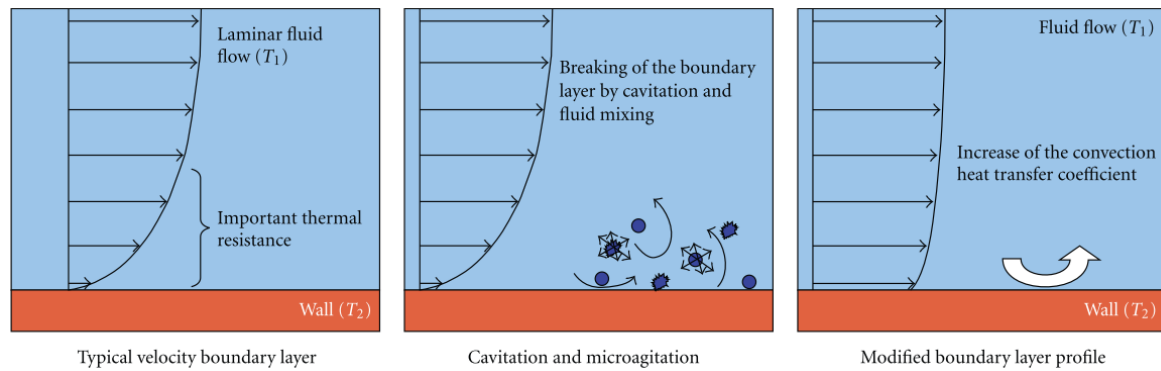


Figure 2.3 - Acoustic cavitation effect on a boundary layer [4].

2.1.3. Fouling factor

Over time, the accumulation of deposits on heat transfer surfaces deteriorate the performance of heat exchangers by decreasing the heat transfer area [1]. The reduction of the fouling factor is yet another advantage that the use of ultrasounds provides in heat exchangers along with the heat transfer enhancement. It was observed that the use of ultrasonic power decreases fouling present in microstructured heat exchangers, that are more prone to fouling [5]. On a double-tube heat exchanger, by using ultrasounds in a range of frequencies between 20 kHz and 40 kHz, it was noted that for both frequencies the antifouling effect was remarkable, with better results for 20 kHz [7].

2.2. Lithium Bromide

Lithium bromide (LiBr) is a compound of lithium and bromine. In its solid form, it resembles common salt (sodium chloride). It is, however, mostly used as an aqueous solution in air-conditioning systems for a concentration of 50-60% and in absorption chillers/transformers [16].

Absorption heat transformers (AHT) can use low-grade temperature streams to obtain higher temperature streams in order to reduce thermal energy waste. Since AHT require a working pair of refrigerant/absorbent, the $H_2O/LiBr$ pair is very frequently used due to its advantages like high latent heat, high stability, high affinity, high relative volatility and high safety, even though at moderate concentrations the lithium bromide tends to get corrosive [17].

A study combining LiBr solution with ultrasonic heat transfer enhancement was already made in 2016 [18]. In this study where it investigates the heat transfer enhancement using ultrasounds on three different structural tubes (smooth, screwed and finned) with a LiBr solution in sub-cooled boiling regime, it was concluded that the boiling heat transfer performance of the LiBr solution is poor compared to water because of its physical properties like low thermal conductivity, high viscosity and high surface tension. The ultrasonic enhancement in the LiBr solution was not as efficient as that in water either.

Preliminary studies on the influence of ultrasounds on the heat transfer rate in a crossflow heat exchanger

Preliminary studies on the influence of ultrasounds on the heat transfer rate in a crossflow heat exchanger

3. Lab Installation

In this section the multiple components of the installation provided at INEGI are presented. The installation was specifically made for this project with various components owned by the “Laboratório de Combustão” (Combustion Laboratory) at INEGI. The overall look of the installation is shown in figure 3.1.

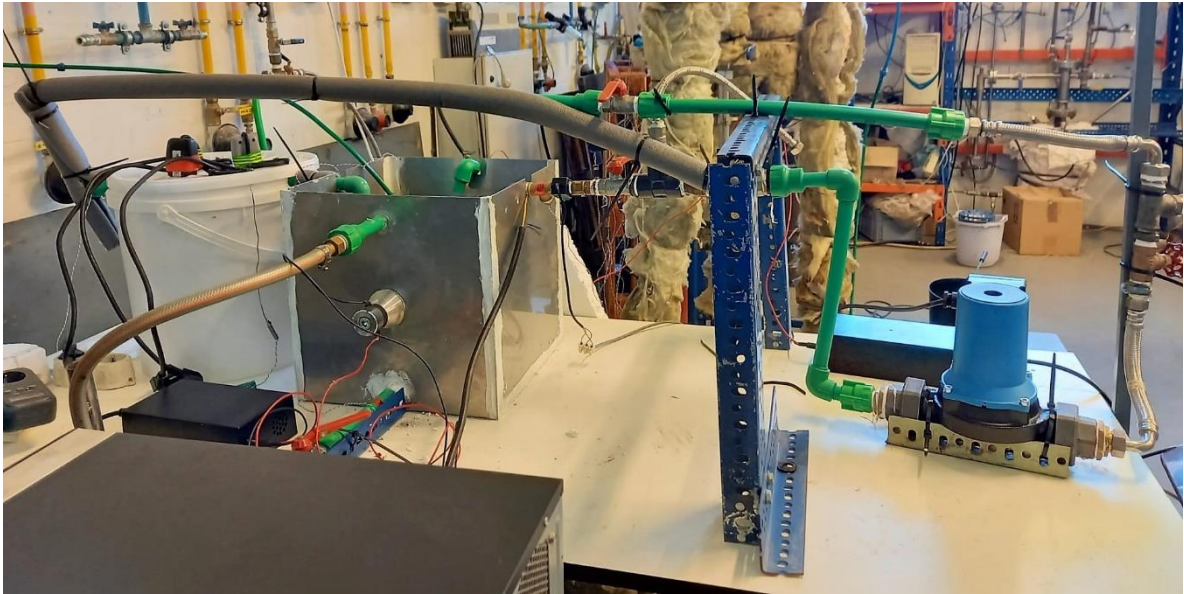


Figure 3.1 - Overall installation.

In the installation, two different fluid flows are present – the hot fluid and the cold fluid (water) – making two different circuits without them mixing. The circuits of the installation are represented in the following scheme.

Preliminary studies on the influence of ultrasounds on the heat transfer rate in a crossflow heat exchanger

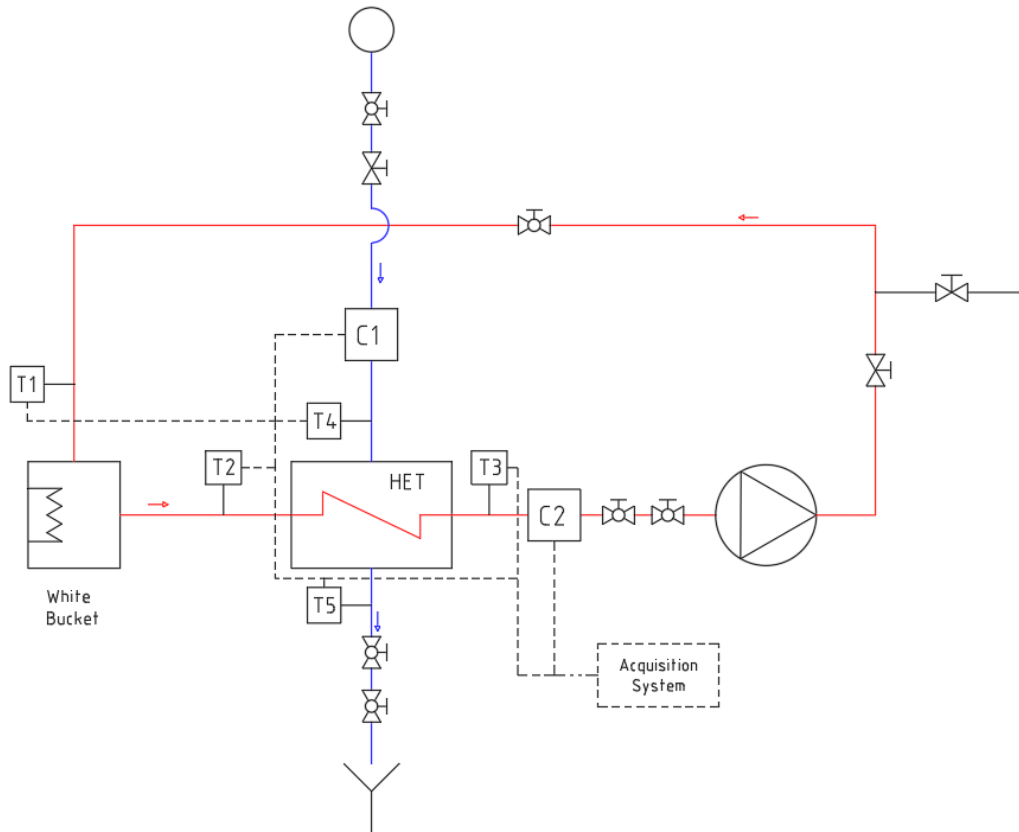


Figure 3.2 – Simplified scheme of the installation (In blue, cold fluid. In red, hot fluid).

In figure 3.2, C1 and C2 represent the present mass flow meters. T1, T2, T3, T4 and T5 represent the thermocouples. The white bucket is where the hot fluid is heated and “HET” stands for heat transfer tank, where the heat transfer between the two fluids happen.

3.1 Pump

The circulation of the hot fluid is guaranteed by an EFAFLU pump, model CD32/120. This pump has the following characteristics (Power = 265 W; Voltage = 230 V; Nominal pressure = 10 bar; Maximum mass flow rate = 9.5 m³/h) and its picture is in figure 3.3. It has three different working positions designated by I, II and III. Because the fluid that will be pumped can go up to 60 °C for a long period of time, a fan was placed next to the pump to help prevent its overheating, figure 3.4.

Preliminary studies on the influence of ultrasounds on the heat transfer rate in a crossflow heat exchanger

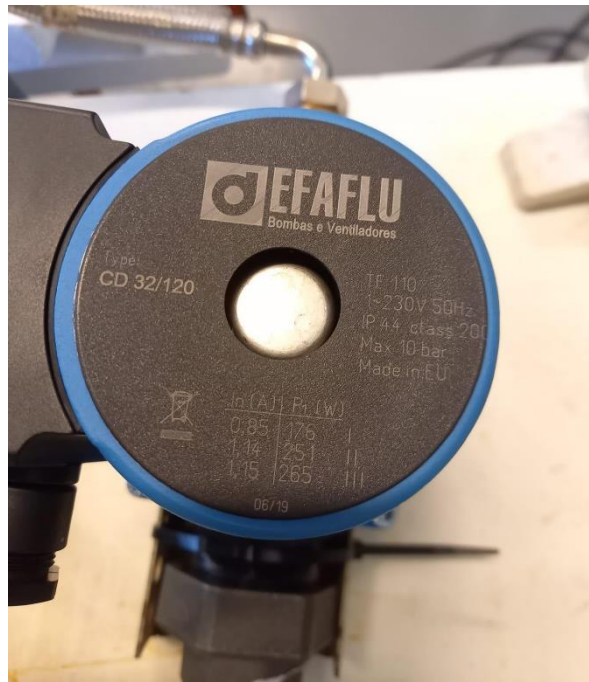


Figure 3.3 – Pump characteristics.



Figure 3.4 – Pump with the cooling fan.

Preliminary studies on the influence of ultrasounds on the heat transfer rate in a crossflow heat exchanger

3.2 Working fluids

Water was the only cold fluid used for testing. The cold water comes from domestic tap water. As for the hot fluid, two kinds of fluid were used. The first round of tests was made with water as also the hot fluid, while for the second round of tests an aqueous solution of lithium bromide 55% v/v provided by “Leverton Clarke Ltd” was used.

3.3 Heating process

The hot fluid was heated in the white bucket using three electrical resistances (figure 3.5 - B). Each one was 1500 W and the ensemble was connected to a watt meter (figure 3.5 - C). This energy monitor system permits readouts of electricity consumption of the connected appliances. A PID controller (proportional integral derivative) was incorporated in the heating process to control the electrical resistances in reaching and maintaining the desired temperature (figure 3.6). The PID controller was connected to a thermocouple with a probe (figure 3.5 - A). The probe was immersed in the hot fluid, close to the fluid exit to properly measure the temperature of the water that exits the bucket.



Figure 3.5 – Heating process. A – Probe; B – The three resistances; C – Watt meter.

Preliminary studies on the influence of ultrasounds on the heat transfer rate in a crossflow heat exchanger



Figure 3.6 – PID controller.

3.4 Regulating valves and piping

Both cold and hot fluid flow rates were controlled through gate valves (figure 3.7 – A) that are present in their respective circuits, one for each circuit. There were also ball valves (figure 3.7 –B) in both circuits to shut-off the circulation of fluids whenever was needed.

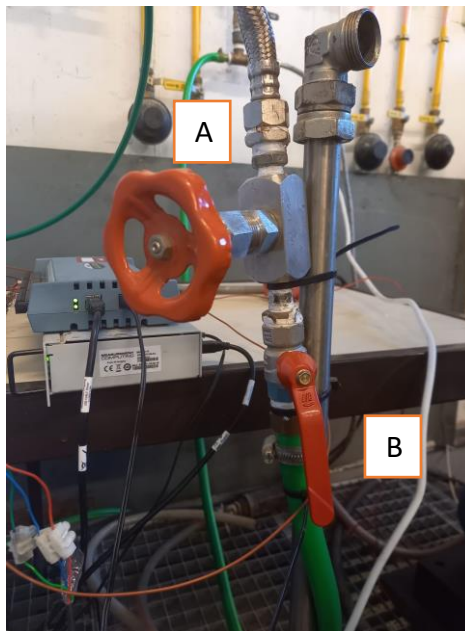


Figure 3.7 – Valves present in the installation. A – Gate valve; B – Ball valve.

The piping used in the hot fluid circuit was made of PPR (Polypropylene Random Copolymer) with an external diameter of 20 mm and 2.8 mm of thickness. For the cold-water circuit, hoses were used to connect the piped water supply to the circuit, and after going through the heat exchanger tank it was discharged to the sewers.

Preliminary studies on the influence of ultrasounds on the heat transfer rate in a crossflow heat exchanger

In the hot fluid circuit, an insulant made of polyethylene was applied covering part of the piping, so that it reduced the heat loss of the hot fluid towards the surroundings, as shown in figure 3.8.



Figure 3.8 – Insulant applied in the hot fluid circuit.

3.5 Bubbling

The bubbling was the product of compressed air being released through a few holes in a plastic tube underwater in the heat exchanger tank (figure 3.12 – C). When the tank was full of water, the air expelled from the green tube caused great agitation as shown in figure 3.9. This compressed air came from pipe compressed air supply and went through a pressure regulator that measured and regulated the pressure of the air that passes through it, figure 3.10. This option of regulating the bubbling air flow only by means of the pressure regulator appeared lately to be a rough approach and resulted in a less precise definition of the bubbling intensity. It was however the initial adopted choice and, as will be explained later, lead to two different operating bubbling intensities, with the corresponding experimental drawbacks.

Preliminary studies on the influence of ultrasounds on the heat transfer rate in a crossflow heat exchanger



Figure 3.9 – Bubbling effect.

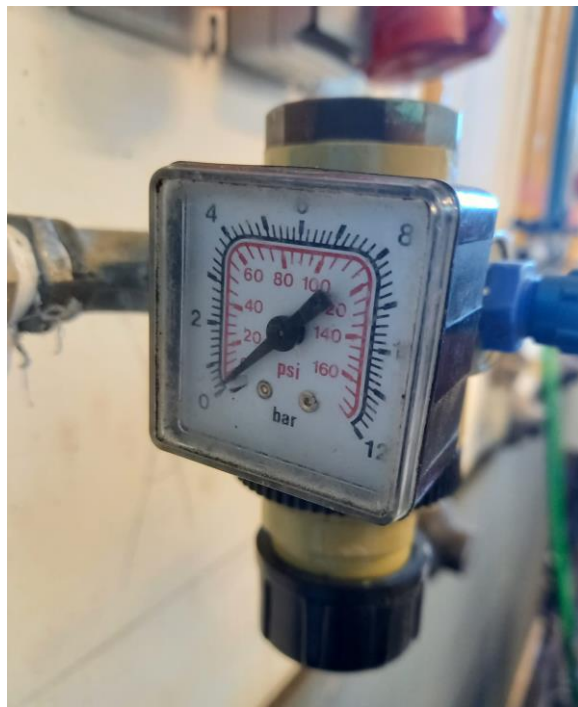


Figure 3.10 – Pressure regulator and corresponding manometer attached to the air pipe supply.

3.6 Ultrasounds

The ultrasounds were generated in a two custom-made devices, each with an ultrasound frequency of 28 kHz and 100 W of power. The two devices were applied to the heat exchanger tank, on opposing sides, generating a total of 200 W ultrasounds. Figure 3.11 displays how the ultrasound generators connected to the heat exchanger tank.

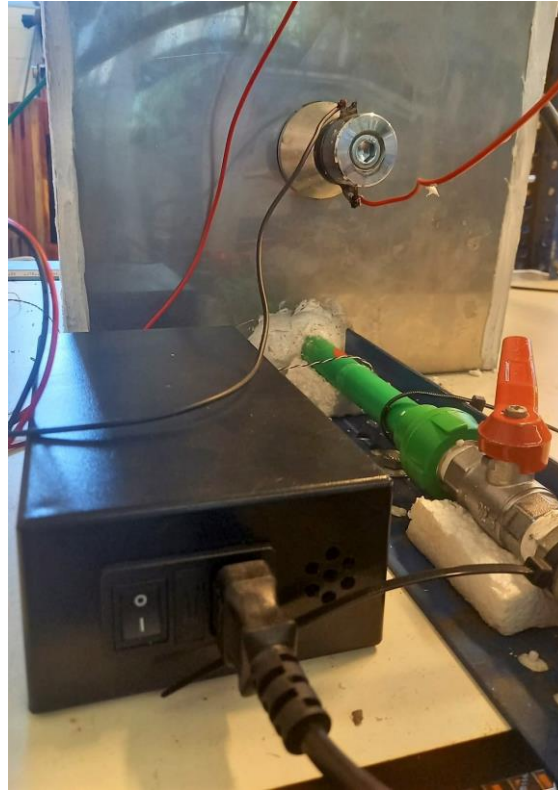


Figure 3.11 – Ultrasound generator applied onto the heat exchanger tank.

3.7 Heat exchanger tank

The heat exchanger tank was where the two fluids exchanged heat between them. The tank was filled with cold water and inside there was a copper coil in which the hot fluid flowed (figure 3.12– A). There was one entry point of the cold water and two exit points, one on the bottom and one at the top for safety purposes (to prevent the tank from overflowing). The tank was made of steel and had silicone on its borders to prevent leakage.

Table 3.1 displays the dimensions of the heat exchanger tank. Since the tank was a cube, the height, width and length all had the same measure. For the tests, a certain mark (figure 3.12 – B) was made at a height of 26.1 cm as a way to make sure that in all tests the volume of cold water, V_{test} was equal.

Table 3.1– Dimensions of the heat exchanger tank

Length [cm]	33
V_{total} [cm³]	35 937
V_{test} [cm³]	28 422.9

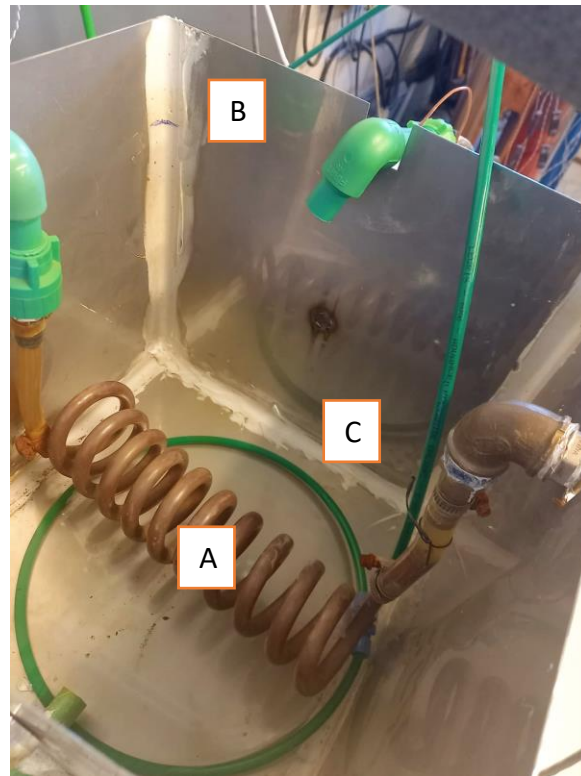


Figure 3.12– Heat exchanger tank. A – copper coil; B – height mark; C – bubbling tube.

3.8 Data acquisition system

In order to properly gather and analyze all the data in each test, a data acquisition system consisting of two boards by Measurement Computing™ (TC-32 and USB-2416) was used to register the temperatures and mass flow rates, respectively. Additionally, the data acquisition software “DASYLab” was used. “DASYLab” allows the user to store, do an early data processing and graphically analyze the evolution of the test as it is running. Additional information is found in Appendix A.

In the installation, there were a total of 5 thermocouples (T_1, T_2, \dots, T_5) and 2 mass flow meters (C_1 and C_2) installed (figure 3.2).

Board TC-32 (figure 3.13) has 11 reading channels and was used for temperature measurement, therefore it was where the thermocouples were connected. Board USB-2416 (figure 3.14) was used to register voltage variation that the mass flow meters pick up and transmit, which was then converted to the corresponding mass flow rate in the “DASYLab” software using a calibration curve. The calibration process of both mass flow meters is presented in Appendix B.

Preliminary studies on the influence of ultrasounds on the heat transfer rate in a crossflow heat exchanger



Figure 3.13 – Data acquisition board TC-32 [19]



Figure 3.14 – Data acquisition board USB-2416 [19].

4. Tests with water

4.1 Test conditions

Before starting tests, operating conditions were established. For each test, after applying the chosen operating conditions into the experimental setup, the experiment started running, and when the steady state operating conditions were reached, meaning the exit temperatures of both fluids stabilized, the testing procedure started. Each steady state test operation lasted between 5 and 10 minutes.

4.1.1. Mass flow rates

For the first set of tests, the mass flow rate values of both cold (\dot{m}_c) and hot fluids (\dot{m}_h) were carefully chosen, and values in the 2 to 5 kg/min range were adopted. From these initial values, it was possible to draw some mass flow rate combinations as shown in table 4.1. For each pair of cold and hot mass flow rates, an experimental condition was defined, for example, point “1.a” is for both cold and hot mass flow rates of approximately 2 kg/min.

Table 4.1 – Test points with water arranged by cold and hot mass flow rates

	$\dot{m}_h = 2 \text{ kg/min}$	$\dot{m}_h = 5 \text{ kg/min}$	$\dot{m}_h = 8 \text{ kg/min}$
$\dot{m}_c = 2 \text{ kg/min}$	1.a	1.b	1.c
$\dot{m}_c = 5 \text{ kg/min}$	2.a	2.b	2.c

The minimum chosen value of both cold and hot mass flow rates was 2 kg/min. If it were much lower, it would be problematic because by throttling the mass flow rate too much, a few operating problems could happen like overheating the water pump. The maximum tested hot fluid mass flow rate was 8 kg/min. This value was chosen because at higher mass flow rates the heat transfer probably would not be affected by neither ultrasounds nor bubbling, as it was observed later in chapter 4.2 (Data analysis). Then a medium value was picked, 5 kg/min, equally between the minimum and maximum values.

The maximum value of cold water mass flow rate was chosen as 5 kg/min. Higher mass flow rates would be too much because since the volume of cold water (volume of the tank) is so much bigger than the hot water crossflow volume, it would be too difficult to maintain the temperature of the hot bucket at approximately 60 °C with the three resistances on. So 5 kg/min was chosen as the maximum cold fluid mass flow rate.

After performing all the tests “1.a” through “2.c” and analyzing the initial results, it was quickly concluded that the ultrasounds had little to no effect when the flow rates of both cold and hot fluids were at 5 kg/min or higher. Therefore, three more tests were made in order to get a better understanding of the influence of ultrasounds and bubbling for lower mass flow rate testing conditions. The corresponding mass flow rates for these new test points are in table 4.2.

Table 4.2 – New test points with water arranged by cold and hot mass flow rates

	$\dot{m}_h = 1.5 \text{ kg/min}$	$\dot{m}_h = 3 \text{ kg/min}$	$\dot{m}_h = 4 \text{ kg/min}$
$\dot{m}_c = 1.5 \text{ kg/min}$	3.d	3.e	3.f

4.1.2. Other test variables

For each defined test point in table 4.1 and 4.2, eight different experiments were done, each applying a combination of different variables, namely tank insulation, ultrasounds and bubbling. The experiments started with a standard one, or base condition, where no other variable was used, and then ultrasounds, bubbling and a mix of the two were applied. Then the same tests were repeated but this time with the tank insulation applied as well.

With these different conditions, it was possible to compare the heat transfer rate for each pair of hot and cold mass flow rates with and without the ultrasounds, bubbling or the two combined. This way, it was possible to tell if these effects enhanced the heat transfer rate or not and which ones represented a bigger enhancement. The thermal insulation of the heat exchanger tank helps reduce the heat dissipation from the tank to the environment and there was interest in confirming if the insulation affected or not the effects of the ultrasounds or bubbling. After confirming that it did not with points from “1.a” to “2.c”, as it will be seen later, points “3.d”, “3.e” and “3.f” were all executed without insulation to save time.

4.2. Data analysis

Each test ran for about 5 to 10 minutes, and the data acquisition software “DASYLab” recorded the measured values every second. The average of each variable was calculated and used in the data analysis.

Some important data regarding the installation, specifically the coil, which will be crucial for future calculations, is shown in table 4.3. The diameters, external and internal, were measured with a pachymeter and the length of the coil was measured with a measuring tape. The formulas used for the calculation of areas and pipe resistance are the following:

$$A_i = \frac{\pi D_i^2}{4} \quad (4.1)$$

$$A_{coil,i} = \pi D_i L_{total} \quad (4.2)$$

$$RW_{cond} = \frac{\ln(D_e/D_i)}{2\pi L_{total} k_{copper}} \quad (4.3)$$

Table 4.3 – Dimensions of the copper coil of the installation

D_i [m]	0.0105
D_e [m]	0.0127
Thickness [m]	0.0011
L_{coil} [m]	0.257
$L_{remaining}$ [m]	0.255
L_{total} [m]	2.825
A_{int} [m ²]	8.659×10^{-05}
A_{ext} [m ²]	1.267×10^{-04}
$A_{coil.ext}$ [m ²]	1.127×10^{-01}
$A_{coil.int}$ [m ²]	9.319×10^{-02}
k_{copper} [W/m.K]	372 [20]
RW_{cond} [K/W]	2.881×10^{-05}

4.2.1. The Logarithmic Mean Temperature Difference (LMTD) method

For simple heat exchangers in steady-state operation and crossflow of the hot and cold fluids, a log-mean temperature difference is defined (equation 4.4). Assuming that the overall heat transfer coefficient U is constant throughout the heat exchanger, the mass flow rate and specific heat of both fluids are constant and there is no phase change [21], this log-mean temperature difference is given by,

$$\Delta T_{ml} = \frac{\Delta T_2 - \Delta T_1}{\ln(\Delta T_2 / \Delta T_1)} \quad (4.4)$$

in which ΔT_1 and ΔT_2 are

$$\Delta T_1 = T_{hi} - T_{co} \quad (4.5)$$

$$\Delta T_2 = T_{ho} - T_{ci} \quad (4.6)$$

From the diagram of the installation (figure 3.2), the following equivalences were drawn:

- $T_{hi} = T_2$
- $T_{ho} = T_3$
- $T_{ci} = T_4$
- $T_{co} = T_5$

4.2.2. The variation of UA with the test conditions

For crossflow heat exchangers such as this one, figure 3.12, a correction factor F must be accounted for in the calculation of the $LMTD$ [21]. F depends on the parameters R and P , that are given by the following expressions [21].

$$R = \frac{T_{hi} - T_{ho}}{T_{co} - T_{ci}} \quad (4.7)$$

$$P = \frac{T_{co} - T_{ci}}{T_{hi} - T_{ci}} \quad (4.8)$$

From there, F is obtained with figure 4.1 [21] that is applicable to crossflow heat exchangers with one fluid mixed and the other unmixed.

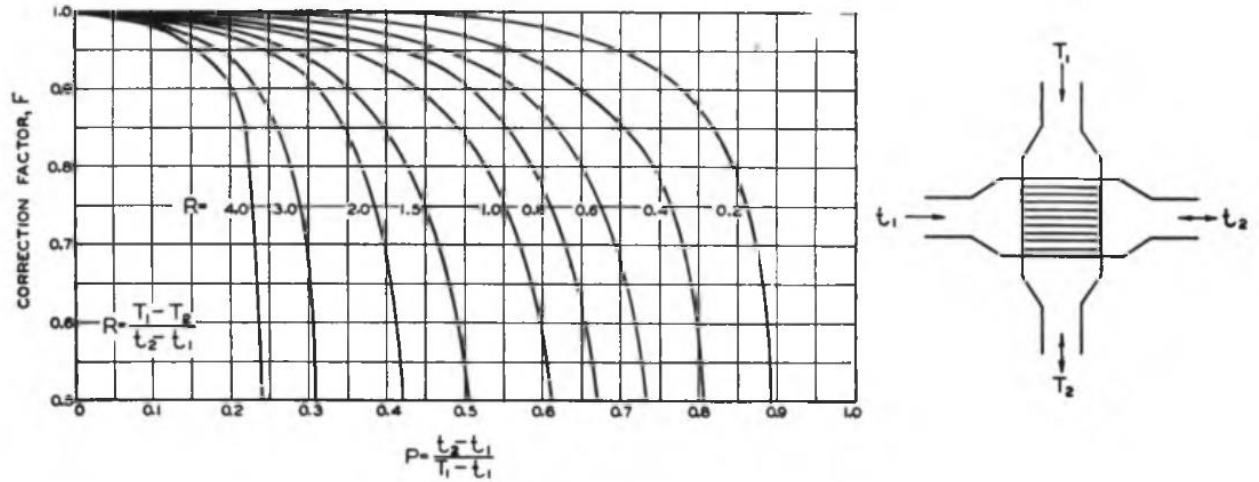


Figure 4.1 – Correction factor plot for single pass crossflow heat exchanger, one fluid mixed, other unmixed [21].

The software calculates the value of the heat power of both hot and cold fluids. Equation 4.9 shows how the heat power of the hot fluid was calculated in the “DASYLab”. After obtaining the values of ΔT_{ml} , F and Q , it is possible to find the overall heat transfer coefficient through equation 4.10.

$$Q_h = \dot{m}_h c (T_{hi} - T_{ho}) \quad (4.9)$$

$$Q = UA \Delta T_{ml} F \quad (4.10)$$

Using the mean value of the heat power of the cold fluid of each point and having calculated ΔT_{ml} and F as described before, then the UA of each point is attained as represented in tables C.1–C.9 (Appendix C). The mean hot temperature T_{mh} was also calculated for purposes that will be discussed ahead.

In order to better perceive the effects that the different conditions (ultrasounds, bubbling, insulation) have in the overall heat transfer coefficient with a variety of mass flow rates, it was thought to be relevant to compare its values along with the changes in the Reynolds number of the hot fluid, Re_i . That way, the comparison of the overall heat transfer coefficient with the mass flow rates is “fair” because Reynolds is a dimensionless number that takes into account the thermal properties of the fluid used. As such, the Reynolds number was calculated with equation 4.11.

$$Re_i = \frac{\rho v D_i}{\mu} \quad (4.11)$$

The density ρ and the dynamic viscosity μ of the fluid were calculated through polynomials which depend on the temperature of the hot fluid, in °C. Equation 4.12 is a trend-line obtained through data collected from a thermodynamic table and equation 4.13 was found in a website concerning water properties [22].

Since the hot fluid temperature decreases along the coil, the mean hot temperature $T_{mh} = (T_{ho} + T_{hi})/2$ was considered instead for the calculations of its thermal properties.

Preliminary studies on the influence of ultrasounds on the heat transfer rate in a crossflow heat exchanger

$$\rho = -1.036 \times 10^{-7} T_{mh}^4 + 3.681 \times 10^{-5} T_{mh}^3 - 7.275 \times 10^{-3} T_{mh}^2 + 5.048 \times 10^{-2} T_{mh} + 999.9 \quad (4.12)$$

$$\mu = 1.684 \times 10^{-3} - 4.264 \times 10^{-5} T_{mh} + 5.062 \times 10^{-7} T_{mh}^2 - 2.244 \times 10^{-9} T_{mh}^3 \quad (4.13)$$

The velocity of the hot fluid was calculated by:

$$v = \frac{\dot{m}_h}{\rho A_{int}} \quad (4.14)$$

As such, all the resulting values are shown in tables 4.4 – 4.12.

Table 4.4 – Reynolds and other properties of point “1.a” ($\dot{m}_c=2$ kg/min; $\dot{m}_h=2$ kg/min)

Test reference	UA [W/K]	μ [N.s/m ²]	ρ [kg/m ³]	v [m/s]	Re _i
base	55.37	0.000555	989.0658	0.395	7384
bubbling	70.74	0.000577	990.0187	0.397	7160
ultrasounds	57.56	0.000534	988.0234	0.375	7286
ultrasounds,bubbling	77.86	0.000548	988.7495	0.400	7573
insulation	56.76	0.000521	987.3578	0.389	7743
insulation,bubbling	71.13	0.000530	987.8196	0.403	7888
insulation,ultrasounds	57.38	0.000512	986.8070	0.380	7690
insulation,ultrasounds,bubbling	76.75	0.000531	987.8522	0.384	7507

Table 4.5 – Reynolds and other properties of test point “1.b” ($\dot{m}_c=2$ kg/min; $\dot{m}_h=5$ kg/min)

Test reference	UA [W/K]	μ [N.s/m ²]	ρ [kg/m ³]	v [m/s]	Re _i
base	62.85	0.000484	984.9718	0.968	20687
bubbling	85.73	0.000490	985.3746	0.969	20466
ultrasounds	63.37	0.000483	984.9143	0.996	21309
ultrasounds,bubbling	84.15	0.000487	985.2124	0.970	20589
insulation	65.24	0.000476	984.3758	0.965	20955
insulation,bubbling	83.18	0.000496	985.7803	1.010	21088
insulation,ultrasounds	64.90	0.000478	984.5209	0.999	21604
insulation,ultrasounds,bubbling	84.93	0.000476	984.3813	1.006	21840

Table 4.6 – Reynolds and other properties of test point “1.c” ($\dot{m}_c=2$ kg/min; $\dot{m}_h=8$ kg/min)

Test reference	UA [W/K]	μ [N.s/m ²]	ρ [kg/m ³]	v [m/s]	Re_i
base	69.20	0.000476	984.3466	1.591	34573
bubbling	94.17	0.000472	984.0686	1.584	34663
ultrasounds	66.69	0.000474	984.2348	1.591	34683
ultrasounds,bubbling	93.50	0.000473	984.1178	1.583	34593
insulation	71.10	0.000473	984.1506	1.579	34489
insulation,bubbling	90.66	0.000471	983.9676	1.580	34671
insulation,ultrasounds	66.35	0.000473	984.1462	1.568	34259
insulation,ultrasounds,bubbling	82.72	0.000471	983.9681	1.572	34502

Table 4.7 – Reynolds and other properties of test point “2.a” ($\dot{m}_c=5$ kg/min; $\dot{m}_h=2$ kg/min)

Test reference	UA [W/K]	μ [N.s/m ²]	ρ [kg/m ³]	v [m/s]	Re_i
base	73.10	0.000548	988.7567	0.384	7272
bubbling	88.22	0.000570	989.7067	0.390	7115
ultrasounds	73.67	0.000550	988.8319	0.388	7321
ultrasounds,bubbling	86.78	0.000558	989.2201	0.386	7177
insulation	73.22	0.000541	988.4044	0.411	7882
insulation,bubbling	85.61	0.000537	988.2104	0.396	7649
insulation,ultrasounds	73.74	0.000541	988.3719	0.402	7712
insulation,ultrasounds,bubbling	84.33	0.000555	989.0724	0.394	7376

Table 4.8 – Reynolds and other properties of test point “2.b” ($\dot{m}_c=5$ kg/min; $\dot{m}_h=5$ kg/min)

Test reference	UA [W/K]	μ [N.s/m ²]	ρ [kg/m ³]	v [m/s]	Re_i
base	91.88	0.000482	984.8258	0.999	21428
bubbling	101.08	0.000488	985.2217	1.005	21316
ultrasounds	90.70	0.000481	984.7281	1.000	21517
ultrasounds,bubbling	99.58	0.000484	984.9631	1.001	21398
insulation	90.74	0.000482	984.7969	1.005	21574
insulation,bubbling	103.35	0.000492	985.5322	1.000	21033
insulation,ultrasounds	89.52	0.000482	984.8077	0.996	21379
insulation,ultrasounds,bubbling	102.52	0.000492	985.5100	0.996	20962

Table 4.9 – Reynolds and other properties of test point “2.c” ($\dot{m}_c=5$ kg/min; $\dot{m}_h=8$ kg/min)

Test reference	UA [W/K]	μ [N.s/m ²]	ρ [kg/m ³]	v [m/s]	Re_i
base	94.34	0.000473	984.1143	1.557	34045
bubbling	108.68	0.000494	985.6715	1.572	32919
ultrasounds	92.30	0.000472	984.0438	1.561	34178
ultrasounds,bubbling	106.69	0.000489	985.3153	1.556	32917
insulation	97.89	0.000482	984.7934	1.574	33797
insulation,bubbling	109.22	0.000498	985.9332	1.578	32807
insulation,ultrasounds	97.28	0.000478	984.5340	1.572	33978
insulation,ultrasounds,bubbling	105.62	0.000492	985.5428	1.570	33009

Table 4.10 – Reynolds and other properties of test point “3.d” ($\dot{m}_c=1.5$ kg/min; $\dot{m}_h=1.5$ kg/min)

Test reference	UA [W/K]	μ [N.s/m ²]	ρ [kg/m ³]	v [m/s]	Re_i
base	49.83	0.000557	989.1359	0.286	5334
bubbling	64.90	0.000577	990.0087	0.300	5410
ultrasounds	51.01	0.000556	989.1184	0.302	5637
ultrasounds,bubbling	65.55	0.000591	990.5650	0.291	5120

Table 4.11 – Reynolds and other properties of test point “3.e” ($\dot{m}_c=1.5$ kg/min; $\dot{m}_h=3$ kg/min)

Test reference	UA [W/K]	μ [N.s/m ²]	ρ [kg/m ³]	v [m/s]	Re_i
base	57.86	0.000486	985.1040	0.591	12576
bubbling	76.97	0.000508	986.5498	0.592	12075
ultrasounds	56.61	0.000486	985.1212	0.580	12338
ultrasounds,bubbling	74.85	0.000497	985.8354	0.592	12351

Table 4.12 – Reynolds and other properties of test point “3.f” ($\dot{m}_c=1.5$ kg/min; $\dot{m}_h=4$ kg/min)

Test reference	UA [W/K]	μ [N.s/m ²]	ρ [kg/m ³]	v [m/s]	Re_i
base	56.71	0.000478	984.5076	0.766	16572
bubbling	78.01	0.000493	985.6000	0.778	16332
ultrasounds	57.67	0.000476	984.3403	0.796	17294
ultrasounds,bubbling	74.82	0.000480	984.7047	0.791	17017

Gathering all the data from all the points, it was thought to be insightful comparing for each certain condition (base, ultrasounds, insulation, etc.) how all the UA values evolved with the increase of Re_i to have a clear understanding of which condition has more influence with the increase of Reynolds number. Therefore, graphics of figures 4.2 – 4.9 show the overall heat transfer coefficient per cold fluid flow rate. For better understanding of the upcoming graphics, the colors blue, orange and red always represent the cold water mass flow rates of 1.5, 2 and 5 kg/min, respectively. Also, each geometric mark represents one type of condition, as shown in table 4.13, in which when the tank insulation is present, the marks have a black edge over them.

Preliminary studies on the influence of ultrasounds on the heat transfer rate in a crossflow heat exchanger

Table 4.13 – Figure marks representing each set of conditions

	Base	Ultrasounds	Bubbling	Ultrasounds + Bubbling
Figure mark	●	▲	■	◆

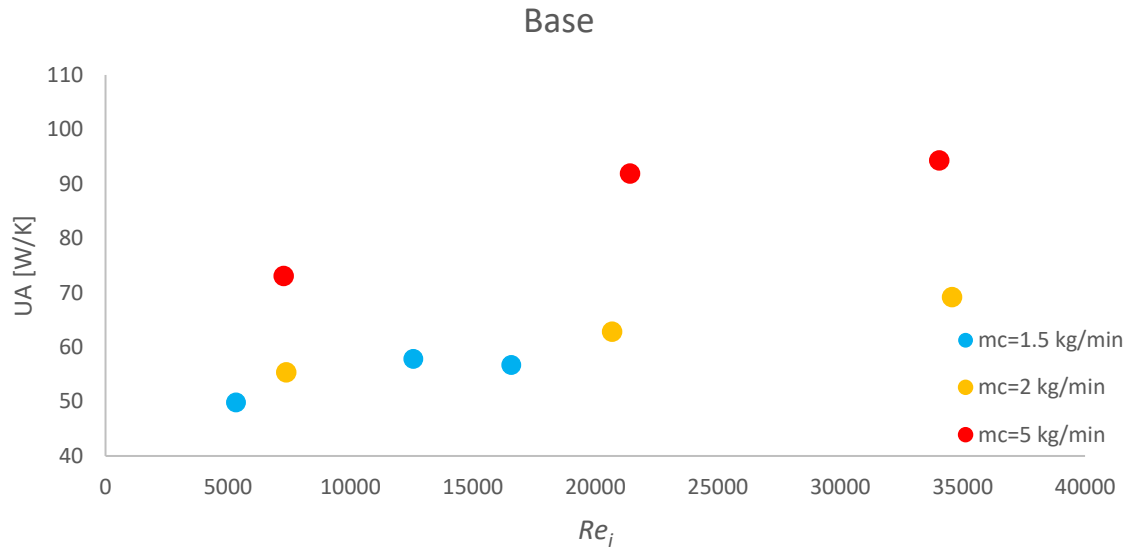


Figure 4.2 – Evolution of the UA with the increase of Re_i for the “base” condition.

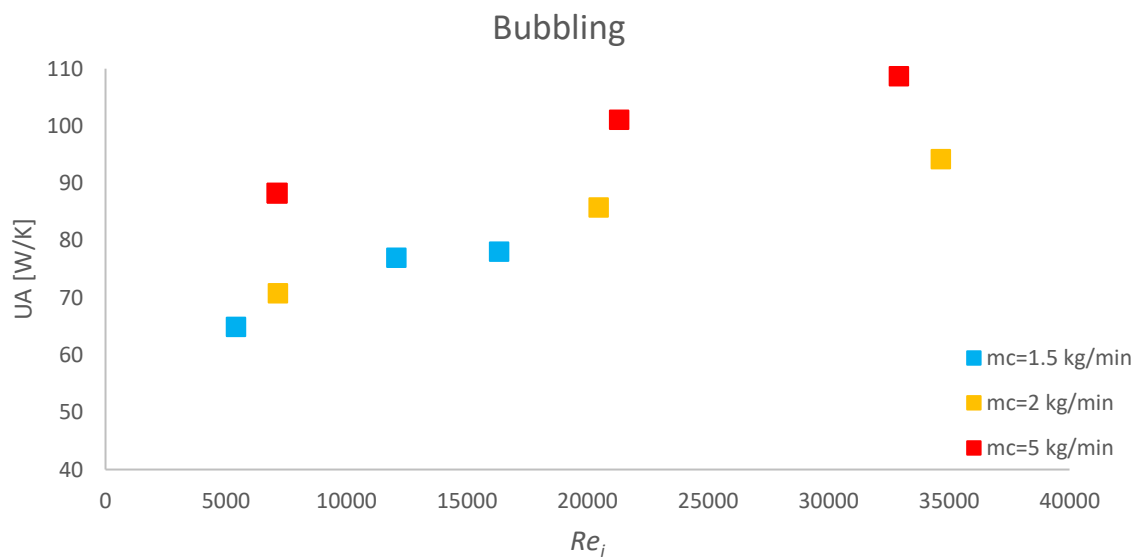


Figure 4.3 – Evolution of the UA with the increase of Re_i for the “bubbling” condition.

Preliminary studies on the influence of ultrasounds on the heat transfer rate in a crossflow heat exchanger

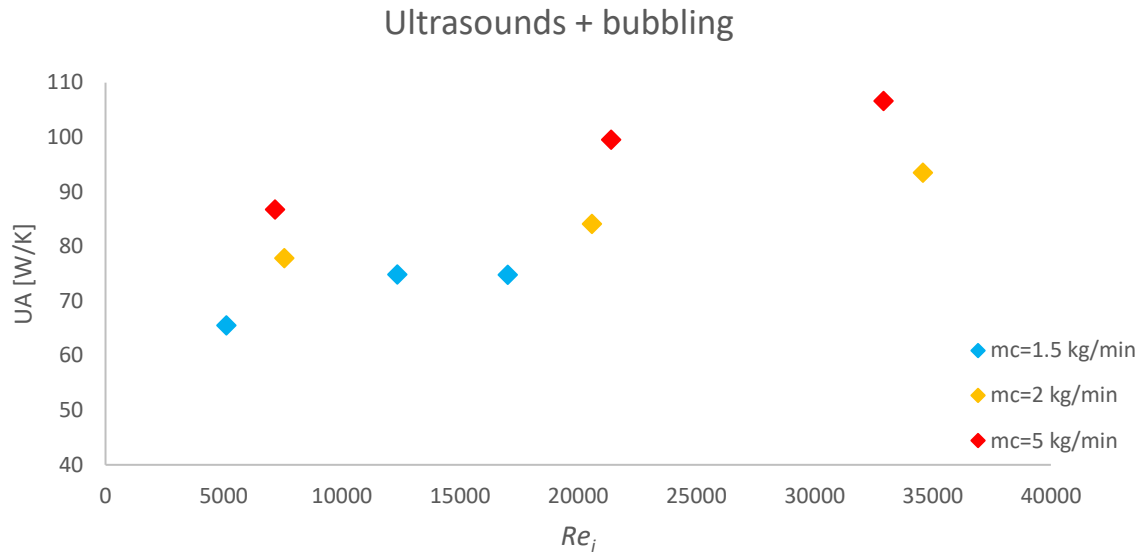


Figure 4.4 – Evolution of the UA with the increase of Re_i for the “ultrasounds, bubbling” condition.

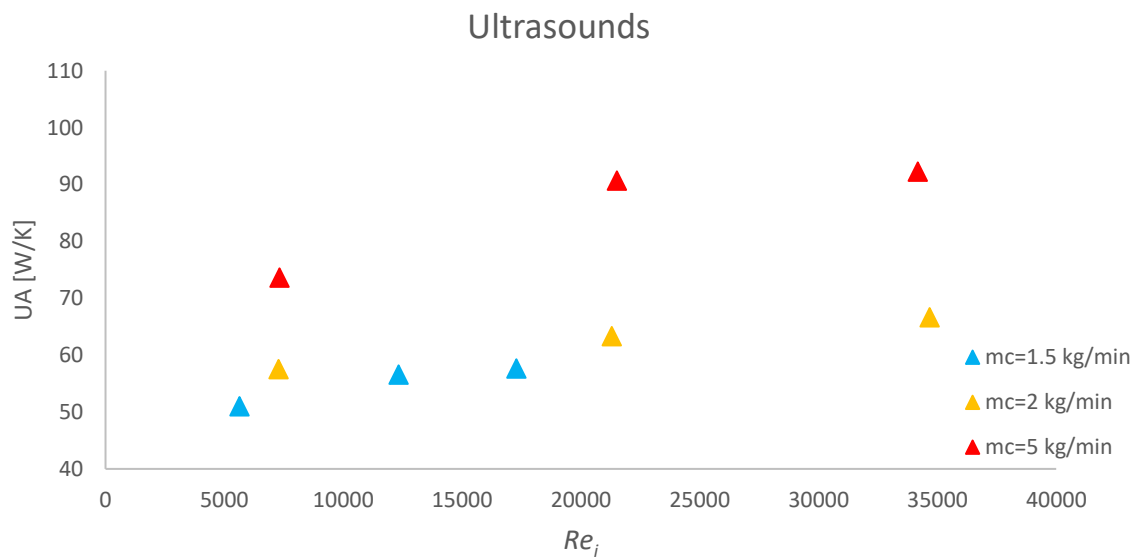


Figure 4.5 – Evolution of the UA with the increase of Re_i for the “ultrasounds” condition.

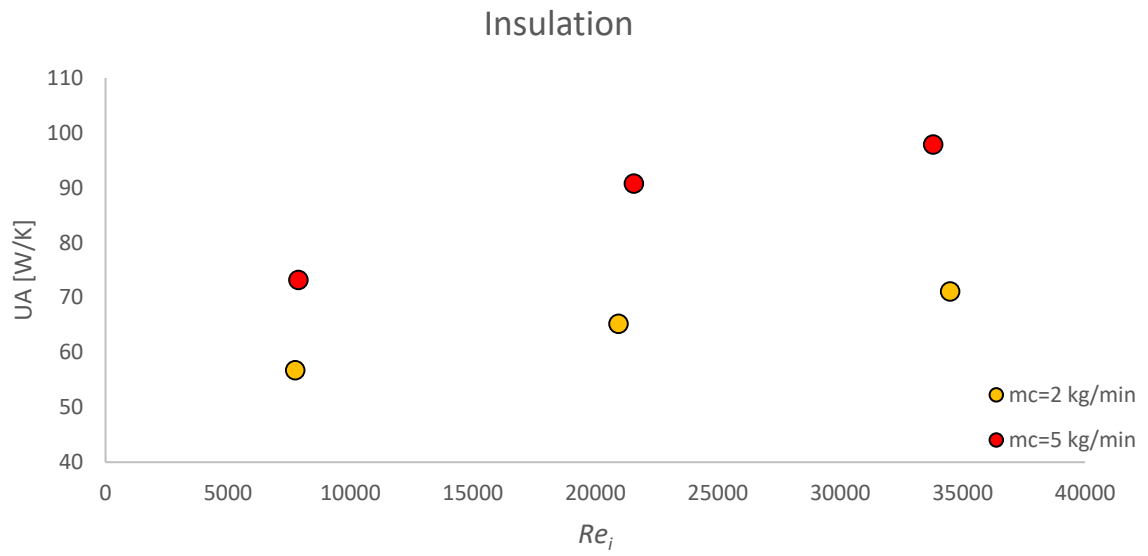


Figure 4.6 – Evolution of the UA with the increase of Re_i for the “base” condition with insulation.

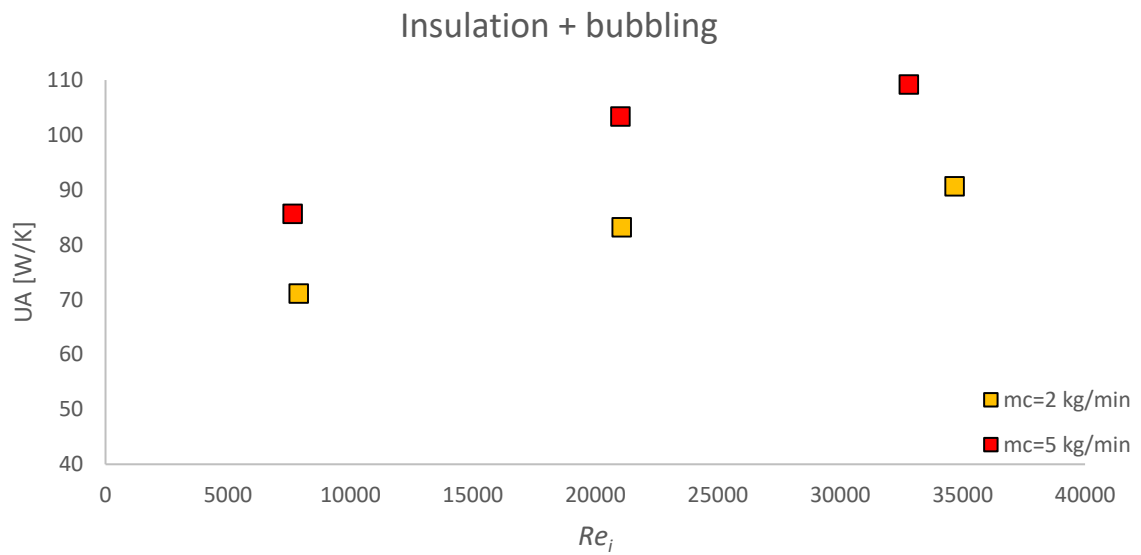


Figure 4.7 – Evolution of the UA with the increase of Re_i for the “bubbling” condition with insulation.

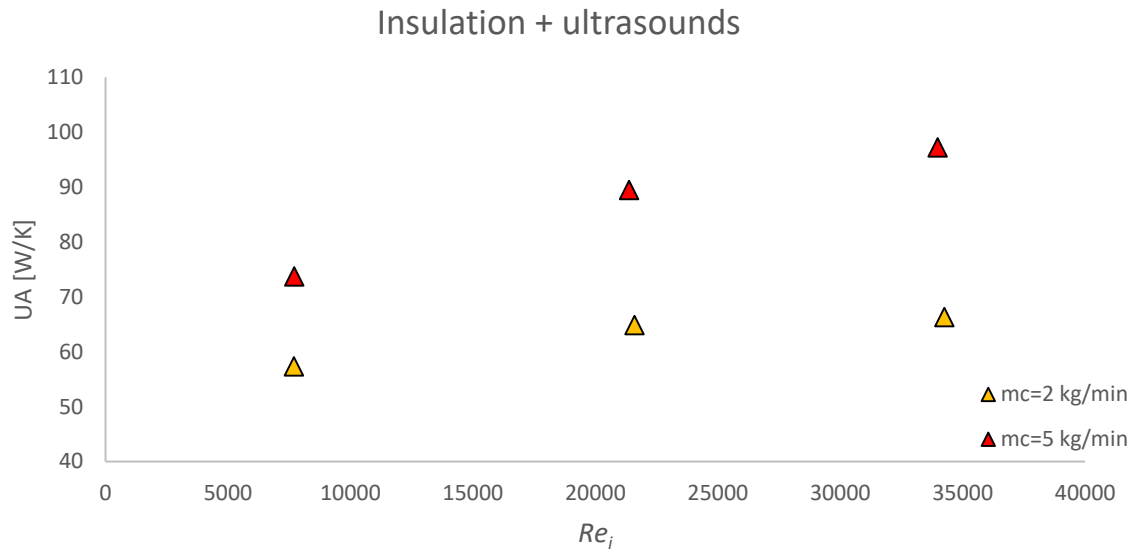


Figure 4.8 – Evolution of the UA with the increase of Re_i for the “ultrasounds” condition with insulation.

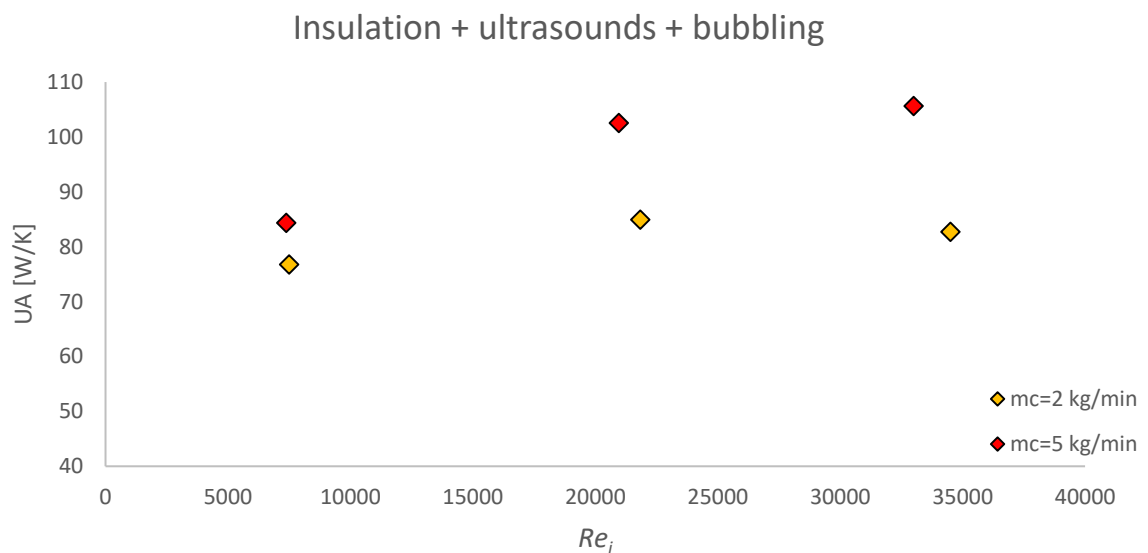


Figure 4.9 – Evolution of the UA with the increase of Re_i for the “ultrasounds, bubbling” condition with insulation.

As expected, if the Reynolds number of the hot fluid increases, consequence of the increase in the flow rate, then the overall heat transfer coefficient generally increases, except for the test point at the highest Re_i and $\dot{m}_c = 2$ kg/min (figure 4.9), which could be due to experimental error. The same is observed with the increase of the cold water flow rate ($\dot{m}_c = 5$ kg/min). The graphics 4.2-4.9 were presented to clearly see the tendency of the evolution of the UA values with the Reynolds number.

Now, figures 4.10 – 4.15 show two different test conditions for comparison.

Preliminary studies on the influence of ultrasounds on the heat transfer rate in a crossflow heat exchanger

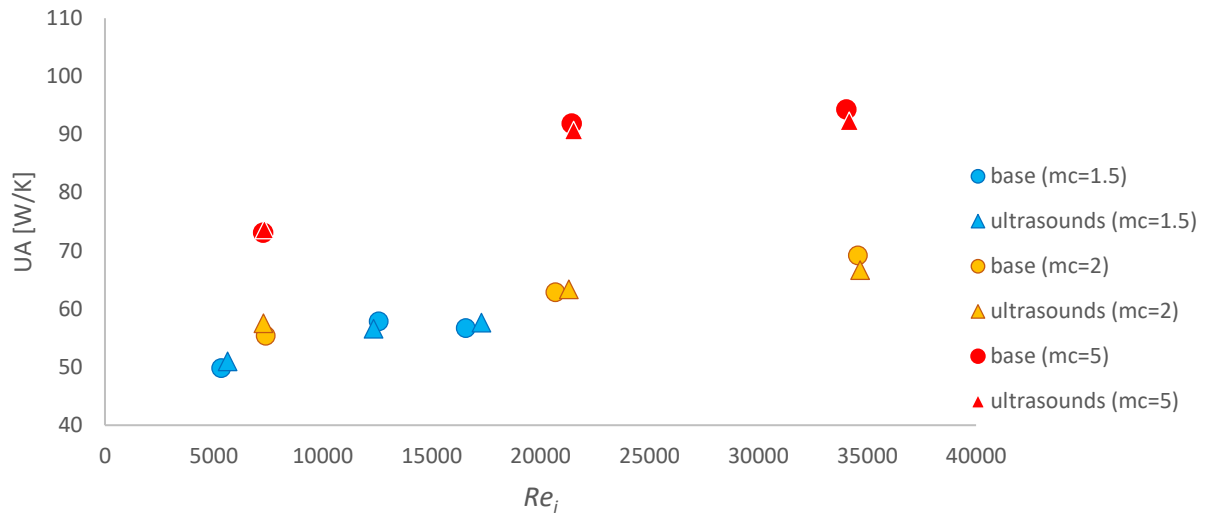


Figure 4.10 – Evolution of the UA with the increase of Re_i : “base” vs “ultrasounds”.

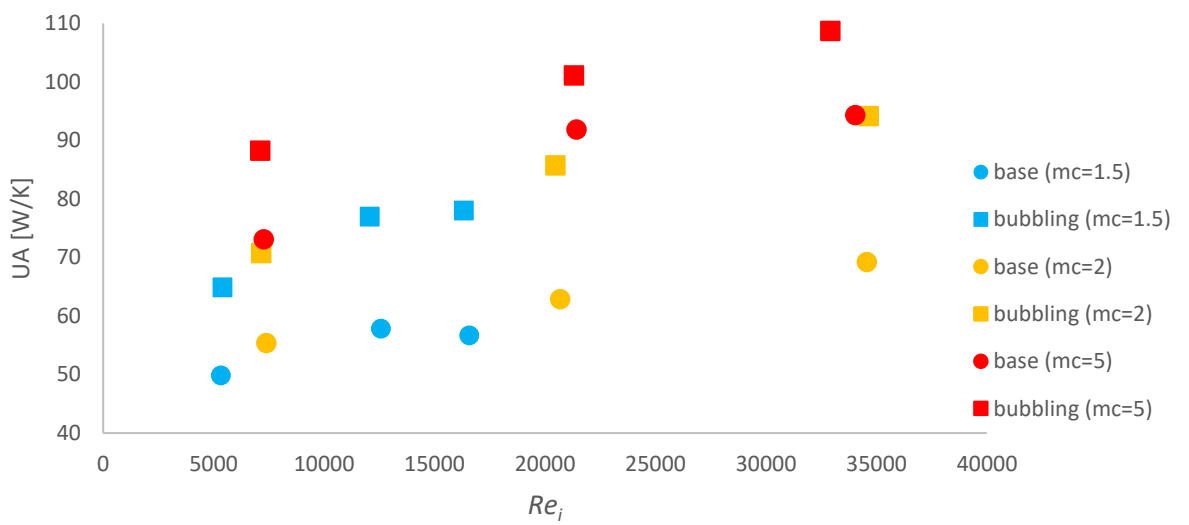


Figure 4.11 – Evolution of the UA with the increase of Re_i : “base” vs “bubbling”.

Preliminary studies on the influence of ultrasounds on the heat transfer rate in a crossflow heat exchanger

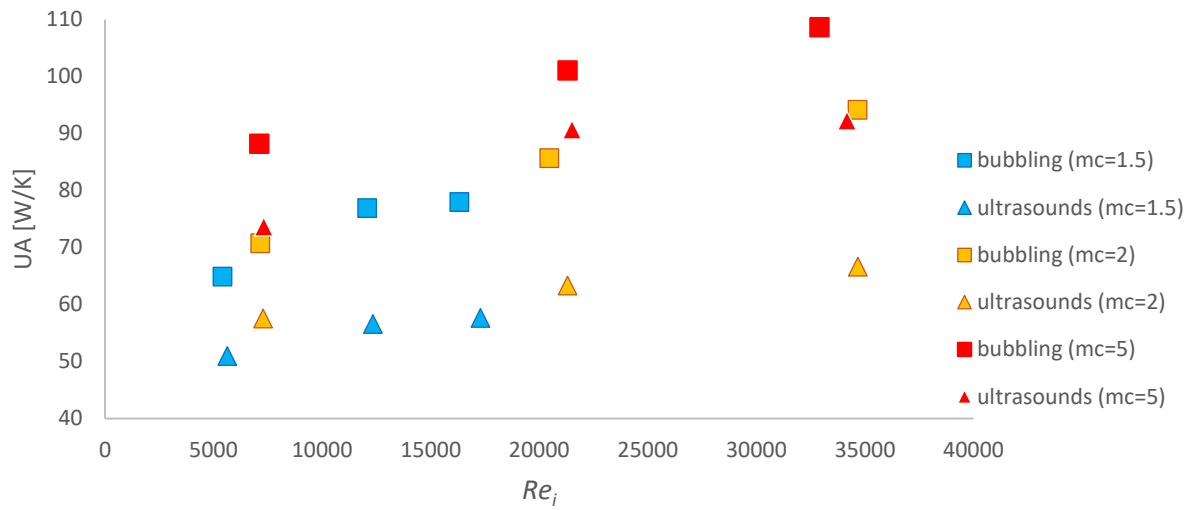


Figure 4.12 – Evolution of the UA with the increase of Re_i : “bubbling” vs “ultrasounds”.

It can be observed through figure 4.10 that the effects of the ultrasounds are negligible, compared with the bubbling effects shown in figure 4.11. Also, for higher flow rates the ultrasounds have no enhancement effect whatsoever. Figure 4.12 shows that the effects of the bubbling surpass the ultrasounds effects for the entire Re_i range.

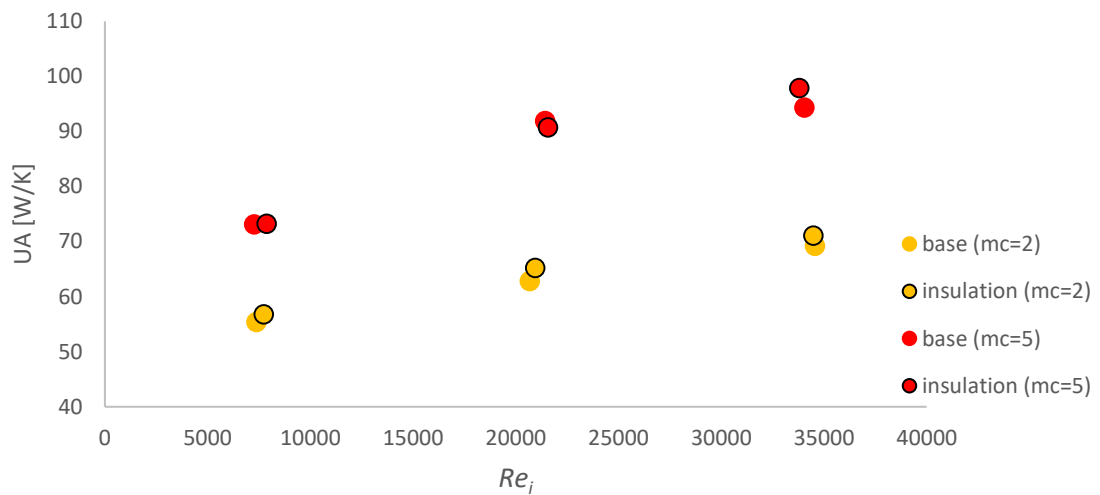


Figure 4.13 – Evolution of the UA with the increase of Re_i : “base” vs “insulation”.

Figure 4.13 shows that the tank insulation does not have a significant effect in the heat transfer rate. The few variations presented are in the experimental error range.

Preliminary studies on the influence of ultrasounds on the heat transfer rate in a crossflow heat exchanger

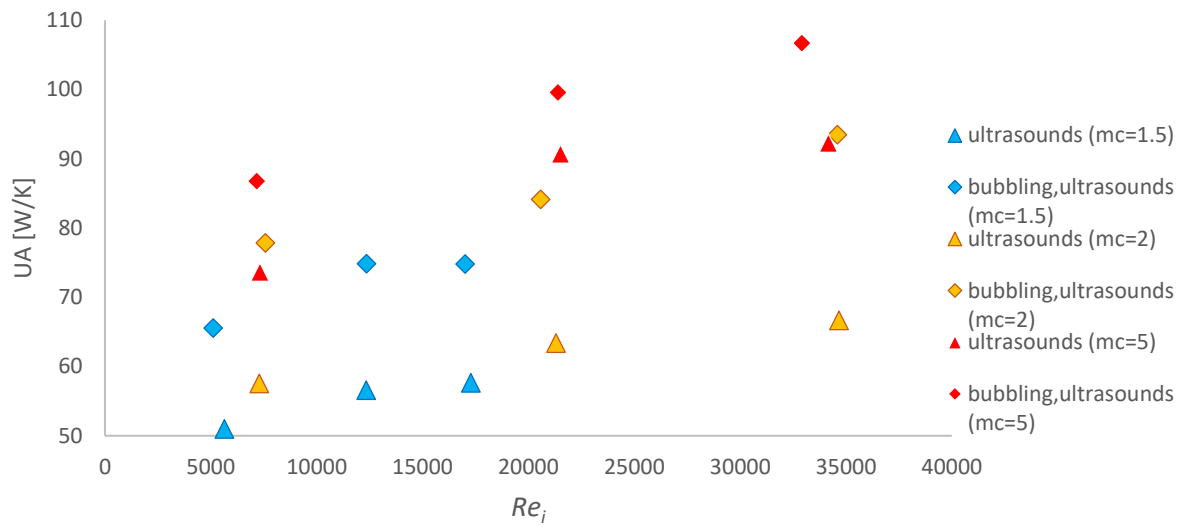


Figure 4.14 – Evolution of the UA with the increase of Re_i : “ultrasounds” vs “ultrasounds, bubbling”.

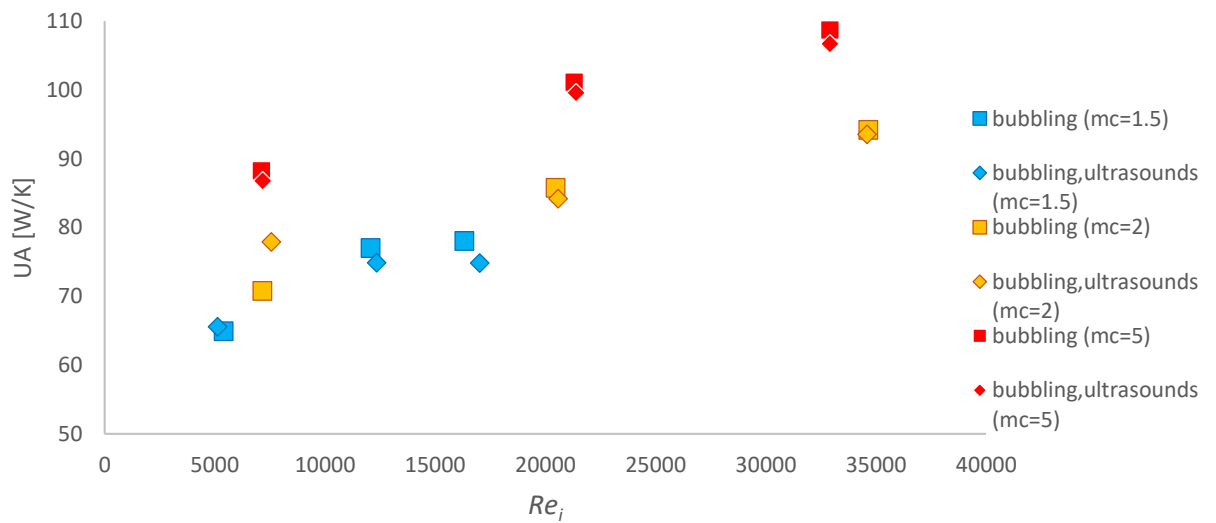


Figure 4.15 – Evolution of the UA with the increase of Re_i : “bubbling” vs “ultrasounds, bubbling”.

Figures 4.14 and 4.15 compare results with both “ultrasounds and bubbling” with the results using ultrasounds or bubbling alone. They show that there is not much difference between the bubbling alone and the bubbling mixed with ultrasounds, as expected due to the previous results. Most times the mixed condition even has lower UA than only the bubbling effect, which is likely due to experimental error.

4.2.3. The convective heat transfer coefficient

The next step to better characterize the effects of both ultrasounds and bubbling was to find both convection heat transfer coefficients h , inside the coil and in the exterior of the coil. The desirable effects of both ultrasounds and bubbling in this heat exchanger were to increase the convection heat transfer coefficient in the exterior of the coil, h_e , so that the heat transfer efficiency also improves. The overall heat transfer coefficient of this type of heat exchanger [1] can be written as in equation 4.15:

$$\frac{1}{UA} = \frac{1}{U_i A_i} = \frac{1}{U_e A_e} = \frac{1}{h_i A_i} + \frac{R_{fi}}{A_i} + R_{w_{cond}} + \frac{R_{fe}}{A_e} + \frac{1}{h_e A_e} \quad (4.15)$$

However, the fouling factor of both inner and outer surface of the coil, R_{fi} and R_{fe} , can be cut off of the equation since the tests are not relatively long, and the experimental setup was brand new, leaving only both the convective heat transfer coefficients, the inner and outer areas of the coil (table 4.3) and the thermal resistance of the coil's wall, $R_{w_{cond}}$, already previously calculated with equation 4.3. Therefore, the right side of the equation 4.15 is left with only three terms. By moving the coil's wall thermal resistance to the left side of the equation, this results in:

$$\frac{1}{UA} - R_{w_{cond}} = \frac{1}{h_i A_{coil.int}} + \frac{1}{h_e A_{coil.ext}} \quad (4.16)$$

In order to find h_i so that it is possible to get to h_e , one turns to the Nusselt number for the inner flow. The Nu in a pipe is defined as shown in equation 4.17, where D_i is the internal diameter of the pipe (coil) inside where the hot fluid flows and k_{hf} is the thermal conductivity of the hot fluid in question. In this case, water.

$$Nu = \frac{h_i D_i}{k_{hf}} \quad (4.17)$$

The water thermal conductivity k_{water} can be determined based on the temperature of the hot water according to the following polynomial, with temperature in °C. By consulting table A2.1 of the form of the lecture course "Transferência de Calor" of MIEM (Mestrado Integrado de Engenharia Mecânica) [23], a trend line was made using a few values of temperature and thermal conductivity, resulting in the polynomial seen in equation 4.18.

$$k_{water} = -1 \times 10^{-5} T_{mh}^2 + 0.0026 T_{mh} + 0.546 \quad (4.18)$$

After that, so that one may obtain the Nusselt number, the correlation of Dittus-Boelter was used [1]. According to this correlation that is shown in equation 4.19, the Nusselt number can be determined by knowing both the Reynolds and Prandtl numbers, if certain conditions are met:

- If the difference in temperature between the fluid and the wall is not very large;
- If $0.7 < Pr < 160$ and $Re_i > 4000$, as fluid properties are evaluated at the hot mean temperature T_{mh} ;
- The flow must be fully developed.

$$Nu = 0.023 Re_i^{0.8} Pr^n \quad (4.19)$$

where $n = 0.4$ for heating and 0.3 for cooling, which is the case.

Even though the Reynolds number is at least 5000 (minimum value for a flow rate of 1.5 kg/min), one must confirm if the turbulent flow inside the coil is fully developed. For that, the length necessary for the fluid flow to be fully developed thermally and dynamically inside a pipe can be determined with the following expression [23]:

$$L_{h,turb} = 1.359Re_i^{0.25}D_i \quad (4.20)$$

Using the tests where the hot fluid flow rate is maximum, for example test point “1.c” where the $\dot{m}_h=8$ kg/min, and the mean number of Reynolds is the biggest, i. e., $Re_i \cong 34500$, then $L_{h,turb}$ is at most 0.1946 m. Since the total length of the coil is 2.825 m, the hydrodynamic entry length is just 6.9 % of the total length, meaning that the Dittus-Boelter correlation is valid to use.

The Prandtl number can be written as the following polynomial, which depends on the hot water mean temperature in °C. Equation 4.21 was obtained by using the same method as the water thermal conductivity in equation 4.18, resorting to [23].

$$Pr = 0.001T_{mh}^2 - 0.1725T_{mh} + 9.56 \quad (4.21)$$

With all this, both the convection heat transfer coefficients can be determined, using equations 4.16 and 4.17. Thus, tables 4.14 – 4.22 show all the resulting values for each test point, presenting the alterations that each test condition imposes in the convective heat transfer coefficients. Note that it’s assumed that the convective heat transfer coefficient of the coil’s inner wall h_i is not affected by the conditions implemented, as it depends on the inner diameter which is constant, the Nusselt number and thermal conductivity of the hot fluid. These last two properties depend on the temperature and flow rate of the hot fluid, making whatever is happening outside the coil irrelevant to the h_i values. So only the convective heat transfer coefficient of the outer wall of the coil h_e were altered according to the conditions implanted in the tests.

Table 4.14 – Reynolds, Prandtl and Nusselt numbers and convective heat transfer coefficients for test point “1.a” ($\dot{m}_c=2$ kg/min; $\dot{m}_h=2$ kg/min)

Test reference	Re_i	Pr	Nu	h_i [W/(m ² .K)]	k_{water} (T)	h_e [W/(m ² .K)]
base	7384	3.581	41.933	2587	0.648	639.029
bubbling	7160	3.755	41.497	2546	0.644	896.932
ultrasounds	7286	3.409	40.879	2537	0.652	676.524
ultrasounds,bubbling	7573	3.527	42.596	2633	0.649	1015.314
insulation	7743	3.307	42.527	2648	0.654	655.390
insulation,bubbling	7888	3.377	43.434	2698	0.652	882.627
insulation,ultrasounds	7690	3.227	41.988	2622	0.656	666.788
insulation,ultrasounds,bubbling	7507	3.382	41.767	2594	0.652	1000.885

Preliminary studies on the influence of ultrasounds on the heat transfer rate in a crossflow heat exchanger

Table 4.15 – Reynolds, Prandtl and Nusselt numbers and convective heat transfer coefficients for test point “1.b”
($\dot{m}_c=2$ kg/min; $\dot{m}_h=5$ kg/min)

Test reference	Re_i	Pr	Nu	h_i [W/(m ² .K)]	k_{water} (T)	h_e [W/(m ² .K)]
base	20687	2.989	90.562	5704	0.661	633.714
bubbling	20466	3.038	90.225	5673	0.660	910.485
ultrasounds	21309	2.982	92.671	5839	0.662	637.707
ultrasounds,bubbling	20589	3.018	90.481	5693	0.661	889.867
insulation	20955	2.920	90.862	5738	0.663	660.630
insulation,bubbling	21088	3.089	92.874	5829	0.659	873.853
insulation,ultrasounds	21604	2.937	93.264	5886	0.663	654.504
insulation,ultrasounds,bubbling	21840	2.921	93.925	5932	0.663	892.883

Table 4.16 – Reynolds, Prandtl and Nusselt numbers and convective heat transfer coefficients for test point “1.c”
($\dot{m}_c=2$ kg/min; $\dot{m}_h=8$ kg/min)

Test reference	Re_i	Pr	Nu	h_i [W/(m ² .K)]	k_{water} (T)	h_e [W/(m ² .K)]
base	34573	2.917	135.581	8564	0.663	673.675
bubbling	34663	2.886	135.432	8564	0.664	950.231
ultrasounds	34683	2.904	135.750	8578	0.664	646.905
ultrasounds,bubbling	34593	2.892	135.289	8554	0.664	942.675
insulation	34489	2.895	135.012	8535	0.664	694.286
insulation,bubbling	34671	2.875	135.300	8560	0.664	910.202
insulation,ultrasounds	34259	2.895	134.285	8489	0.664	643.889
insulation,ultrasounds,bubbling	34502	2.875	134.773	8526	0.664	821.339

Table 4.17 – Reynolds, Prandtl and Nusselt numbers and convective heat transfer coefficients for test point “2.a”
($\dot{m}_c=5$ kg/min; $\dot{m}_h=2$ kg/min)

Test reference	Re_i	Pr	Nu	h_i [W/(m ² .K)]	k_{water} (T)	h_e [W/(m ² .K)]
base	7272	3.528	41.239	2549	0.649	939.838
bubbling	7115	3.696	41.094	2526	0.645	1257.035
ultrasounds	7321	3.541	41.507	2564	0.649	947.848
ultrasounds,bubbling	7177	3.608	41.084	2533	0.647	1222.491
insulation	7882	3.470	43.765	2710	0.650	917.641
insulation,bubbling	7649	3.438	42.610	2642	0.651	1168.993
insulation,ultrasounds	7712	3.464	42.989	2663	0.650	933.664
insulation,ultrasounds,bubbling	7376	3.582	41.904	2585	0.648	1155.437

Preliminary studies on the influence of ultrasounds on the heat transfer rate in a crossflow heat exchanger

Table 4.18 – Reynolds, Prandtl and Nusselt numbers and convective heat transfer coefficients for test point “2.b”
($\dot{m}_c=5$ kg/min; $\dot{m}_h=5$ kg/min)

Test reference	Re_i	Pr	Nu	h_i [W/(m ² .K)]	k_{water} (T)	h_e [W/(m ² .K)]
base	21428	2.972	92.986	5861	0.662	983.128
bubbling	21316	3.019	93.037	5854	0.661	1104.672
ultrasounds	21517	2.961	93.190	5876	0.662	967.475
ultrasounds,bubbling	21398	2.988	93.036	5861	0.661	1084.285
insulation	21574	2.969	93.462	5892	0.662	967.442
insulation,bubbling	21033	3.058	92.399	5805	0.660	1137.722
insulation,ultrasounds	21379	2.970	92.797	5850	0.662	953.246
insulation,ultrasounds,bubbling	20962	3.055	92.124	5789	0.660	1127.111

Table 4.19 – Reynolds, Prandtl and Nusselt numbers and convective heat transfer coefficients for test point “2.c”
($\dot{m}_c=5$ kg/min; $\dot{m}_h=8$ kg/min)

Test reference	Re_i	Pr	Nu	h_i [W/(m ² .K)]	k_{water} (T)	h_e [W/(m ² .K)]
base	34045	2.891	133.566	8445	0.664	953.928
bubbling	32919	3.075	132.448	8316	0.659	1125.606
ultrasounds	34178	2.883	133.876	8467	0.664	930.210
ultrasounds,bubbling	32917	3.031	131.864	8293	0.660	1102.109
insulation	33797	2.968	133.838	8437	0.662	995.239
insulation,bubbling	32807	3.109	132.520	8311	0.658	1132.225
insulation,ultrasounds	33978	2.938	134.001	8457	0.663	987.731
insulation,ultrasounds,bubbling	33009	3.059	132.526	8326	0.660	1088.608

Table 4.20 – Reynolds, Prandtl and Nusselt numbers and convective heat transfer coefficients for test point “3.d”
($\dot{m}_c=1.5$ kg/min; $\dot{m}_h=1.5$ kg/min)

Test reference	Re_i	Pr	Nu	h_i [W/(m ² .K)]	k_{water} (T)	h_e [W/(m ² .K)]
base	5334	3.593	32.361	1996	0.648	605.113
bubbling	5410	3.753	33.158	2034	0.644	878.087
ultrasounds	5637	3.590	33.815	2086	0.648	614.798
ultrasounds,bubbling	5120	3.862	32.001	1956	0.642	910.774

Table 4.21 – Reynolds, Prandtl and Nusselt numbers and convective heat transfer coefficients for test point “3.e”
($\dot{m}_c=1.5$ kg/min; $\dot{m}_h=3$ kg/min)

Test reference	Re_i	Pr	Nu	h_i [W/(m ² .K)]	k_{water} (T)	h_e [W/(m ² .K)]
base	12576	3.005	60.912	3835	0.661	613.704
bubbling	12075	3.191	60.037	3754	0.657	878.041
ultrasounds	12338	3.007	60.004	3777	0.661	599.642
ultrasounds,bubbling	12351	3.096	60.582	3801	0.659	844.373

Table 4.22 – Reynolds, Prandtl and Nusselt numbers and convective heat transfer coefficients for test point “3.f” ($\dot{m}_c=1.5$ kg/min; $\dot{m}_h=4$ kg/min)

Test reference	Re_i	Pr	Nu	h_i [W/(m ² .K)]	k_{water} (T)	h_e [W/(m ² .K)]
base	16572	2.935	75.424	4761	0.663	577.916
bubbling	16332	3.066	75.534	4744	0.660	842.750
ultrasounds	17294	2.916	77.892	4920	0.663	586.332
ultrasounds,bubbling	17017	2.958	77.218	4870	0.662	796.980

At last, to confirm if either ultrasounds, bubbling or the mix of them give out any advantage to that heat transfer rate, an enhancement factor α is calculated by using the following expression,

$$\alpha = \frac{h'_e}{h_e} \quad (4.22)$$

where h'_e is the convection heat transfer coefficient for when any of the new conditions are applied and h_e is for the standard testing (base, insulation). These factors are presented in tables 4.23 – 4.31 for each test point, showing the heat transfer enhancement that the test conditions provoked in every test point. Even though a comparison is made between the experiments with and without test conditions, the experiments were not exactly equal between them, with a few discrepancies like mass flow rate or inlet temperatures. Therefore, variations under 10% could be discarded as irrelevant.

Table 4.23 – Enhancement factors obtained in point “1.a” ($\dot{m}_c=2$ kg/min; $\dot{m}_h=2$ kg/min)

	h_e	h'_e (ultrasounds)	h'_e (bubbling)	h'_e (ultrasounds,bubbling)
No insulation	639.029	676.524	896.932	1015.314
α	-	1.059	1.404	1.589
W/ insulation	655.390	666.788	882.627	1000.885
α	-	1.017	1.347	1.527

Table 4.24 – Enhancement factors obtained in point “1.b” ($\dot{m}_c=2$ kg/min; $\dot{m}_h=5$ kg/min)

	h_e	h'_e (ultrasounds)	h'_e (bubbling)	h'_e (ultrasounds,bubbling)
No insulation	633.714	637.707	910.485	889.867
α	-	1.006	1.437	1.404
W/ insulation	660.630	654.504	873.853	892.883
α	-	0.991	1.323	1.352

Table 4.25 – Enhancement factors obtained in point “1.c” ($\dot{m}_c=2$ kg/min; $\dot{m}_h=8$ kg/min)

	h_e	h'_e (ultrasounds)	h'_e (bubbling)	h'_e (ultrasounds,bubbling)
No insulation	673.675	646.905	950.231	942.675
α	-	0.960	1.411	1.399
W/ insulation	694.286	643.889	910.202	821.339
α	-	0.927	1.311	1.183

Preliminary studies on the influence of ultrasounds on the heat transfer rate in a crossflow heat exchanger

Table 4.26 – Enhancement factors obtained in point “2.a” ($\dot{m}_c=5$ kg/min; $\dot{m}_h=2$ kg/min)

	h_e	$h'_e(\text{ultrasounds})$	$h'_e(\text{bubbling})$	$h'_e(\text{ultrasounds,bubbling})$
No insulation	939.838	947.848	1257.035	1222.491
α	-	1.009	1.338	1.301
W/ insulation	917.641	933.664	1168.993	1155.437
α	-	1.017	1.274	1.259

Table 4.27 – Enhancement factors obtained in point “2.b” ($\dot{m}_c=5$ kg/min; $\dot{m}_h=5$ kg/min)

	h_e	$h'_e(\text{ultrasounds})$	$h'_e(\text{bubbling})$	$h'_e(\text{ultrasounds,bubbling})$
No insulation	983.128	967.475	1104.672	1084.285
α	-	0.984	1.124	1.103
W/ insulation	967.442	953.246	1137.722	1127.111
α	-	0.985	1.176	1.165

Table 4.28 – Enhancement factors obtained in point “2.c” ($\dot{m}_c=5$ kg/min; $\dot{m}_h=8$ kg/min)

	h_e	$h'_e(\text{ultrasounds})$	$h'_e(\text{bubbling})$	$h'_e(\text{ultrasounds,bubbling})$
No insulation	953.928	930.210	1125.606	1102.109
α	-	0.975	1.180	1.155
W/ insulation	995.239	987.731	1132.225	1088.608
α	-	0.992	1.138	1.094

Table 4.29 – Enhancement factors obtained in point “3.d” ($\dot{m}_c=1.5$ kg/min; $\dot{m}_h=1.5$ kg/min)

	h_e	$h'_e(\text{ultrasounds})$	$h'_e(\text{bubbling})$	$h'_e(\text{ultrasounds,bubbling})$
No insulation	605.113	614.798	878.087	910.774
α	-	1.016	1.451	1.505

Table 4.30 – Enhancement factors obtained in point “3.e” ($\dot{m}_c=1.5$ kg/min; $\dot{m}_h=3$ kg/min)

	h_e	$h'_e(\text{ultrasounds})$	$h'_e(\text{bubbling})$	$h'_e(\text{ultrasounds,bubbling})$
No insulation	613.704	599.642	878.041	844.373
α	-	0.977	1.431	1.376

Table 4.31 – Enhancement factors obtained in point “3.f” ($\dot{m}_c=1.5$ kg/min; $\dot{m}_h=4$ kg/min)

	h_e	$h'_e(\text{ultrasounds})$	$h'_e(\text{bubbling})$	$h'_e(\text{ultrasounds,bubbling})$
No insulation	577.916	586.332	842.750	796.980
α	-	1.015	1.458	1.378

For every point, the α is bigger for the bubbling effect than for the ultrasound effect. And sometimes the ultrasounds do not have any notable influence in the convection heat

Preliminary studies on the influence of ultrasounds on the heat transfer rate in a crossflow heat exchanger

transfer coefficient, making the mixed condition “ultrasounds, bubbling” basically the same as the bubbling alone. To understand the influence of the mass flow rate of both hot and cold fluids, figures 4.16 and 4.17 are presented.

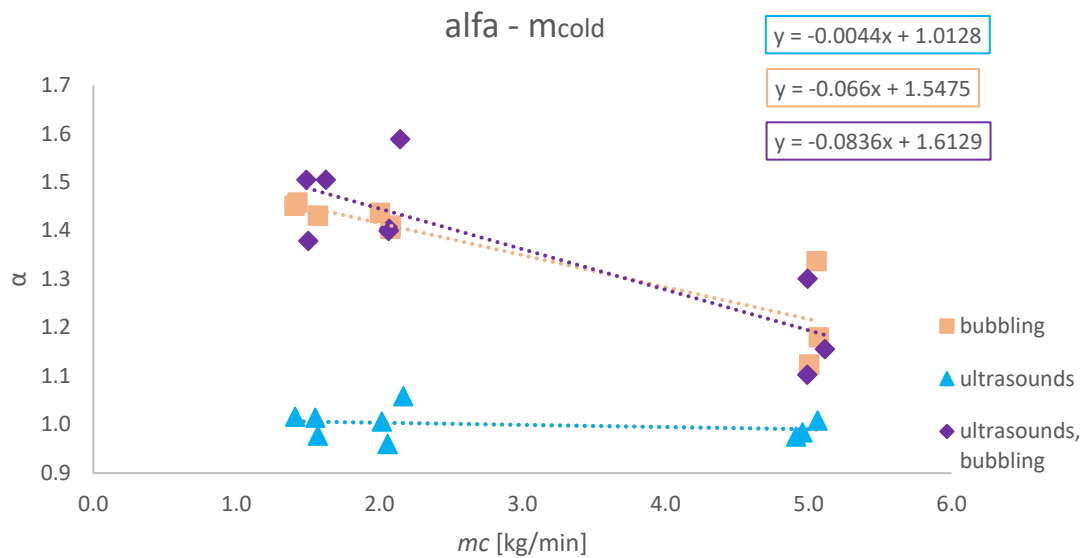


Figure 4.16 – Evolution of the enhancement factor with the increase in cold water mass flow rate.

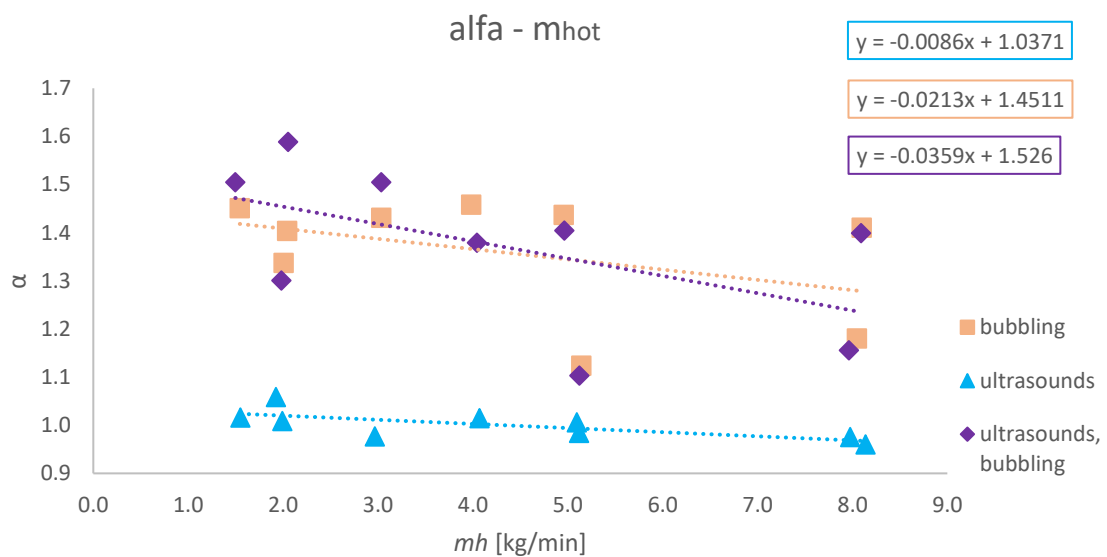


Figure 4.17 – Evolution of the enhancement factor with the increase in hot water mass flow rate.

In figures 4.16 and 4.17 a trend-line was drawn for each condition. The equations of each trend-line are presented in their respective figure and inside a box of their respective color. The trend-lines were presented as an indication to confirm the overall tendency that each test condition had with the increase of the cold fluid mass flow rate, figure 4.16, or the increase of hot fluid mass flow rate, figure 4.17.

For the “ultrasounds” condition, the slope, even though negative for both figures, is not very significant, remaining almost unchanged for the entire mass flow rate range.

As for the “bubbling” and “ultrasounds, bubbling” conditions, the slopes are negative in both figures, meaning that with increase of the fluids mass flow rates, there is less enhancement. The slopes of figure 4.16 are even steeper, which means the cold fluid mass flow rate has more impact in the heat transfer enhancement for the “bubbling” and “ultrasounds, bubbling” conditions.

It was then concluded that the “bubbling” and “ultrasounds, bubbling” conditions provided bigger heat transfer enhancements for lower mass flow rates, both cold and hot fluids. The “ultrasounds” condition did not have much impact in the heat transfer rate for any test.

4.3. Tests with water II

4.3.1. Influence of the cold water entrance position

In the previous tests the entrance position of the cold water was down below in the tank, basically in front of the coil, figure 4.18 – A, and the cold water exit. This meant that the inlet cold water rapidly contacted with the hot water inside the heat exchanger tank, facilitating the heat transfer. The tests shown in this section were performed to understand how the cold water entry point influenced the results.

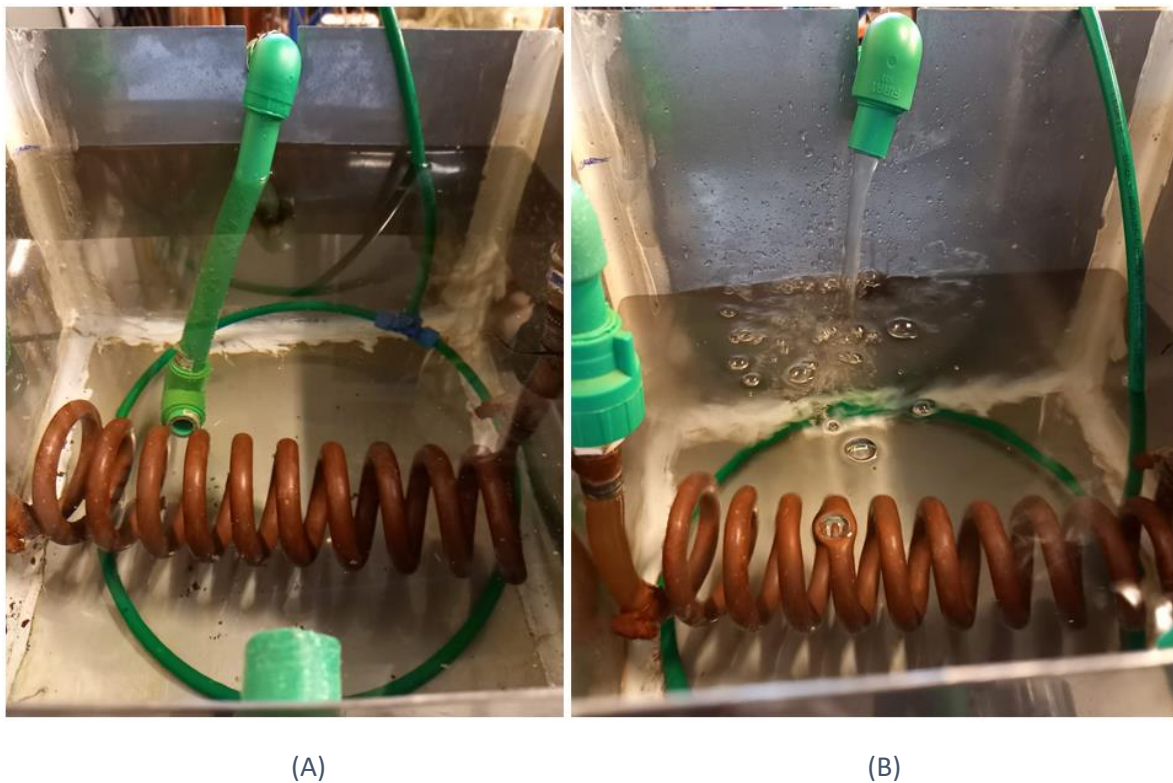


Figure 4.18 – Different cold water entry positions. A – Below; B – Top.

A few tests were made for the “base” and “bubbling” conditions where the entrance position of the cold water was moved to the top of the tank, figure 4.18 – B. In this position, when the tank is full, the cold water is not introduced underwater but instead above, creating a little natural bubbling at the surface of the water. The tests done with the new position were repetitions of tests points already made, from point “1.a” to “2.c”, but only for the “base” and “bubbling” conditions, with the mass flow rates already discussed.

Preliminary studies on the influence of ultrasounds on the heat transfer rate in a crossflow heat exchanger

In order to calculate the overall heat transfer coefficient and Reynolds number, the same methods as described in previous section were used. The parameters R , P and F were obtained the same way as previously.

In tables 4.32 and 4.33, the overall heat transfer coefficient and the Reynolds number are displayed for “base” and “bubbling” conditions respectively.

Table 4.32 - UA and Re_i for each test point in “base” condition for the new entry point.

Base	UA [W/K]	Re_i
R1.a	54.56	8263
R1.b	68.00	21563
R1.c	72.38	34847
R2.a	64.30	7563
R2.b	81.27	21656
R2.c	85.42	34226

Table 4.33 - UA and Re_i for each test point in “bubbling” condition for the new entry point.

Bubbling	UA [W/K]	Re_i
R1.a	72.50	7534
R1.b	84.59	20853
R1.c	91.48	34684
R2.a	79.82	7752
R2.b	97.61	21090
R2.c	101.42	33819

Figures 4.19 and 4.20 show the comparison between the previous results, obtained when the cold water entry point was “below” (underwater), and the current results obtained with the entry point placed at the “top”.

Preliminary studies on the influence of ultrasounds on the heat transfer rate in a crossflow heat exchanger

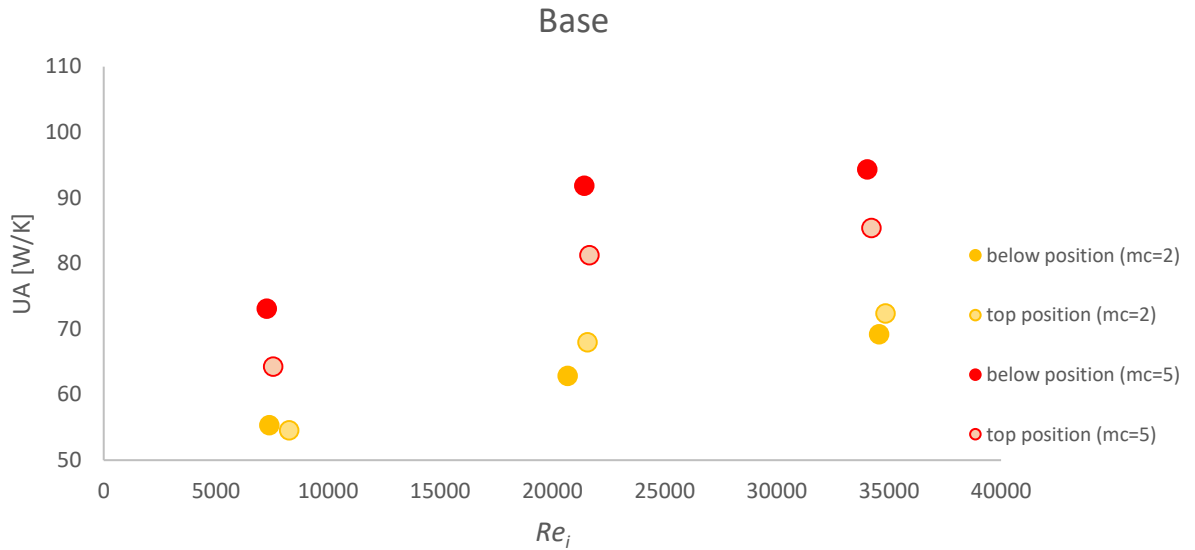


Figure 4.19 - Evolution of the UA with the increase of Re_i in “base” condition: “below” vs “top” position of the cold water entrance.

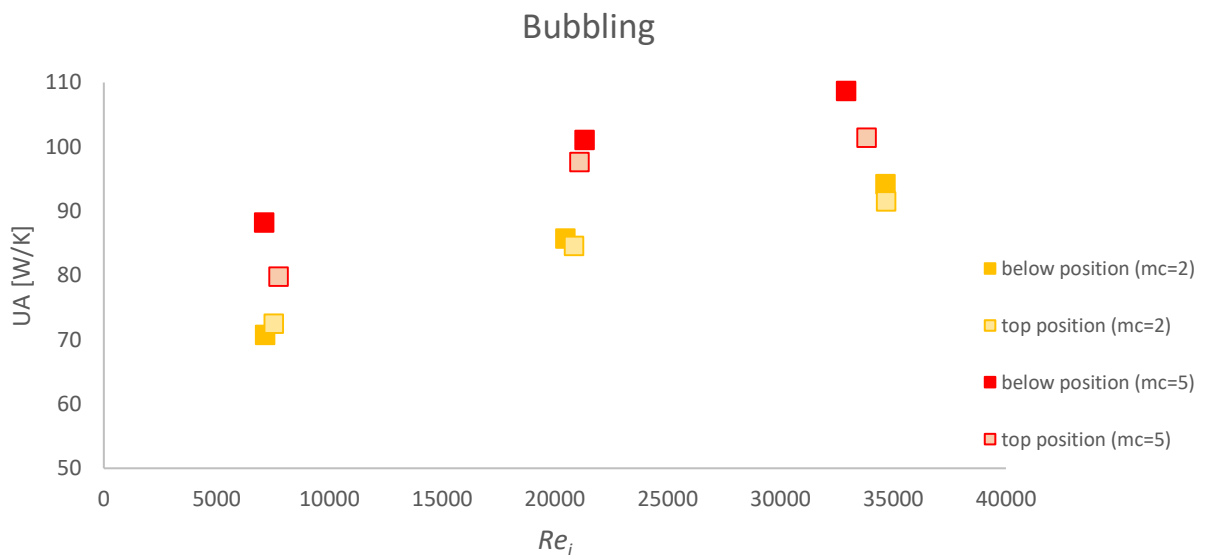


Figure 4.20 - Evolution of the UA with the increase of Re_i in “bubbling” condition: “below” vs “top” position of the cold water entrance.

Analyzing figure 4.19, for higher cold water mass flow rate ($\dot{m}_c = 5 \text{ kg/min}$) the difference between the overall heat transfer coefficient of the original tests (top) and the new ones (below) is noticeably higher than for the lower cold mass flow rate ($\dot{m}_c = 2 \text{ kg/min}$). This means that the influence of the cold water entry point is clearer at higher cold water flow rates and according to figure 4.19, that influence is that the overall heat transfer coefficient decreases because the entrance point of the cold water is now at the top of the tank. For the tests with $\dot{m}_c = 2 \text{ kg/min}$, the disparity between the original and new tests is small, with no clear tendency, and can be justified by experimental errors.

Looking at figure 4.20, there is still the tendency of the UA values of the top entry point tests being slightly lower than the ones for the bottom point of entry for $\dot{m}_c = 5 \text{ kg/min}$. However,

Preliminary studies on the influence of ultrasounds on the heat transfer rate in a crossflow heat exchanger

this difference between the tests with different entrance positions is less significant than the one observed in figure 4.19. This could be due to the dynamic effect that the bubbling introduces. By causing a huge turmoil within the volume of cold water, this agitation reduces whatever influence the cold-water entrance position has. As for the tests with $\dot{m}_c = 2 \text{ kg/min}$, once again no definite conclusion can be made.

Preliminary studies on the influence of ultrasounds on the heat transfer rate in a crossflow heat exchanger

5. Tests with LiBr solution

The hot fluid was subsequently changed to an aqueous LiBr solution and another set of heat transfer experiments was carried out, still using water as the cold fluid.

Before starting the tests, it was necessary to properly calibrate the flow meter C_2 for the LiBr solution, because its physical properties are different from those of water, mainly the density. Therefore, the calibration process done is explained in Appendix E.

5.1. Tests conditions

5.1.1. Mass flow rates

With the purpose of comparing the results of the lithium bromide solution with the water test results already done, the mass flow rates planned were to copy the ones used in the tests made with water. Only some test points were copied, which were the test points with the lowest mass flow rates for both cold and hot water. The reason is because looking at the results of the tests with water, for the lowest mass flow rates, the ultrasounds seemed to have a bit more effect than for higher mass flow rates, so this was a way to confirm it.

Thus, for the cold fluid mass flow rates devised, it was chosen $\dot{m}_c = 1.5$ kg/min and $\dot{m}_c = 2$ kg/min, the lowest values of those used in the water tests. As for the hot fluid mass flow rates, the values $\dot{m}_h = 2$ kg/min, $\dot{m}_h = 5$ kg/min, $\dot{m}_h = 1.5$ kg/min and $\dot{m}_h = 3$ kg/min were picked, with the aim of copying the test points “1.a”, “1.b”, “3.d” and “3.e”. So, new test points for the LiBr solution experiments were made as shown in table 5.1.

Table 5.1 – Test points for the LiBr experiments

Water test points		LiBr test points	Mass flow rates
“1.a”	⇒	“11.a”	$\dot{m}_c = 2$ kg/min; $\dot{m}_h = 2$ kg/min
“1.b”	⇒	“11.b”	$\dot{m}_c = 2$ kg/min; $\dot{m}_h = 5$ kg/min
“3.d”	⇒	“13.d”	$\dot{m}_c = 1.5$ kg/min; $\dot{m}_h = 1.5$ kg/min
“3.e”	⇒	“13.e”	$\dot{m}_c = 1.5$ kg/min; $\dot{m}_h = 3$ kg/min

5.1.2. Test variables

Once again, the variable conditions used for the experiments were the base condition, ultrasound, bubbling and the mix of ultrasound with bubbling. The tank insulation changes was not used as it was already concluded that it did not markedly contribute to the heat transfer enhancement.

Like the tests with water, the main objective here was to study the heat transfer enhancement that the conditions implemented have on the overall heat transfer coefficient. The results will be compared with ones obtained in the water only tests.

5.2. Data analysis

The duration of each test was again from 5 to 10 minutes, and the measured values derived from the “DASYLab” software had their average calculated and used in the data analysis.

5.2.1. The variation of UA with the test conditions

Just as with the tests with water, the path to find the overall heat transfer coefficient involves calculating the logarithmic mean temperature through equations 4.4 - 4.6. Also, the parameters R and P are obtained by resorting to equations 4.7 and 4.8, so then the correction factor is obtained by consulting figure 4.1. Finally the UA is calculated with equation 4.10, using the calorific power Q of the LiBr solution. The tables where these values can be observed are in Appendix D.

Once more, the Reynolds number was calculated, using equation 4.11 with the LiBr properties for the mean hot temperature. The D_i is still the same, as it is the same installation and both μ and ρ of the LiBr solution were calculated in Appendix F for various temperatures. The velocity was calculated with equation 4.14. Tables 5.2 – 5.7 present the obtained Reynolds and other properties for all the test points. Tables 5.6 and 5.7 show the values of the test points “11.z” that were later added, as explained further in chapter 5.2.2.

Table 5.2 - Reynolds and other properties of test point “11.a” ($\dot{m}_c=2$ kg/min; $\dot{m}_h=2$ kg/min)

Test reference	UA [W/K]	μ [N.s/m ²]	ρ [kg/m ³]	v [m/s]	Re_i
base	35.12	0.003155	1605.5907	0.247	1320
bubbling	48.30	0.003304	1607.0818	0.246	1254
ultrasounds	34.39	0.003142	1605.4576	0.245	1312
ultrasounds,bubbling	46.62	0.003311	1607.1523	0.237	1206

Table 5.3 - Reynolds and other properties of test point “11.b” ($\dot{m}_c=2$ kg/min; $\dot{m}_h=5$ kg/min)

Test reference	UA [W/K]	μ [N.s/m ²]	ρ [kg/m ³]	v [m/s]	Re_i
base	45.70	0.002735	1601.3741	0.606	3722
bubbling	70.76	0.002822	1602.2411	0.609	3628
ultrasounds	45.84	0.002740	1601.4208	0.601	3688
ultrasounds,bubbling	68.84	0.002825	1602.2750	0.589	3507

Table 5.4 - Reynolds and other properties of test point “13.d” ($\dot{m}_c=1.5$ kg/min; $\dot{m}_h=1.5$ kg/min)

Test reference	UA [W/K]	μ [N.s/m ²]	ρ [kg/m ³]	v [m/s]	Re_i
base	28.51	0.003322	1607.2636	0.186	944
bubbling	40.28	0.003492	1608.9743	0.190	917
ultrasounds	28.38	0.003388	1607.9328	0.185	921
ultrasounds,bubbling	39.66	0.003523	1609.2899	0.186	893

Preliminary studies on the influence of ultrasounds on the heat transfer rate in a crossflow heat exchanger

Table 5.5 - Reynolds and other properties of test point "13.e" ($\dot{m}_c=1.5$ kg/min; $\dot{m}_h=3$ kg/min)

Test reference	UA [W/K]	μ [N.s/m ²]	ρ [kg/m ³]	v [m/s]	Re_i
base	37.16	0.002820	1602.2256	0.354	2113
bubbling	53.84	0.002920	1603.2261	0.358	2062
ultrasounds	37.41	0.002810	1602.1226	0.369	2212
ultrasounds,bubbling	54.65	0.002919	1603.2154	0.364	2097

Table 5.6 - Reynolds and other properties of test point "11.z (10)" ($\dot{m}_c=2$ kg/min; $\dot{m}_h=10$ kg/min)

Test reference	UA [W/K]	μ [N.s/m ²]	ρ [kg/m ³]	v [m/s]	Re_i
base	58.04	0.002683	1600.8445	1.193	7475
bubbling	93.80	0.002753	1601.5464	1.214	7417

Table 5.7 - Reynolds and other properties of test point "11.z (12.5)" ($\dot{m}_c=2$ kg/min; $\dot{m}_h=12.5$ kg/min)

Test reference	UA [W/K]	μ [N.s/m ²]	ρ [kg/m ³]	v [m/s]	Re_i
base	59.83	0.002656	1600.5794	1.502	9501
bubbling	98.02	0.002738	1601.4026	1.507	9251

Figures 5.1 – 5.4 show the evolution of the UA with the increase in the Reynolds number of the inner fluid (LiBr solution) for the various test conditions.

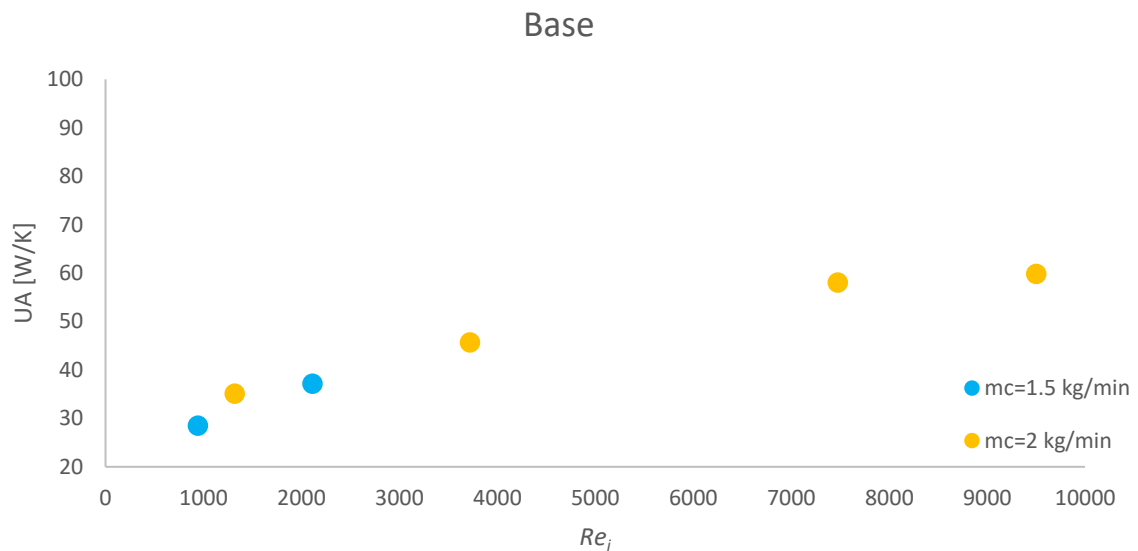


Figure 5.1 - Evolution of the UA with the increase of Re_i for the "base" condition.

Preliminary studies on the influence of ultrasounds on the heat transfer rate in a crossflow heat exchanger

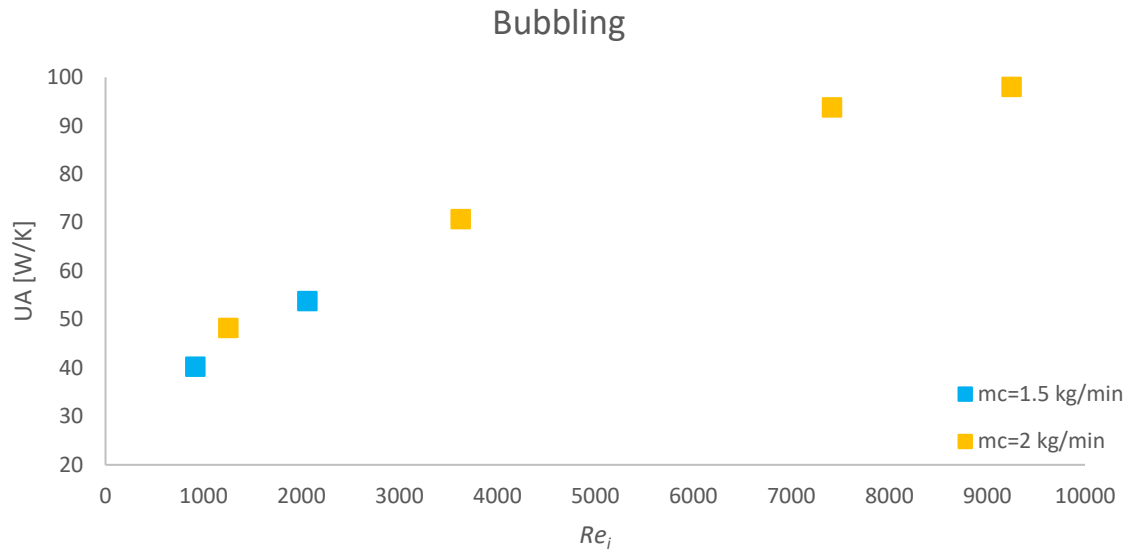


Figure 5.2 - Evolution of the UA with the increase of Re_i for the “bubbling” condition.

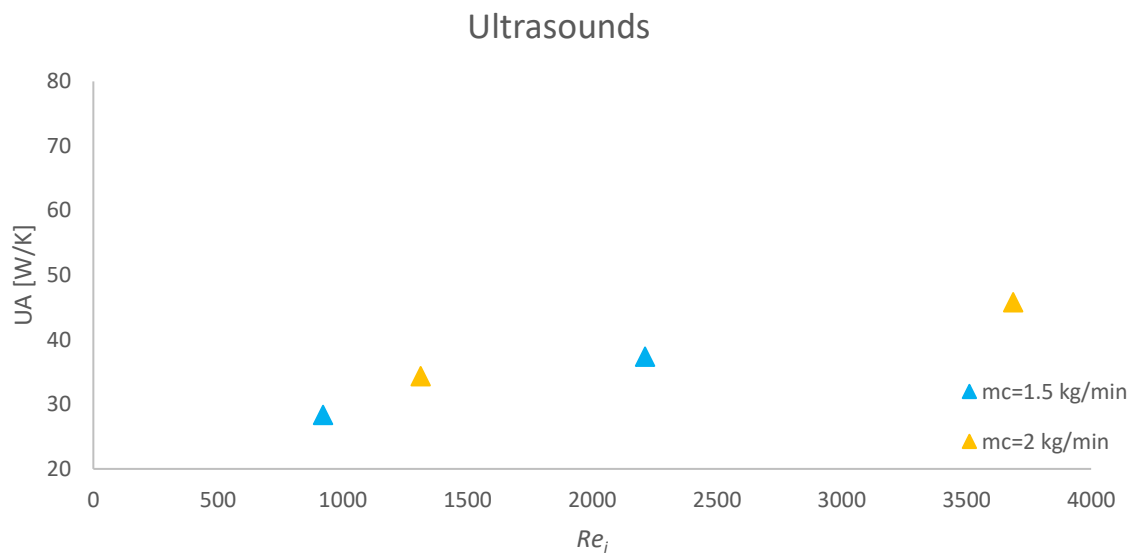


Figure 5.3 - Evolution of the UA with the increase of Re_i for the “ultrasounds” condition.

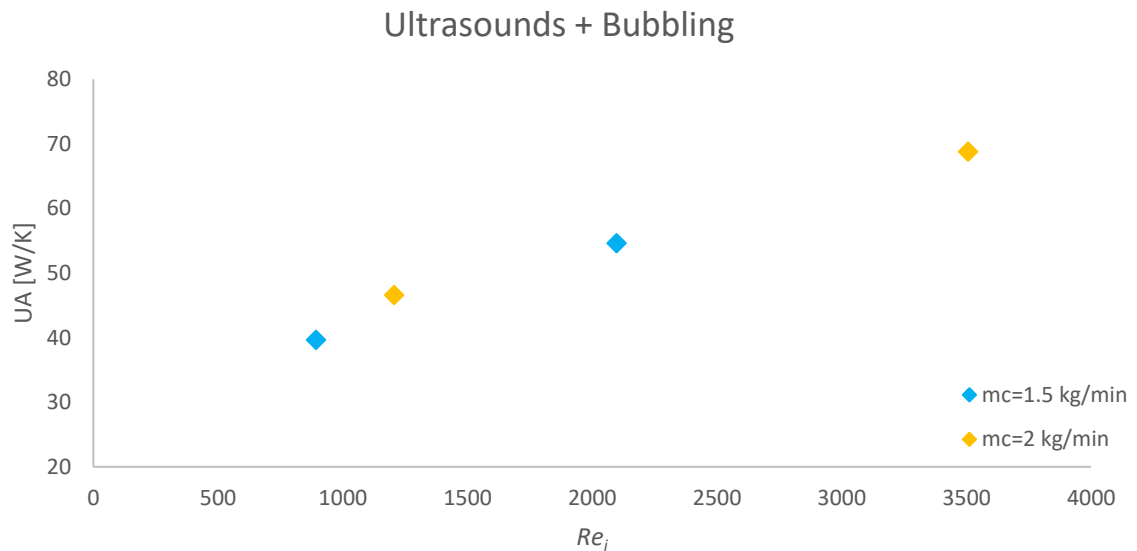


Figure 5.4 - Evolution of the UA with the increase of Re_i for the "ultrasounds, bubbling" condition.

Once again, it is shown that with the increase of the LiBr solution (hot fluid) mass flow rate, thus higher Re_i , raises the overall heat transfer coefficient values, for any given test conditions. For bigger cold water mass flow rate, the UA values should also be higher, but since the values of the cold water mass flow rate tests are very close ($\dot{m}_c = 1.5$ kg/min and $\dot{m}_c = 2$ kg/min), that tendency is not that noticeable.

Now, figures 5.5 – 5.8 will show how the test conditions compare with each other.

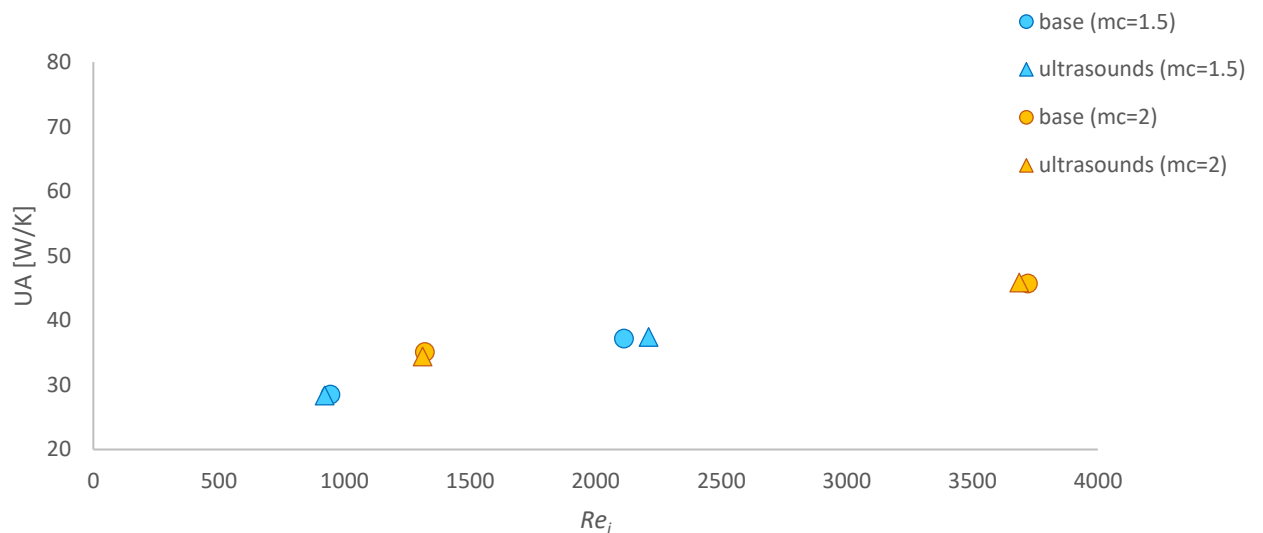


Figure 5.5 - Evolution of the UA with the increase of Re_i : "base" vs "ultrasounds".

Preliminary studies on the influence of ultrasounds on the heat transfer rate in a crossflow heat exchanger

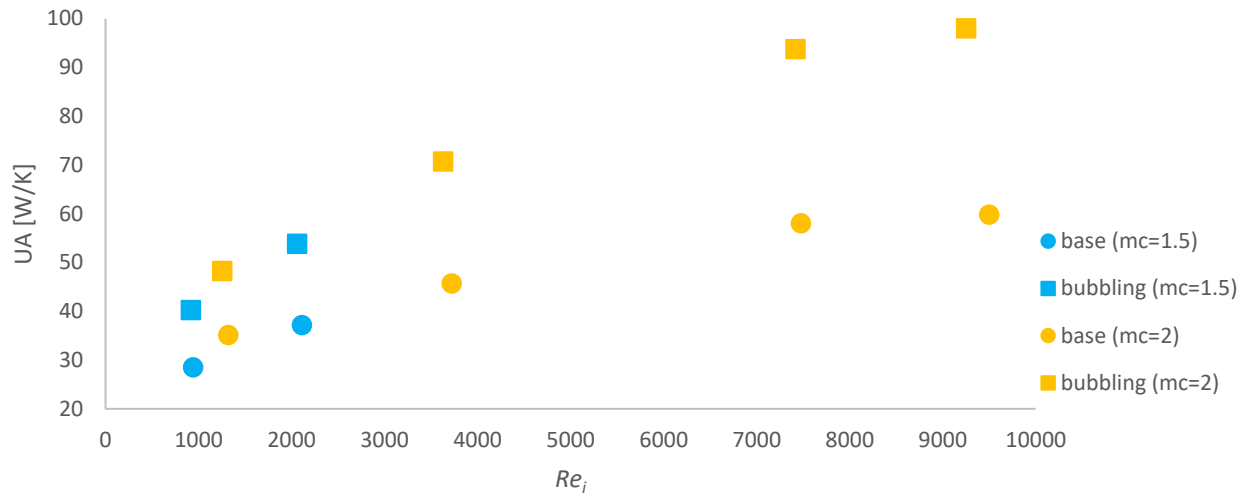


Figure 5.6 - Evolution of the UA with the increase of Re_i : "base" vs "bubbling".

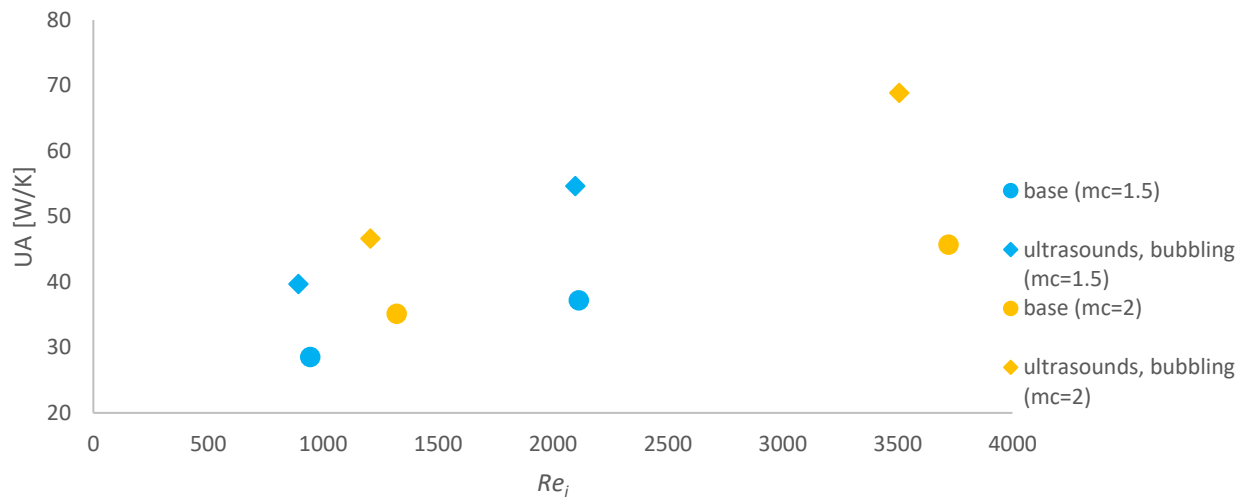


Figure 5.7 - Evolution of the UA with the increase of Re_i : "base" vs "ultrasounds, bubbling".

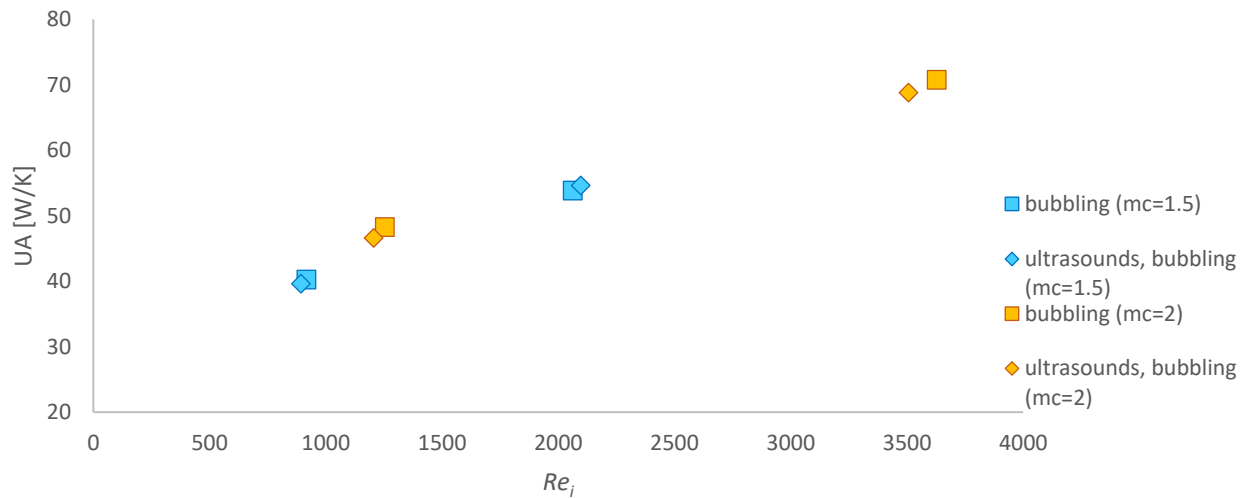


Figure 5.8 - Evolution of the UA with the increase of Re_i : “bubbling” vs “ultrasounds, bubbling”.

After analyzing figure 5.5, it can be concluded that the ultrasounds do not have any effect on the heat transfer rate. It can be verified with figure 5.8, where the “bubbling” and “ultrasounds, bubbling” conditions have identical results, hence the similarity between figure 5.6 and 5.7.

As for the “bubbling” condition, figure 5.6 displays that the bubbling has a significant positive effect on the overall heat transfer coefficient, just as seen with the tests with water only.

5.2.2. Comparison of the LiBr tests with the water tests

In order to see how the LiBr solution matches with water in terms of heat transfer rate, figures 5.9 – 5.12 present the evolution of the UA values with the Reynolds of both hot fluids. As said previously in this chapter, the aim of the picked mass flow rates of the LiBr solution tests was to copy the ones from the tests with water. Therefore, the water tests points used to compare with the LiBr solution are those that were used as reference: “1.a”; “1.b”; “3.d”; “3.e”.

Because the physical properties of the LiBr solution are very different from the water properties, the same mass flow rate of both fluids translates into different Reynolds numbers. So, by need, two more test points were created, where the $\dot{m}_h = 10$ kg/min and $\dot{m}_h = 12.5$ kg/min. The cold water mass flow rate is 2 kg/min, just like with points “11.a” and “11.b”. For these new test points “11.z”, only the base condition and bubbling conditions were tested, as it was already confirmed that the ultrasounds have no effect on the heat transfer rate.

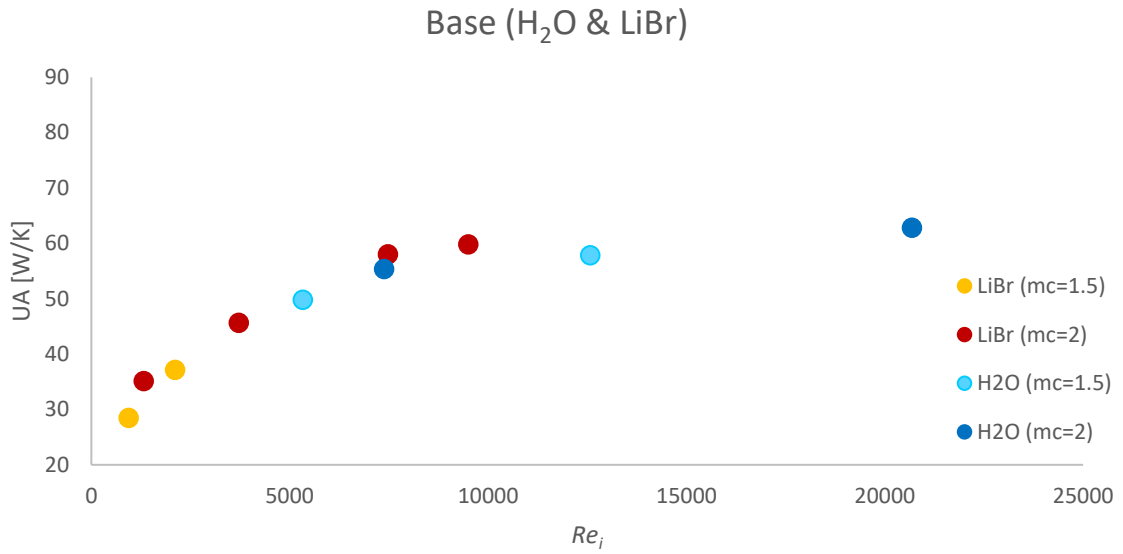


Figure 5.9 - Evolution of the UA with the increase of Re_i in "base" condition: "water" vs "LiBr".

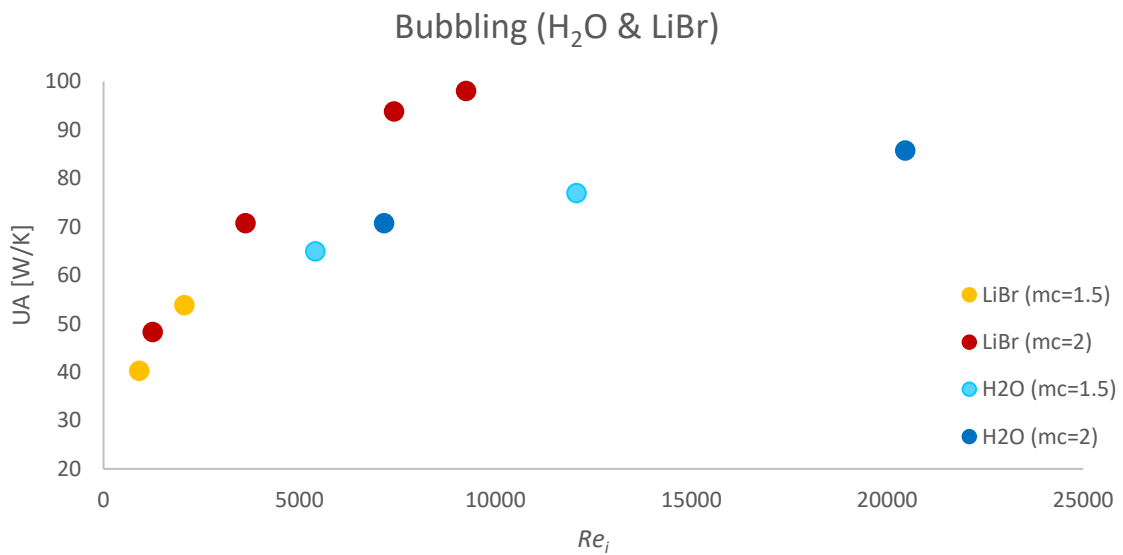


Figure 5.10 - Evolution of the UA with the increase of Re_i in "bubbling" condition: "water" vs "LiBr".

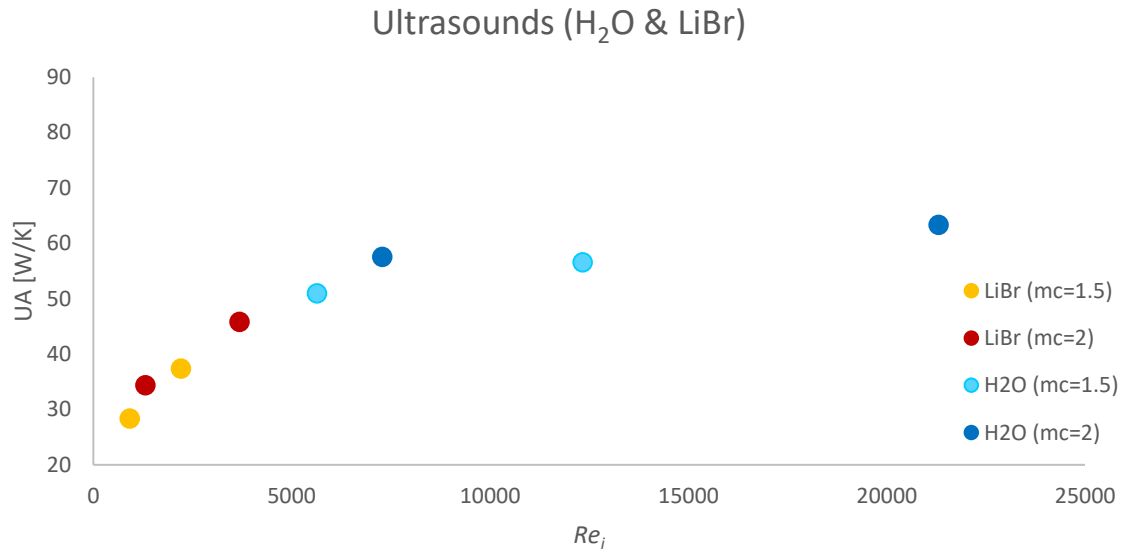


Figure 5.11 - Evolution of the UA with the increase of Re_i in “ultrasounds” condition: “water” vs “LiBr”.

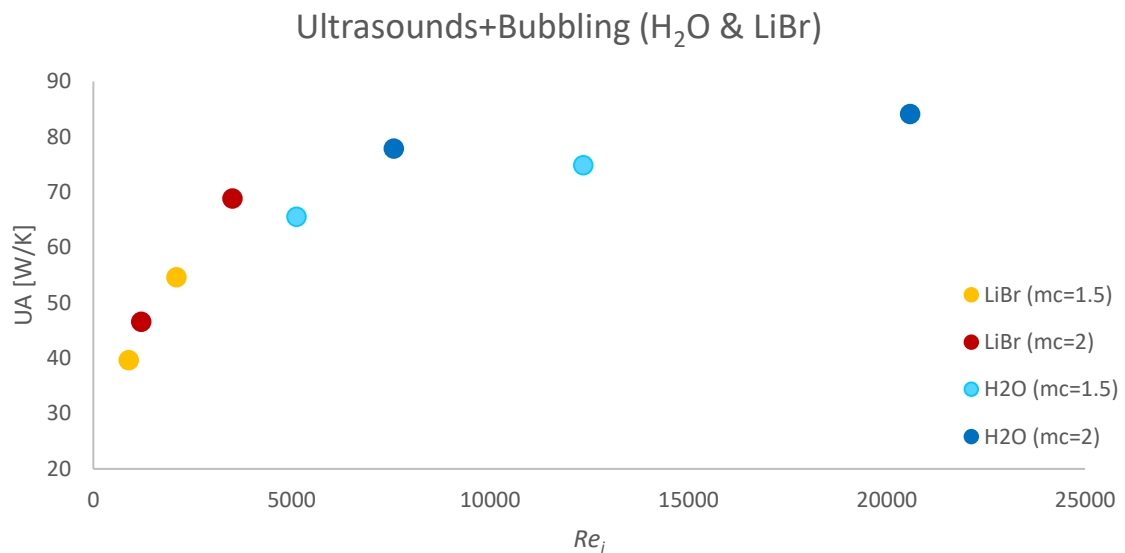


Figure 5.12 - Evolution of the UA with the increase of Re_i in “ultrasounds + bubbling” condition: “water” vs “LiBr”.

For the same mass flow rates the difference between the Re_i of both fluids is such that it is hard to compare them, given the big spectrum of the Reynolds in the graphics, hence the need for a couple more test points with greater mass flow rate.

For the “base” condition (figure 5.9), the LiBr solution seems to be equivalent to the water in terms of overall heat transfer coefficients for Reynolds of 5000 to 10000, approximately.

For the “bubbling” condition (figure 5.10), the LiBr solution gets much higher UA values than water. However, this is because in the time between the end of the tests with water and the start of the LiBr tests, the pipe that supplied the compressed air for the tests was used for an unrelated activity. Because the manometer attached to the pipe is not very precise and does not have a clear resolution or enough sensitivity, it was impossible to return to the exact same

air pressure as in the previous experiments. The “bubbling” results in this section reflect that imprecision. As figure 5.10 shows, the tests with LiBr solution had a bigger bubbling intensity than the water tests. Otherwise, there is no other explanation as to why the tests with the LiBr solution higher UA values were obtained.

5.2.3. Convective heat transfer coefficient

Once again, in order to reach the convective heat transfer coefficient, equation 4.15 is used. Since the installation did not change, the same conditions can be applied, thus arriving at equation 4.16. The path to find the inner convective heat transfer coefficient is the same as in chapter 4.2.3, resorting to the number of Nusselt with equation 4.17. The D_i is the same, but the thermal conductivity coefficient is now of the LiBr solution (k_{LiBr}), obtained as indicated in Appendix F. The Nu is obtained through the Dittus-Boelter correlation (equation 4.19) if all the conditions are met. The Re_i is calculated as explained in chapter 5.2.1 and the Prandtl number is calculated with equation 5.1.

$$Pr = \frac{c\mu}{k_{LiBr}} \quad (5.1)$$

Where c is the specific heat of the LiBr solution and is obtained through equation F.1 in Appendix F and μ is the dynamic viscosity of the LiBr solution.

To check if the flow is fully developed, one must calculate the hydrodynamic entry length for the worst possible situation, which means the longest possible entry length. In this case, it is for the test point where the Re_i is the highest, when the $\dot{m}_h = 12.5$ kg/min. The highest Reynolds if for the base condition of “11.z(12.5)”, with a value of 9501. Resorting to equation 4.20 once more, the resulting value of the $L_{h,turb}$ is 0.141 m. The total length of the coil is much bigger than that, concluding that the flow is fully developed. As to verify if the Prandtl is between 0.7 and 160, tables 5.8 and 5.9 confirm that Pr is indeed in the correct range of values to use the Dittus-Boelter correlation.

After obtaining the Nusselt and then the h_i , the h_e can finally be calculated with equation 4.16. The values used to obtain the h_e are presented in the following tables for test points “11.z(10)” and “11.z(12.5)”.

Table 5.8 - Reynolds, Prandtl, Nusselt numbers and convective heat transfer coefficients of point “11.z(10)” ($\dot{m}_c=2$ kg/min; $\dot{m}_h=10$ kg/min)

Test reference	Re_i	c [J/(kg.°C)]	Pr	Nu	h_i [W/(m ² .K)]	k_{LiBr} (T)	h_e [W/(m ² .K)]
base	7475	2063.396	12.030	60.913	2669	0.460	673.122
bubbling	7417	2061.701	12.363	61.031	2668	0.459	1342.070

Table 5.9 - Reynolds, Prandtl, Nusselt numbers and convective heat transfer coefficients of point “11.z(12.5)” ($\dot{m}_c=2$ kg/min; $\dot{m}_h=12.5$ kg/min)

Test reference	Re_i	c [J/(kg.°C)]	Pr	Nu	h_i [W/(m ² .K)]	k_{LiBr} (T)	h_e [W/(m ² .K)]
base	9501	2064.037	11.905	73.565	3227	0.461	664.156
bubbling	9251	2062.049	12.294	72.710	3180	0.459	1305.000

To confirm the suspicions of the bubbling being more intense in the LiBr tests than in the water tests, the enhancement factor was calculated for these two test points analyzed above, using equation 4.22 with the coil external convective heat transfer coefficient for the bubbling and base conditions. The results are as observed in table 5.10.

Table 5.10 – Enhancement factor of the bubbling effect for test point “11.z(10)” and “11.z(12.5)”

	h_e (base)	h'_e (bubbling)	α
11.z (10)	673.122	1342.070	1.994
11.z (12.5)	664.156	1305.000	1.939

As predicted, the enhancement is indeed much higher compared to the tests with water as the hot fluid that have an enhancement factor with a range of $1.2 < \alpha < 1.4$, approximately. The increase of the h_e provided by the bubbling effect from the water tests to the tests with LiBr is around 40%, confirming that the intensity of the bubbling rose in the LiBr tests.

For the remaining test points of the experiments with the LiBr solution, since the flow of the hot fluid is laminar ($Re_i < 4000$), the Dittus-Boelter correlation is no longer applicable. Therefore, it is not possible to obtain the h_i with equation 4.17, if the Nusselt is unknown. And without the h_i , the h_e is also unknown. So for these test points, the process to disclose the desired properties (Nu , h_i and h_e) was reversed.

In theory, if the conditions outside the coil are equal, like the cold water mass flow rate and the conditions imposed (ultrasounds or bubbling for example), then the convective heat transfer coefficient of the coil outer wall should be similar. For example, take test points “1.a”, “1.b” and “1.c” of the tests with water as the hot fluid. They all have the same cold water mass flow rate ($\dot{m}_c = 2$ kg/min) and only the hot water mass flow rate varies (table 4.1). The h_e obtained in the base condition for the three test points are as follows.

Table 5.11 - h_e values for the base condition in test points “1.a”, “1.b” and “1.c”

	“1.a”	“1.b”	“1.c”
h_e [W/(m ² .K)]	639.029	633.714	673.675

For these values the biggest disparity is between “1.b” and “1.c” with a variation of 6%, which is not significant. Thus, one can assume that the values of the h_e obtained in the tests with water can be used in the LiBr tests with the respective conditions imposed. All but the bubbling condition which was not the same between the water tests and the most recent tests. So for the bubbling and ultrasounds + bubbling conditions, the values of the h_e to assume in the remaining LiBr test points will be an approximation of the ones obtained in “11.z”. This is because it is more correct to use the h_e values calculated for the actual bubbling intensity present in the LiBr tests instead of the lower intensity present in the water tests. So, 1300 W/(m².K) will be used as the h_e value for the upcoming experimental points analysis of all tests where higher bubbling intensity was used.

Before presenting the resulting values of the properties obtained in the remaining test points, table 5.12 simplifies how the h_e values were assumed for each test point.

Table 5.12 – Shared values of h_e for both tests

Water tests	Condition	h_e [W/(m ² .K)]		Condition	LiBr tests
"1.a"	Base	639.029	⇒	Base	"11.a"
	Ultrasounds	676.524	⇒	Ultrasounds	
"1.b"	Base	633.714	⇒	Base	"11.b"
	Ultrasounds	637.707	⇒	Ultrasounds	
"3.d"	Base	605.113	⇒	Base	"13.d"
	Ultrasounds	614.798	⇒	Ultrasounds	
"3.e"	Base	613.704	⇒	Base	"13.e"
	Ultrasounds	599.642	⇒	Ultrasounds	

Once the outer convective heat transfer coefficient was determined, the h_i could be calculated with equation 4.16. And then the Nusselt was calculated through equation 4.17 for the LiBr solution. Thus, tables 5.13 – 5.16 displays the obtained properties of the remaining LiBr test points.

Table 5.13 - Reynolds, Prandtl, Nusselt numbers and convective heat transfer coefficients of point "11.a" ($\dot{m}_c=2$ kg/min; $\dot{m}_h=2$ kg/min)

Test reference	Re_i	c [J/(kg.°C)]	Pr	Nu	h_i [W/(m ² .K)]	k_{LiBr} (T)	h_e [W/(m ² .K)]
base	1320	2051.934	14.299	17.095	737.15	0.453	639.03
bubbling	1254	2048.333	15.022	18.059	774.75	0.450	1300.00
ultrasounds	1312	2052.256	14.235	15.609	673.40	0.453	676.52
ultrasounds, bubbling	1206	2048.163	15.056	17.141	735.16	0.450	1300.00

Table 5.14 - Reynolds, Prandtl, Nusselt numbers and convective heat transfer coefficients of point "11.b" ($\dot{m}_c=2$ kg/min; $\dot{m}_h=5$ kg/min)

Test reference	Re_i	c [J/(kg.°C)]	Pr	Nu	h_i [W/(m ² .K)]	k_{LiBr} (T)	h_e [W/(m ² .K)]
base	3722	2062.117	12.281	31.233	1366	0.459	633.71
bubbling	3628	2060.024	12.693	33.805	1474	0.458	1300.00
ultrasounds	3688	2062.005	12.303	31.156	1363	0.459	637.71
ultrasounds, bubbling	3507	2059.942	12.709	32.072	1399	0.458	1300.00

Table 5.15 - Reynolds, Prandtl, Nusselt numbers and convective heat transfer coefficients of point "13.d" ($\dot{m}_c=1.5$ kg/min; $\dot{m}_h=1.5$ kg/min)

Test reference	Re_i	c [J/(kg.°C)]	Pr	Nu	h_i [W/(m ² .K)]	k_{LiBr} (T)	h_e [W/(m ² .K)]
base	944	2047.894	15.111	12.281	527	0.450	605.11
bubbling	917	2043.763	15.947	14.007	597	0.448	1300.00
ultrasounds	921	2046.278	15.437	12.074	516	0.449	614.80
ultrasounds, bubbling	893	2043.000	16.102	13.726	584	0.447	1300.00

Table 5.16 - Reynolds, Prandtl, Nusselt numbers and convective heat transfer coefficients of point "13.e" ($\dot{m}_c=1.5$ kg/min; $\dot{m}_h=3$ kg/min)

Test reference	Re_i	c [J/(kg.°C)]	Pr	Nu	h_i [W/(m ² .K)]	k_{LiBr} (T)	h_e [W/(m ² .K)]
base	2113	2060.061	12.685	19.802	864	0.458	613.70
bubbling	2062	2057.645	13.162	21.063	916	0.456	1300.00
ultrasounds	2212	2060.310	12.636	20.653	901	0.458	599.64
ultrasounds, bubbling	2097	2057.671	13.157	21.570	938	0.456	1300.00

Another way to obtain the Nusselt number and the convective heat transfer coefficients would be to assume the value of Nu for a laminar flow. According to [1], for fully developed laminar flows in circular tubes, $Nu = 3.66$ if the surface temperature is constant and $Nu = 4.36$ if the surface heat flux is constant. Neither are constant, but the Nusselt should be between those two values. They are not, however, as seen in tables 5.13-5.16, but are instead much higher. To confirm if the laminar flow is indeed fully developed, the hydrodynamic entry length should be calculated. For laminar flows in circular tubes, the hydrodynamic entry length $L_{t,laminar}$ is obtained with equation 5.2.

$$L_{t,laminar} = 0.05Re_iPrD_i \quad (5.2)$$

Calculating the entry length for the worst case, which is the test point with the highest LiBr mass flow rate, test point "11.b" ($\dot{m}_h = 5$ kg/min), the resulting $L_{t,laminar}$ is around 24 m. The total length of the coil in the installation is 2.825 m, meaning that the flow is nowhere near being fully developed.

As for the best possible case, test point "13.d" ($\dot{m}_h = 1.5$ kg/min) which has the lowest LiBr mass flow rate, the resulting $L_{t,laminar}$ is around 7.5 m. It still is not a fully developed flow throughout the total length of the coil.

So why is the Nusselt number higher than the expected values? This is because for developing laminar flows, the temperature and velocity profiles are simultaneously developing. These are the combined entry length (thermal and velocity). The graphic in figure 5.13 correlates the Nusselt number with the inverse of the Graetz number [24]. The Graetz number Gz follows the following equation.

$$Gz = \frac{D}{x} RePr \quad (5.3)$$

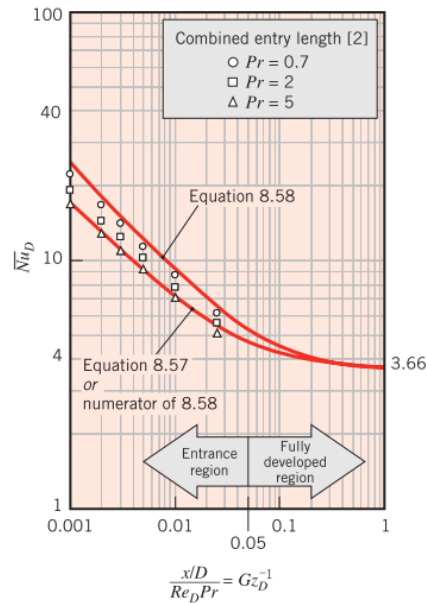


Figure 5.13 – Entry length solution for laminar flow in circular tubes [24].

The inverse of the Graetz number was then calculated for the test points with laminar flow, using $x = 1.4$, a mean value of the total length of the coil. The diameter used was the inner diameter D_i and the Reynolds and Prandtl used were the ones relative of each test point. Its values are represented in tables 5.17 – 5.20.

Table 5.17 – The inverse of Graetz number for test point “11.a” ($\dot{m}_c=2$ kg/min; $\dot{m}_h=2$ kg/min)

Test reference	Re_i	Pr	Nu	Gz^{-1}
base	1320	14.299	17.095	0.007065
bubbling	1254	15.022	18.059	0.007077
ultrasounds	1312	14.235	15.609	0.007140
ultrasounds, bubbling	1206	15.056	17.141	0.007344

Table 5.18 - The inverse of Graetz number for test point “11.b” ($\dot{m}_c=2$ kg/min; $\dot{m}_h=5$ kg/min)

Test reference	Re_i	Pr	Nu	Gz^{-1}
base	3722	12.281	31.233	0.002917
bubbling	3628	12.693	33.805	0.002895
ultrasounds	3688	12.303	31.156	0.002939
ultrasounds, bubbling	3507	12.709	32.072	0.002992

Table 5.19 - The inverse of Graetz number for test point “11.b” ($\dot{m}_c=1.5$ kg/min; $\dot{m}_h=1.5$ kg/min)

Test reference	Re_i	Pr	Nu	Gz^{-1}
base	944	15.111	12.281	0.009350
bubbling	917	15.947	14.007	0.009116
ultrasounds	921	15.437	12.074	0.009380
ultrasounds, bubbling	893	16.102	13.726	0.009272

Preliminary studies on the influence of ultrasounds on the heat transfer rate in a crossflow heat exchanger

Table 5.20 - The inverse of Graetz number for test point "11.b" ($\dot{m}_c=1.5$ kg/min; $\dot{m}_h=3$ kg/min)

Test reference	Re_i	Pr	Nu	Gz^{-1}
base	2113	12.685	19.802	0.004975
bubbling	2062	13.162	21.063	0.004912
usltrasounds	2212	12.636	20.653	0.004771
ultrasounds, bubbling	2097	13.157	21.570	0.004832

Approximately, they all fit between the two red lines of figure 5.13, with the exception of test point "11.b" ($\dot{m}_h= 5$ kg/min). In this test point, with a Reynolds of approximately 3600, the flow is in the transition from laminar to the turbulent region.

Preliminary studies on the influence of ultrasounds on the heat transfer rate in a crossflow heat exchanger

6. Conclusions

With an installation provided by “Laboratório de Combustão” at INEGI, the main objective of this project was to evaluate the influence that the ultrasounds and bubbling might have in the heat transfer rate. A few tests were carried out in a sort of crossflow heat exchanger, with the cold fluid mixed and the hot fluid unmixed. The hot/cold fluid pairs used were water/water and aqueous LiBr solution/water.

For the tests, the temperature of the hot fluid was set to 60 °C and by varying the mass flow rate of both hot and cold fluids, the overall heat transfer coefficient UA was calculated for a few test conditions (base, ultrasounds, bubbling and tank insulation). From that, some dimensionless numbers like Reynolds, Nusselt and Prandtl were calculated for the hot fluid to finally obtain the convective heat transfer coefficients h_i and h_e .

In the water only tests, it was concluded that for higher mass flow rates of both cold and hot fluid, the overall heat transfer coefficient rises. As for the test conditions, it was observed that the ultrasounds have no noticeable effect on the overall heat transfer coefficient, and that the bubbling effect provokes evidently more enhancement in the heat transfer rate than any other condition, obtaining up to 45% increase in the outer convective heat transfer coefficient. Even though for higher cold water mass flow rate the UA increases, the heat transfer enhancement caused by the bubbling is more prominent the lower the \dot{m}_c is.

Still in the tests using water as the hot fluid, a few experimental points were executed where the cold fluid entrance position was altered from below, underwater, to the top of the heat exchanger tank to check if it lead to any change in the heat transfer performance. It was observed that for high cold-water mass flow rates, the difference is noticeable as the overall heat transfer coefficient is lower when the cold fluid entry point is in the top position.

In the tests with the aqueous LiBr solution as the hot fluid, the same correlation between the two mass flow rates and the overall heat transfer coefficient was made as in the water only tests, meaning that the increase in both hot and cold fluids mass flow rate lead to greater UA values. Once more, the use of ultrasounds did not introduce any positive change in the heat transfer rate of the tests with the aqueous LiBr solution. The bubbling produced evidently better results as expected, although the bubbling intensity present in the LiBr solution tests was unintentionally higher than they were in the previous tests with water as the hot fluid.

A comparison was made between the tests that used water as the hot fluid and the ones that had the aqueous LiBr solution as the hot fluid. It was observed that for the same Reynolds number, the difference between both hot fluids mass flow rate is significantly disparate, because of the difference between their physical properties. It was possible to conclude that for the base condition, both hot fluids present similar UA values for the same approximate Reynolds numbers. As for the bubbling condition, it was not possible to equally compare the hot fluids, as the conditions were not the same.

As for the installation, it was concluded that a few upgrades should be made to further investigate the use of ultrasounds and bubbling in heat transfer enhancement. As the installation is now, the ultrasounds generators are not enough to influence the heat transfer present in the heat exchanger tank. More importantly, the pressure of the compressed air should be more easily controlled and measured so that more rigorous tests can be done with the bubbling condition.

Preliminary studies on the influence of ultrasounds on the heat transfer rate in a crossflow heat exchanger

7. Future works

As for future works, to correct the ineffectiveness of the ultrasounds in heat transfer enhancement, duplicating the number of ultrasound generators should be a good bet to get better results, as it seemed that the present ultrasounds power were not effective because of the great volume of the cold water in the heat exchanger tank. Not only that, but perhaps choosing a frequency other than 28 kHz could provide different outcomes.

All tests were executed with the temperature set at 60 °C for heating the hot fluid. Redoing these tests with different temperatures might produce different overall heat transfer coefficients. Studying the different values could give an optimum temperature for better heat transfer for this heat exchanger tank.

Since there was an “accident” with regulating the intensity of the bubbling, it would be pivotal for the installation to set a proper manometer along with the pressure regulator so that changing the bubbling intensity with full control over it should be possible. The way to do it is install the pressure regulator in a different setup with a high-resolution manometer, as the compressed air passes through it. A needle valve should be used to regulate the bubbling air flow. As demonstrated in this project, the bubbling effect is remarkably effective in the heat transfer enhancement and studying it further with different magnitudes is imperative.

It would also be interesting to prove if the inner convective heat transfer coefficient h_i is affected by the ultrasounds like the h_e , and if it is, at what degree. For that matter, different heat exchanger configuration should be tested.

Preliminary studies on the influence of ultrasounds on the heat transfer rate in a crossflow heat exchanger

References

- [1] Y.A. Çengel, Heat Transfer: A Practical Approach, 2nd ed., Mcgraw-Hill, New York, 2002.
- [2] A. Franco, C. Bartoli, The ultrasounds as a mean for the enhancement of heat exchanger performances: An analysis of the available data, J. Phys. Conf. Ser. 1224 (2019). <https://doi.org/10.1088/1742-6596/1224/1/012035>.
- [3] N. Gondrexon, Y. Rousselet, M. Legay, P. Boldo, S. Le Person, A. Bontemps, Intensification of heat transfer process: Improvement of shell-and-tube heat exchanger performances by means of ultrasound, Chem. Eng. Process. Process Intensif. 49 (2010) 936–942. <https://doi.org/10.1016/j.cep.2010.06.007>.
- [4] M. Legay, N. Gondrexon, S. Le Person, P. Boldo, A. Bontemps, Enhancement of heat transfer by ultrasound: Review and recent advances, Int. J. Chem. Eng. 2011 (2011). <https://doi.org/10.1155/2011/670108>.
- [5] W. Benzinger, U. Schygulla, M. Jäger, K. Schubert, Anti Fouling Investigations With Ultrasound in a Microstructured Heat Exchanger, Proc. 6th Int. Conf. Heat Exch. Fouling Clean. - Challenges Oppor. (2005).
- [6] D.W. Zhou, Heat transfer enhancement of copper nanofluid with acoustic cavitation, Int. J. Heat Mass Transf. 47 (2004) 3109–3117. <https://doi.org/10.1016/j.ijheatmasstransfer.2004.02.018>.
- [7] Y. Chen, S. Sun, Y. Lai, C. Ma, Influence of ultrasound to convective heat transfer with fouling of cooling water, Appl. Therm. Eng. 100 (2016) 340–347. <https://doi.org/10.1016/j.applthermaleng.2016.01.144>.
- [8] J.D.N. Cheeke, J.D.N. Cheeke, Fundamentals and Applications of Ultrasonic Waves, 2010. <https://doi.org/10.1201/9781420042139>.
- [9] J.M. Leveque, L. Duclaux, D. Fontvieille, N. Gondrexon, R. Vibert, A. Perrier, Low frequency ultrasonic device Sonitube: A possible gate to pilot and industrial scale applications, 1621 (2014) 250–255. <https://doi.org/10.1063/1.4898474>.
- [10] O. Bulliard-Sauret, J. Berindei, S. Ferrouillat, L. Vignal, A. Momponteil, C. Poncet, J.M. Leveque, N. Gondrexon, Heat transfer intensification by low or high frequency ultrasound: Thermal and hydrodynamic phenomenological analysis, Exp. Therm. Fluid Sci. 104 (2019) 258–271. <https://doi.org/10.1016/j.expthermflusci.2019.03.003>.
- [11] W.H. Tay, K.K. Lau, A.M. Shariff, High frequency ultrasonic-assisted CO₂ absorption in a high pressure water batch system, Ultrason. Sonochem. 33 (2016) 190–196. <https://doi.org/10.1016/j.ultsonch.2016.04.004>.
- [12] S.M.M. Yusof, A.M. Shariff, W.H. Tay, K.K. Lau, N.F.A. Mustafa, Mass transfer intensification of CO₂ absorption in monoethanolamine using high frequency ultrasonic technology in continuous system, Int. J. Greenh. Gas Control. 102 (2020) 103157. <https://doi.org/10.1016/j.ijggc.2020.103157>.
- [13] B. Loh, N. Carolina, P.I. Ro, C. Kleinstreuer, Acoustic streaming induced by ultrasonic flexural vibrations and associated enhancement of convective heat transfer, 111 (2002) 875–883. <https://doi.org/10.1121/1.1433811>.
- [14] M. Ashokkumar, The characterization of acoustic cavitation bubbles - An overview,

- Ultrasound. *Sonochem.* 18 (2011) 864–872.
<https://doi.org/10.1016/j.ultsonch.2010.11.016>.
- [15] J. Chandrapala, C. Oliver, S. Kentish, M. Ashokkumar, Ultrasonics in food processing, *Ultrasound. Sonochem.* 19 (2012) 975–983.
<https://doi.org/10.1016/j.ultsonch.2012.01.010>.
- [16] Wietelmann, U. and Steinbild, M. (2014). Lithium and Lithium Compounds. In *Ullmann's Encyclopedia of Industrial Chemistry*, (Ed.).
https://doi.org/10.1002/14356007.a15_393.pub2
- [17] M. Santos, *Practical Configurations of Small-Scale*, FEUP, 2019.
- [18] M. Zheng, B. Li, Z. Wan, B. Wu, Y. Tang, J. Li, Ultrasonic heat transfer enhancement on different structural tubes in LiBr solution, *Appl. Therm. Eng.* 106 (2016) 625–633.
<https://doi.org/10.1016/j.applthermaleng.2016.06.019>.
- [19] J. Trindade, Projeto , construção e teste de um módulo de acumulação de energia térmica usando material de mudança de fase, FEUP, 2018.
- [20] TABELA DE CONDUTIVIDADE TÉRMICA DE MATERIAIS DE CONSTRUÇÃO, (n.d.).
<http://www.protolab.com.br/Tabela-Conductividade-Material-Construcao.htm>
(accessed May 3, 2021).
- [21] A.R. Mumjord, A.A. Markson, R.A. Bowman, A.C. Mueller, J.R. Connelly, H.C. Keysor, D.H. Pletta, S.J. Needs, C.T. Ripley, *A.s.m.e.*, n.d.
- [22] Syeilendra Pramuditya, *Water Thermodynamic Properties*, (2021).
<https://syeilendrapramuditya.wordpress.com/2011/08/20/water-thermodynamic-properties/> (accessed June 10, 2021).
- [23] F.M.C.T. Pinho, *Formulário TC*, (2015) 1–39, DEMEC, FEUP.
- [24] D.P.D. Theodore L. Bergman, Adrienne S. Lavine, Frank P. Incropera, *Fundamentals of Heat and Mass Transfer*, 7th ed., Don Fowley, USA, 2011.
- [25] R.A. Khairulin, V.A. Gruzdev, S. V. Stankus, O.I. Verba, Experimental study of the density of aqueous solutions of lithium bromide at temperature of up to 250°C in the range of mass concentrations from 30 to 65 %, *Thermophys. Aeromechanics.* 13 (2006) 575–583.
<https://doi.org/10.1134/S0869864306040111>.
- [26] Y. Kaita, Thermodynamic properties of lithium bromide-water solutions at high temperatures, *Int. J. Refrig.* 24 (2001) 374–390. [https://doi.org/10.1016/S0140-7007\(00\)00039-6](https://doi.org/10.1016/S0140-7007(00)00039-6).
- [27] S. Kline, G. Nellis, *LiBrSSC (aqueous lithium bromide) Property Routines*, (2005).

APPENDICES

A. Appendix A – Data acquisition software “DASYLab”

For the data acquisition system, the “DASYLab” software was used. In this software a worksheet (figure A.1) was made in order to process the data received. In this worksheet it is possible to insert formulas (calibration trend lines, polynomials and heat equations) as well as graphics that show the evolution of a certain variable in real time during the tests.

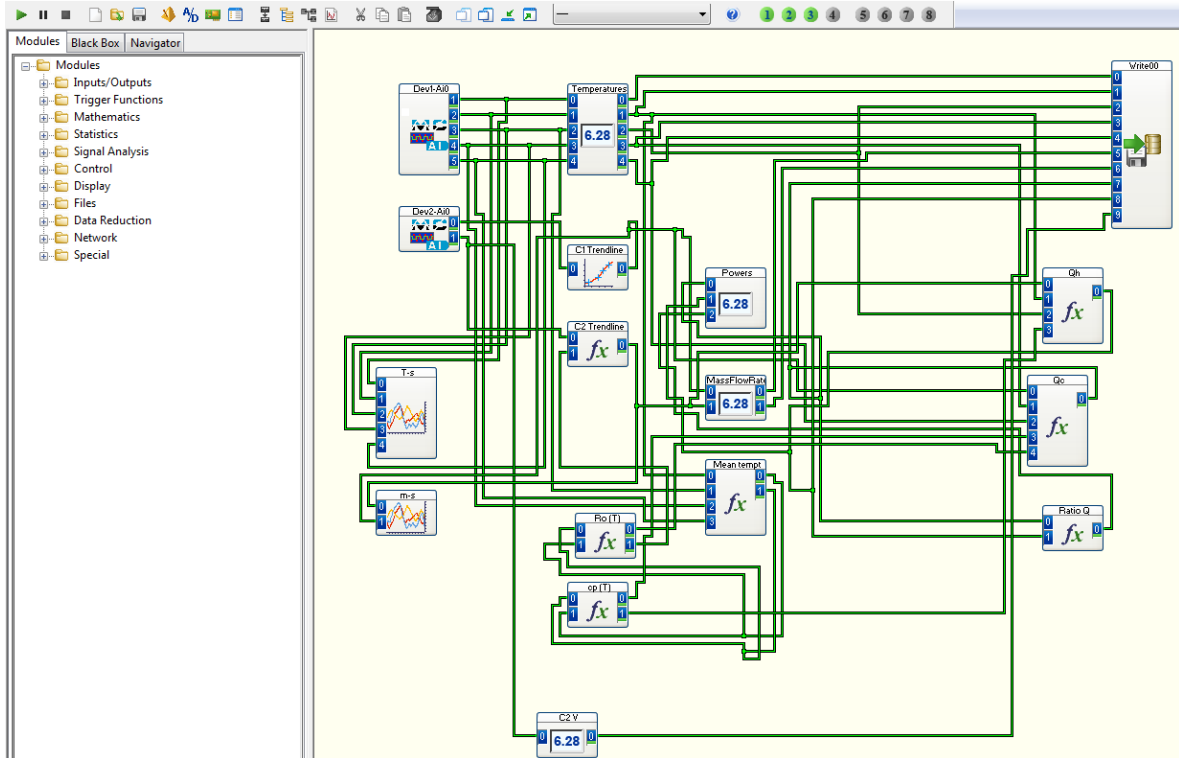


Figure A.1 – “DASYLab” worksheet for the tests.

Preliminary studies on the influence of ultrasounds on the heat transfer rate in a crossflow heat exchanger

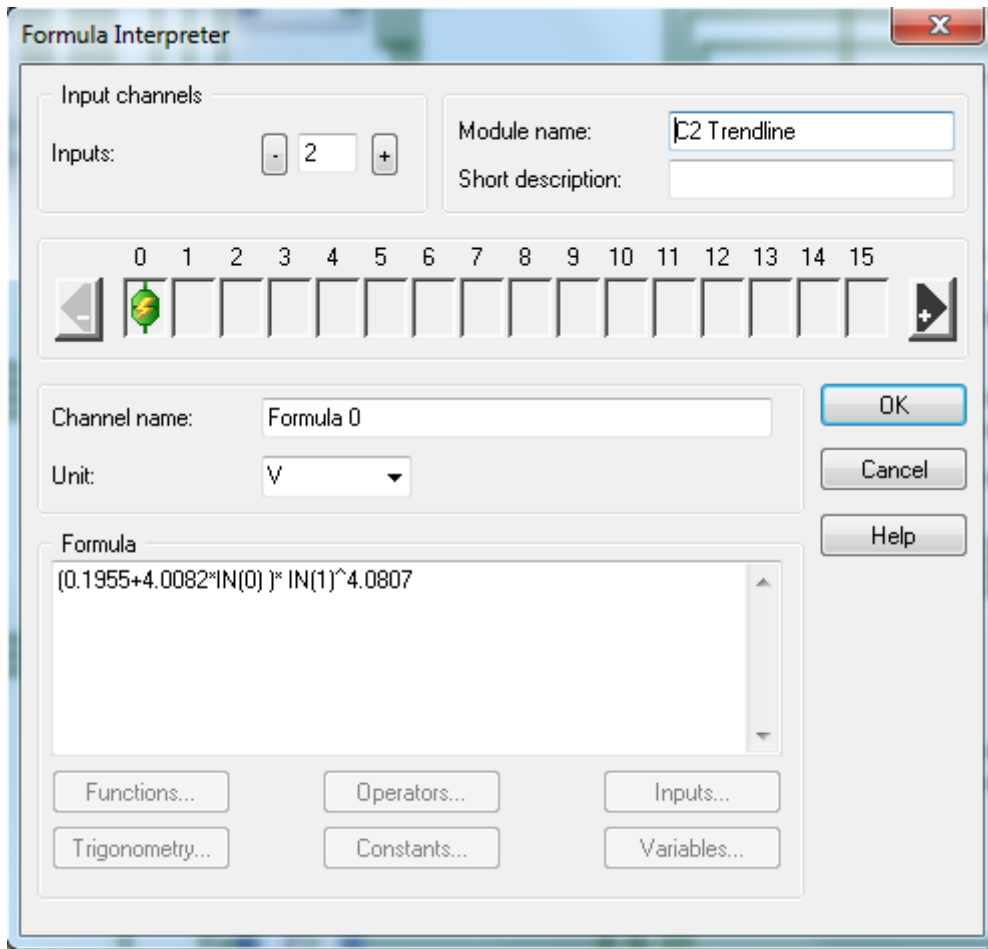


Figure A.2 – Calibration formula of the C₂ flow meter in the “DASYLab” worksheet.

Preliminary studies on the influence of ultrasounds on the heat transfer rate in a crossflow heat exchanger

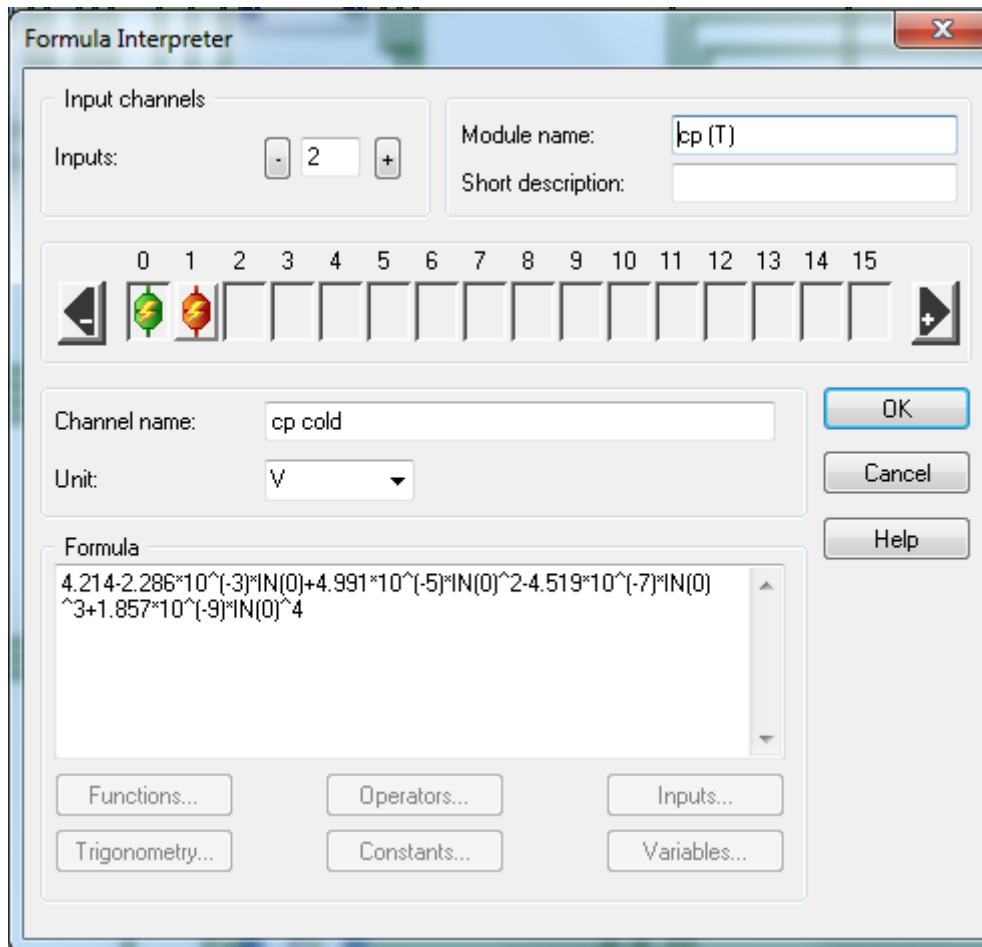


Figure A.3 – Polynomial used for the c of the water, using the mean hot temperature in °C.

B. Appendix B – Calibration of the mass flow meters (Water)

The measurements of the mass flow rates of the cold and hot fluids were made with two flow meters, C_1 and C_2 respectively. In order to properly calibrate the two flow meters, one must simulate as much as possible the real situation in which the flow meter will be subjected to. Both calibration processes were made using water, for the cold and hot fluid.

B.1 – Calibration of the flow meter for the cold water (C_1)

Flow meter C_1 is located in the cold water circuit, just before reaching the heat exchanger tank. Therefore, the water that goes through it is the one that comes from outside at ambient temperature. In the calibration process, the same hose and regulating valve are used but instead of filling the heat exchanger tank, the water is led to an empty bucket. The steps of the calibration process are as it shows:

- 1) At a certain regulating valve position, fill up an empty bucket;
- 2) At the same time, with the aid of the “DASYLab” software, save and store the voltage fluctuations that the flow meter is transmitting at the given flow rate, for the duration of each test run;
- 3) Time with chronometer (in this case a cellphone was used) the duration of the filling of the bucket;
- 4) Weight the bucket using a weighting scale (figure B.1);
- 5) Repeat the process a number of times with a different valve position to vary the flow rate, and in consequence the voltage.



Figure B.1 – Weighting scale used in the calibration of the flow meters.

Having made a total of six test runs and analyzing the data in Excel, figure B.2 reveals the trend line obtained that relates the voltage with the respecting mass flow rate, in kg/min.

Preliminary studies on the influence of ultrasounds on the heat transfer rate in a crossflow heat exchanger

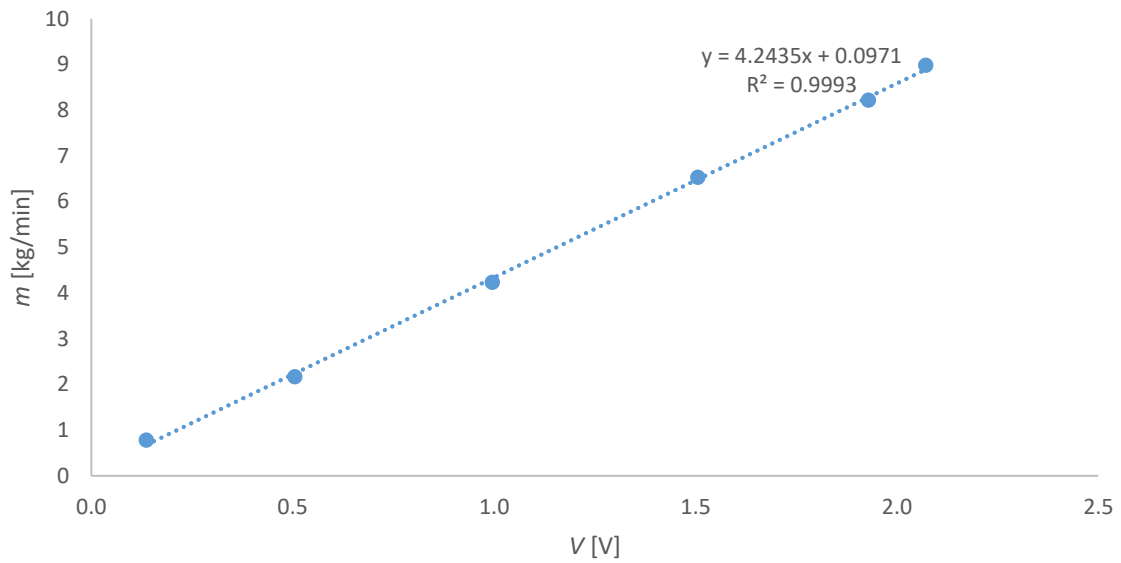


Figure B.2 – Trend line obtained through the calibration process of flow meter C_1 .

The trend line obtained correlates the voltage acquired from the flow meter into the respective mass flow rate in kg/min according to the following equation.

$$\dot{m} = 4.2335V + 0.0971 \quad (\text{B.1})$$

Equation B.1 is then inserted in the “DASYLab” worksheet as suggested in figure B.3.

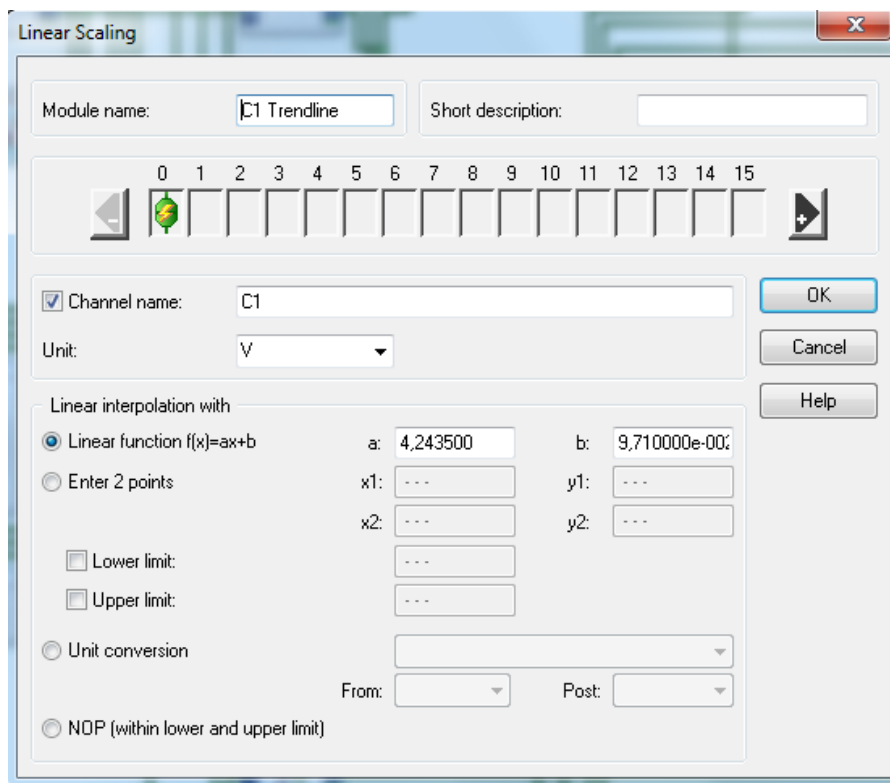


Figure B.3 – C_1 Trend line inserted in the worksheet of “DASYLab”.

B.2 – Calibration of the flow meter for the hot water (C_2)

Flow meter C_2 is located in the hot fluid circuit between the heat exchanger tank and the pump. The working conditions that will be imposed in flow meter C_2 are high temperatures, up to 60 °C, and a wide range of flow rates pumped by the pump. The hot fluid circuit is a closed one. To simulate these conditions while adopting a similar method of calibration used in the calibration of C_1 , one must interrupt the cycle to lead the hot water onto an empty bucket. So, a valve system was assembled with a shut-off valve in the T branch following the gate valve, as represented in figure B.4. This way, the water is heated with the resistances in the white bucket and the pressure drop caused by the pump and the installation itself is accounted for as much as possible when calibrating flow meter C_2 , making the results more realistic.

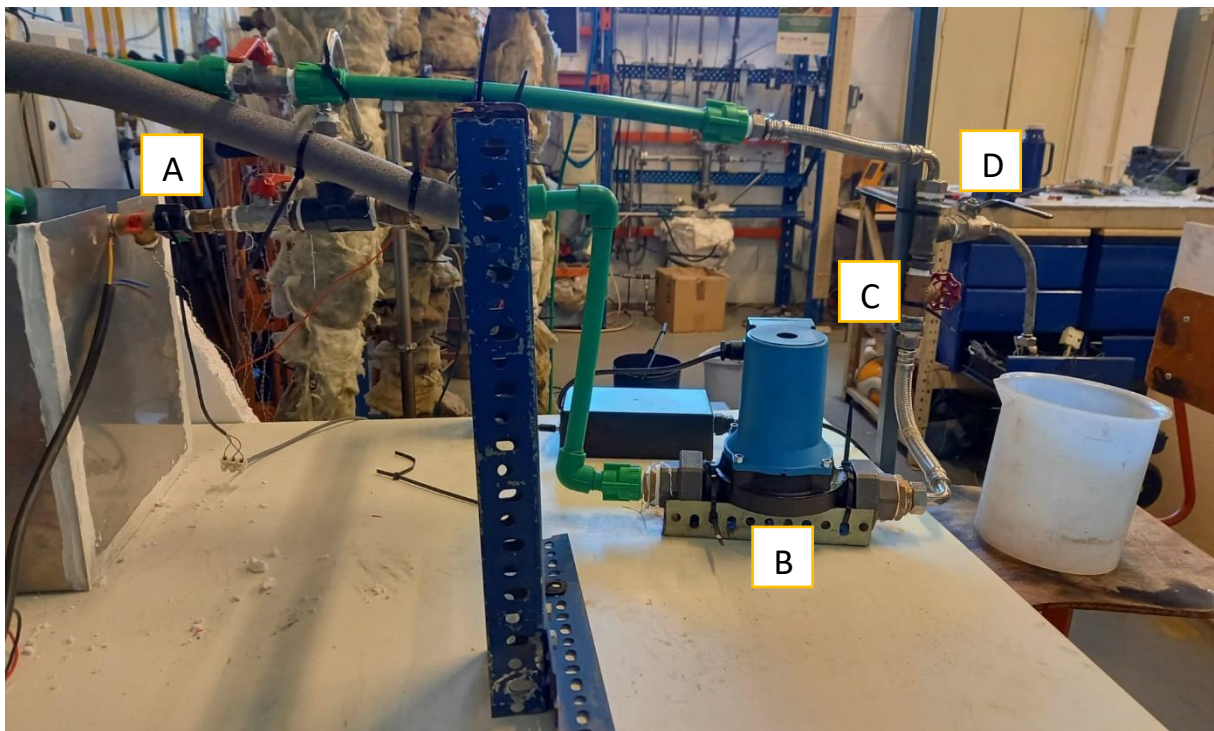


Figure B.4 – Hot water calibration setup; A – Flow meter C_2 ; B – Pump; C – Needle valve; D – Shut-off valve in T.

Unlike the calibration of flow meter C_1 , for the flow meter C_2 the density of the water must be accounted for. While the cold water that goes through C_1 does not vary much in its temperature (always between 18 and 21 °C), its density does not change much either. However, the temperatures of the hot fluid that will go through C_2 will have a wider range of temperatures and consequently different densities. So the resulting equation of the calibration process will have to not only account for the voltage given off by the flow meter but also the density of the hot fluid. This is because for the same flow rate, the weight of the fluid is lightly different if its temperature varies considerably (the higher the temperature, the less dense the fluid), which means the turbine inside the flow meter will spin for a less dense volume of liquid. This could induce misleading mass flow rates, so for that reason the voltage is not the only variable that the C_2 calibration equation should depend on.

The calibration process for flow meter C_2 was similar to the one used for C_1 , involving the same steps. However, this time the temperature was also measured in each test run with the thermocouple T_3 and stored along with the voltage thanks to the “DASYLab” software. This

Preliminary studies on the influence of ultrasounds on the heat transfer rate in a crossflow heat exchanger

process was carried out for temperatures of 24 °C, 42 °C, 55 °C and 60 °C, and the resulting values can be observed all together in figure B.5.

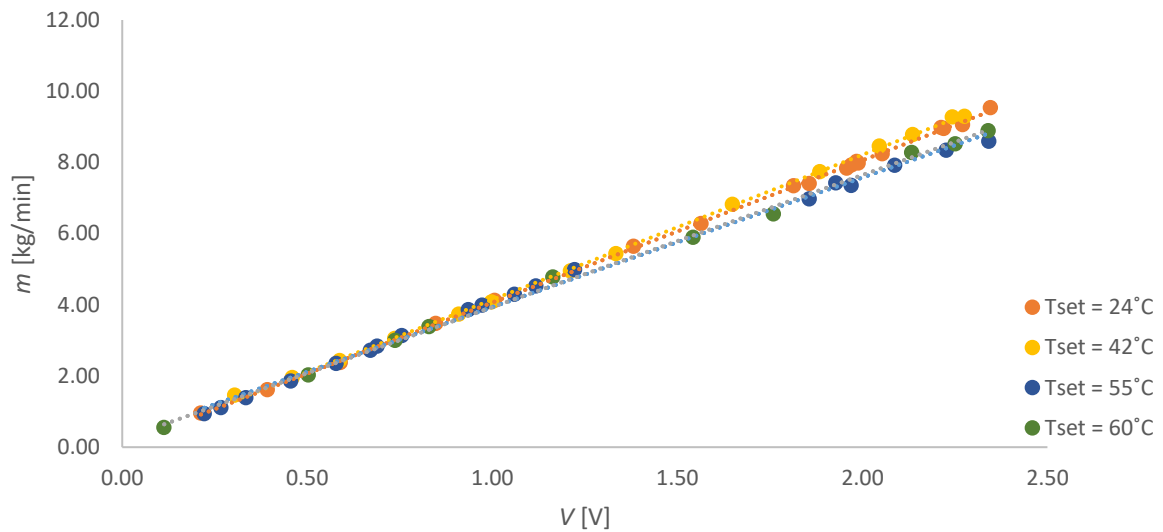


Figure B.5 – Graphic of the values obtained in the calibration process.

After that, the specific gravity of the water was calculated for each test point using a polynomial (equation B.2) with the temperature in °C.

$$d = -1.036 \times 10^{-10}T_3^4 + 3.681 \times 10^{-8}T_3^3 - 7.275 \times 10^{-6}T_3^2 + 5.048 \times 10^{-5}T_3 + 9.999 \times 10^{-1} \quad (\text{B.2})$$

In order to correlate the mass flow rate with the voltage and specific gravity, the software “NLREG” was used. This software allows the user to find the correct parameters for an equation of the user’s choice using all the values of the variables introduced. With the input of all the values of \dot{m} , d and V obtained on all the tests runs of the calibration process, after a few attempts the following correlation was obtained for the least incertitude.

$$\dot{m} = (0.1955 + 4.0082V) \times d^{4.0807} \quad (\text{B.3})$$

Equation B.3 was then input in the “DASYLab” software, along with equation B.2. That way the specific gravity is calculated on real time using the temperature present at the moment. In figure B.6, the mass flow rates obtained during the calibration process are placed along with the correlation, equation B.3, showing the viability of the correlation used. The bigger disparity still observed in higher flow rates can be due to experimental errors.

Preliminary studies on the influence of ultrasounds on the heat transfer rate in a crossflow heat exchanger

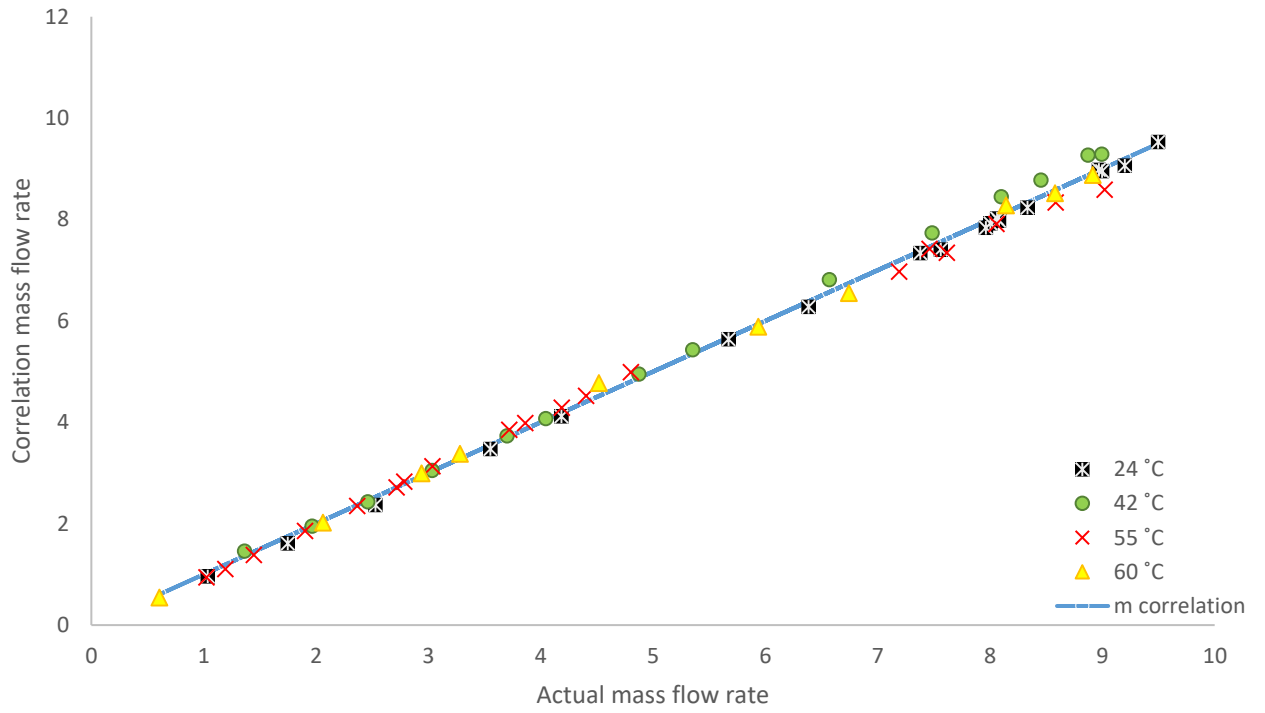


Figure B.6 – Comparison of the actual mass flow rate with the one calculated using equation B.3.

C. Appendix C – Experimental results of the tests with water

The resulting values, such as temperatures, mass flow rates, calorific power and parameters R , P and F are all shown in the following tables, for each test point and conditions implanted. In the tables below, the terms “bubb”, “uss” and “insul” mean bubbling, ultrasounds and insulation, respectively.

Table C.1 – Values obtained for test point “1.a” ($\dot{m}_c = 2$ kg/min; $\dot{m}_h = 2$ kg/min)

Test reference	T_{hi} [°C]	T_{ho} [°C]	T_{ci} [°C]	T_{co} [°C]	T_{mh} [°C]	ΔT_1	ΔT_2	ΔT_{mi}	\dot{m}_c [kg/min]	\dot{m}_h [kg/min]	Q_c [kW]	Q_h [kW]	Q_c/Q_h	R	P	F	UA [W/K]
base	52.727	43.348	19.552	27.445	48.037	25.282	23.796	24.531	2.064	2.028	1.134	1.324	0.856	1.188	0.238	0.975	55.37
bubb	50.982	40.680	19.614	28.851	45.831	22.131	21.066	21.594	2.078	2.044	1.335	1.467	0.911	1.115	0.294	0.96	70.74
uss	56.069	44.666	18.457	27.767	50.367	28.302	26.209	27.242	2.168	1.924	1.404	1.529	0.919	1.225	0.248	0.975	57.56
uss,bubb	55.191	42.315	18.759	29.667	48.753	25.524	23.556	24.527	2.146	2.055	1.628	1.843	0.884	1.180	0.299	0.965	77.86
insul	57.431	46.199	19.371	28.015	51.815	29.416	26.828	28.102	2.103	1.998	1.265	1.563	0.809	1.299	0.227	0.98	56.76
insul,bubb	57.095	44.532	19.236	29.904	50.814	27.192	25.296	26.232	2.120	2.068	1.573	1.810	0.869	1.178	0.282	0.97	71.13
insul,uss	58.961	47.020	19.079	28.948	52.991	30.013	27.941	28.965	2.176	1.948	1.494	1.620	0.922	1.210	0.247	0.975	57.38
insul,uss,bubb	57.573	43.912	19.310	30.989	50.742	26.584	24.602	25.580	2.203	1.971	1.789	1.875	0.954	1.170	0.305	0.955	76.75

Preliminary studies on the influence of ultrasounds on the heat transfer rate in a crossflow heat exchanger

Table C.2 - Values obtained for test point "1.b" ($\dot{m}_c = 2$ kg/min; $\dot{m}_h = 5$ kg/min)

Test reference	T_{hi} [°C]	T_{ho} [°C]	T_{ci} [°C]	T_{co} [°C]	T_{mh} [°C]	ΔT_1	ΔT_2	ΔT_{ml}	\dot{m}_c [kg/min]	\dot{m}_h [kg/min]	Q_c [kW]	Q_h [kW]	Q_c/Q_h	R	P	F	UA [W/K]
base	59.730	53.838	18.078	30.530	56.784	29.200	35.760	32.369	2.079	4.955	1.801	2.034	0.885	0.473	0.299	1	62.85
bubb	59.588	52.345	18.283	33.693	55.967	25.895	34.062	29.792	2.004	4.960	2.146	2.503	0.858	0.470	0.373	0.98	85.73
uss	59.777	54.022	18.670	30.438	56.900	29.339	35.352	32.252	2.018	5.095	1.652	2.044	0.808	0.489	0.286	1	63.37
uss,bubb	59.860	52.733	18.061	34.536	56.297	25.324	34.672	29.754	2.070	4.966	2.371	2.466	0.961	0.433	0.394	0.985	84.15
insul	61.017	54.939	18.852	32.100	57.978	28.917	36.087	32.370	2.032	4.936	1.872	2.091	0.895	0.459	0.314	0.99	65.24
insul,bubb	58.280	51.990	19.299	34.833	55.135	23.448	32.691	27.814	2.087	5.172	2.253	2.267	0.994	0.405	0.398	0.98	83.18
insul,uss	60.539	54.839	19.278	32.614	57.689	27.924	35.560	31.589	2.023	5.109	1.875	2.030	0.924	0.427	0.323	0.99	64.90
insul,uss,bubb	61.489	54.445	19.419	35.656	57.967	25.833	35.026	30.197	2.113	5.145	2.384	2.526	0.944	0.434	0.386	0.985	84.93

Preliminary studies on the influence of ultrasounds on the heat transfer rate in a crossflow heat exchanger

Table C.3 – Values obtained for test point “1.c” ($\dot{m}_c = 2$ kg/min; $\dot{m}_h = 8$ kg/min)

Test reference	T_{hi} [°C]	T_{ho} [°C]	T_{ci} [°C]	T_{co} [°C]	T_{mh} [°C]	ΔT_1	ΔT_2	ΔT_{ml}	\dot{m}_c [kg/min]	\dot{m}_h [kg/min]	Q_c [kW]	Q_h [kW]	Q_c/Q_h	R	P	F	UA [W/K]
base	60.018	56.054	18.506	32.098	58.036	27.920	37.548	32.496	2.026	8.137	1.915	2.249	0.852	0.292	0.327	1	69.20
bubb	61.117	56.057	18.559	36.727	58.587	24.390	37.499	30.476	2.081	8.097	2.627	2.856	0.920	0.278	0.427	0.995	94.17
uss	60.169	56.347	18.713	32.319	58.258	27.850	37.634	32.497	2.058	8.138	1.947	2.167	0.898	0.281	0.328	1	66.69
uss,bubb	60.996	55.984	18.643	36.649	58.490	24.347	37.341	30.382	2.065	8.091	2.583	2.827	0.914	0.278	0.425	0.995	93.50
insul	60.512	56.338	18.445	31.903	58.425	28.609	37.893	33.034	2.054	8.074	1.922	2.349	0.818	0.310	0.320	1	71.10
insul,bubb	61.260	56.313	18.117	36.701	58.786	24.559	38.196	30.877	2.102	8.077	2.714	2.785	0.974	0.266	0.431	0.995	90.66
insul,uss	60.319	56.548	18.786	33.868	58.434	26.451	37.761	31.771	1.996	8.019	2.092	2.108	0.992	0.250	0.363	1	66.35
insul,uss,bubb	61.049	56.521	18.911	36.142	58.785	24.907	37.610	30.824	1.996	8.038	2.389	2.537	0.942	0.263	0.409	0.995	82.72

Preliminary studies on the influence of ultrasounds on the heat transfer rate in a crossflow heat exchanger

Table C.4 – Values obtained for test point “2.a” ($\dot{m}_c = 5$ kg/min; $\dot{m}_h = 2$ kg/min)

Test reference	T_{hi} [°C]	T_{ho} [°C]	T_{ci} [°C]	T_{co} [°C]	T_{mh} [°C]	ΔT_1	ΔT_2	ΔT_{ml}	\dot{m}_c [kg/min]	\dot{m}_h [kg/min]	Q_c [kW]	Q_h [kW]	Q_c/Q_h	R	P	F	UA [W/K]
base	55.813	41.660	18.502	23.920	48.737	31.893	23.158	27.293	5.086	1.973	1.919	1.945	0.987	2.612	0.145	0.975	73.10
bubb	54.268	38.856	18.266	24.225	46.562	30.044	20.589	25.019	5.058	2.005	2.099	2.152	0.975	2.587	0.166	0.975	88.22
uss	55.628	41.506	18.266	23.846	48.567	31.783	23.240	27.289	5.063	1.992	1.968	1.960	1.004	2.531	0.149	0.975	73.67
uss,bubb	55.612	39.759	18.343	24.381	47.685	31.231	21.415	26.015	4.995	1.983	2.100	2.190	0.959	2.626	0.162	0.97	86.78
insul	56.385	42.665	18.178	23.981	49.525	32.404	24.488	28.261	5.003	2.111	2.022	2.018	1.002	2.364	0.152	0.975	73.22
insul,bubb	58.257	41.653	18.181	24.765	49.955	33.492	23.473	28.186	4.923	2.034	2.257	2.353	0.960	2.522	0.164	0.975	85.61
insul,uss	56.647	42.547	18.262	24.173	49.597	32.474	24.286	28.182	4.945	2.063	2.036	2.026	1.005	2.385	0.154	0.975	73.74
insul,uss,bubb	55.586	40.458	18.733	24.849	48.022	30.738	21.725	25.971	5.073	2.026	2.160	2.135	1.012	2.474	0.166	0.975	84.33

Table C.5 – Values obtained for test point “2.b” ($\dot{m}_c = 5$ kg/min; $\dot{m}_h = 5$ kg/min)

Test reference	T_{hi} [°C]	T_{ho} [°C]	T_{ci} [°C]	T_{co} [°C]	T_{mh} [°C]	ΔT_1	ΔT_2	ΔT_{mi}	\dot{m}_c [kg/min]	\dot{m}_h [kg/min]	Q_c [kW]	Q_h [kW]	Q_c/Q_h	R	P	F	UA [W/K]
base	61.451	52.705	18.315	27.334	57.078	34.117	34.390	34.253	4.888	5.111	3.069	3.116	0.985	0.970	0.209	0.99	91.88
bubb	60.889	51.666	18.094	27.731	56.278	33.158	33.573	33.365	5.006	5.142	3.358	3.305	1.016	0.957	0.225	0.98	101.08
uss	61.625	52.923	18.110	27.288	57.274	34.337	34.813	34.575	4.960	5.118	3.169	3.105	1.021	0.948	0.211	0.99	90.70
uss,bubb	61.439	52.164	18.079	27.983	56.801	33.455	34.084	33.769	4.992	5.124	3.441	3.312	1.039	0.936	0.228	0.985	99.58
insul	61.415	52.857	18.481	27.514	57.136	33.900	34.376	34.138	5.089	5.142	3.200	3.067	1.043	0.947	0.210	0.99	90.74
insul,bubb	60.221	51.068	18.494	28.291	55.645	31.931	32.574	32.251	5.067	5.121	3.454	3.267	1.057	0.934	0.235	0.98	103.35
insul,uss	61.332	52.896	18.527	27.735	57.114	33.597	34.369	33.982	5.037	5.097	3.228	2.996	1.077	0.916	0.215	0.985	89.52
insul,uss,bubb	60.271	51.109	18.517	28.367	55.690	31.904	32.593	32.247	5.054	5.100	3.464	3.256	1.064	0.930	0.236	0.985	102.52

Preliminary studies on the influence of ultrasounds on the heat transfer rate in a crossflow heat exchanger

Table C.6 – Values obtained for test point “2.c” ($\dot{m}_c = 5$ kg/min; $\dot{m}_h = 8$ kg/min)

Test reference	T_{hi} [°C]	T_{ho} [°C]	T_{ci} [°C]	T_{co} [°C]	T_{mh} [°C]	ΔT_1	ΔT_2	ΔT_{mi}	\dot{m}_c [kg/min]	\dot{m}_h [kg/min]	Q_c [kW]	Q_h [kW]	Q_c/Q_h	R	P	F	UA [W/K]
base	61.437	55.557	19.026	28.372	58.497	33.064	36.530	34.769	4.929	7.962	3.205	3.264	0.982	0.629	0.220	0.995	94.34
bubb	58.401	52.317	18.852	28.685	55.359	29.716	33.465	31.553	5.073	8.048	3.471	3.412	1.017	0.619	0.249	0.995	108.68
uss	61.532	55.740	18.908	28.501	58.636	33.030	36.832	34.897	4.913	7.978	3.280	3.221	1.018	0.604	0.225	1	92.30
uss,bubb	59.159	53.016	18.889	28.977	56.087	30.183	34.127	32.114	5.115	7.963	3.590	3.409	1.053	0.609	0.251	0.995	106.69
insul	60.095	54.191	18.301	27.874	57.143	32.221	35.891	34.023	4.997	8.054	3.329	3.314	1.005	0.617	0.229	0.995	97.89
insul,bubb	57.851	51.789	18.314	28.388	54.820	29.463	33.475	31.426	4.973	8.085	3.486	3.415	1.021	0.602	0.255	0.995	109.22
insul,uss	60.636	54.689	18.307	28.106	57.663	32.530	36.383	34.420	4.996	8.039	3.407	3.332	1.023	0.607	0.231	0.995	97.28
insul,uss,bubb	58.595	52.651	19.016	28.777	55.623	29.819	33.635	31.688	4.962	8.039	3.370	3.330	1.012	0.609	0.247	0.995	105.62

Table C.7 – Values obtained for test point “3.d” ($\dot{m}_c = 1.5$ kg/min; $\dot{m}_h = 1.5$ kg/min)

Test reference	T_{hi} [°C]	T_{ho} [°C]	T_{ci} [°C]	T_{co} [°C]	T_{mh} [°C]	ΔT_1	ΔT_2	ΔT_{ml}	\dot{m}_c [kg/min]	\dot{m}_h [kg/min]	Q_c [kW]	Q_h [kW]	Q_c/Q_h	R	P	F	UA [W/K]
base	53.758	41.997	18.928	27.196	47.877	26.562	23.069	24.774	1.437	1.469	0.827	1.204	0.687	1.422	0.237	0.975	49.83
bubb	52.311	39.398	18.917	28.118	45.855	24.192	20.481	22.285	1.407	1.544	0.901	1.389	0.649	1.403	0.276	0.96	64.90
uss	53.639	42.195	18.796	27.258	47.917	26.381	23.399	24.860	1.412	1.551	0.831	1.236	0.672	1.352	0.243	0.975	51.01
uss,bubb	50.944	38.115	18.957	28.154	44.529	22.789	19.157	20.921	1.627	1.497	1.041	1.337	0.779	1.395	0.288	0.975	65.55

Table C.8 – Values obtained for test point “3.e” ($\dot{m}_c = 1.5$ kg/min; $\dot{m}_h = 3$ kg/min)

Test reference	T_{hi} [°C]	T_{ho} [°C]	T_{ci} [°C]	T_{co} [°C]	T_{mh} [°C]	ΔT_1	ΔT_2	ΔT_{ml}	\dot{m}_c [kg/min]	\dot{m}_h [kg/min]	Q_c [kW]	Q_h [kW]	Q_c/Q_h	R	P	F	UA [W/K]
base	60.789	52.243	18.701	31.058	56.516	29.731	33.543	31.599	1.592	3.024	1.368	1.801	0.760	0.692	0.294	0.985	57.86
bubb	58.384	48.683	18.757	33.511	53.534	24.873	29.927	27.322	1.570	3.034	1.611	2.050	0.786	0.657	0.372	0.975	76.97
uss	60.715	52.249	18.677	31.379	56.482	29.336	33.572	31.406	1.570	2.968	1.386	1.751	0.792	0.666	0.302	0.985	56.61
uss,bubb	59.855	50.188	18.814	34.953	55.022	24.902	31.374	28.014	1.490	3.035	1.671	2.044	0.817	0.599	0.393	0.975	74.85

Preliminary studies on the influence of ultrasounds on the heat transfer rate in a crossflow heat exchanger

Table C.9 – Values obtained for test point “3.f” ($\dot{m}_c = 1.5$ kg/min; $\dot{m}_h = 4$ kg/min)

Test reference	T_{hi} [°C]	T_{ho} [°C]	T_{ci} [°C]	T_{co} [°C]	T_{mh} [°C]	ΔT_1	ΔT_2	ΔT_{ml}	\dot{m}_c [kg/min]	\dot{m}_h [kg/min]	Q_c [kW]	Q_h [kW]	Q_c/Q_h	R	P	F	UA [W/K]
base	61.018	54.413	18.920	32.333	57.715	28.685	35.493	31.968	1.477	3.918	1.377	1.804	0.763	0.492	0.319	0.995	56.71
bubb	59.311	51.701	19.215	36.003	55.506	23.308	32.486	27.643	1.427	3.984	1.665	2.113	0.788	0.453	0.419	0.98	78.01
uss	61.241	54.856	19.478	32.919	58.049	28.322	35.379	31.720	1.554	4.070	1.451	1.811	0.802	0.475	0.322	0.99	57.67
uss,bubb	61.146	53.496	19.381	35.980	57.321	25.167	34.114	29.414	1.503	4.045	1.733	2.157	0.803	0.461	0.397	0.98	74.82

D. Appendix D – Experimental results of the tests with LiBr solution

The resulting values of the tests using LiBr solution as the hot fluid, such as temperatures, mass flow rates, calorific power and parameters R , P and F are all shown in the following tables, for each test point and conditions implanted. Like the previous appendix, in the tables the terms “bubb” and “uss” mean bubbling and ultrasounds, respectively.

Table D.1 - Values obtained for test point “11.a” ($\dot{m}_c = 2$ kg/min; $\dot{m}_h = 2$ kg/min)

Test reference	T_{hi} [°C]	T_{ho} [°C]	T_{ci} [°C]	T_{co} [°C]	T_{mh} [°C]	ΔT_1	ΔT_2	ΔT_{ml}	\dot{m}_c [kg/min]	\dot{m}_h [kg/min]	Q_c [kW]	Q_h [kW]	Q_c/Q_h	R	P	F	UA [W/K]
base	55.318	43.731	22.579	28.575	49.524	26.742	21.152	23.838	1.990	2.061	0.830	0.816	1.017	1.932	0.183	0.975	35.12
bubb	54.129	39.775	21.774	28.834	46.952	25.295	18.002	21.442	1.995	2.050	0.980	1.005	0.975	2.033	0.218	0.97	48.30
uss	55.594	43.914	22.301	28.427	49.754	27.167	21.613	24.284	1.999	2.039	0.851	0.814	1.046	1.907	0.184	0.975	34.39
uss,bubb	53.961	39.700	21.723	29.028	46.831	24.933	17.977	21.266	1.993	1.975	1.013	0.962	1.053	1.952	0.227	0.97	46.62

Preliminary studies on the influence of ultrasounds on the heat transfer rate in a crossflow heat exchanger

Table D.2 - Values obtained for test point "11.b" ($\dot{m}_c = 2$ kg/min; $\dot{m}_h = 5$ kg/min)

Test reference	T_{hi} [°C]	T_{ho} [°C]	T_{ci} [°C]	T_{co} [°C]	T_{mh} [°C]	ΔT_1	ΔT_2	ΔT_{ml}	\dot{m}_c [kg/min]	\dot{m}_h [kg/min]	Q_c [kW]	Q_h [kW]	Q_c/Q_h	R	P	F	UA [W/K]
base	60.742	52.855	21.684	31.270	56.798	29.471	31.171	30.313	1.974	5.038	1.316	1.364	0.964	0.823	0.245	0.985	45.70
bubb	60.714	49.891	21.541	34.203	55.303	26.511	28.351	27.420	1.999	5.066	1.759	1.882	0.934	0.855	0.323	0.97	70.76
uss	60.699	52.737	21.605	31.280	56.718	29.418	31.131	30.267	2.003	5.000	1.347	1.367	0.986	0.823	0.247	0.985	45.84
uss,bubb	60.648	49.841	21.573	34.407	55.244	26.240	28.267	27.241	1.991	4.902	1.775	1.819	0.976	0.842	0.328	0.97	68.84

Table D.3 - Values obtained for test point "13.d" ($\dot{m}_c = 1.5$ kg/min; $\dot{m}_h = 1.5$ kg/min)

Test reference	T_{hi} [°C]	T_{ho} [°C]	T_{ci} [°C]	T_{co} [°C]	T_{mh} [°C]	ΔT_1	ΔT_2	ΔT_{ml}	\dot{m}_c [kg/min]	\dot{m}_h [kg/min]	Q_c [kW]	Q_h [kW]	Q_c/Q_h	R	P	F	UA [W/K]
base	52.359	40.918	21.797	27.660	46.639	24.700	19.120	21.791	1.481	1.551	0.604	0.606	0.997	1.952	0.192	0.975	28.51
bubb	50.177	37.198	21.984	28.790	43.688	21.387	15.214	18.126	1.464	1.585	0.693	0.701	0.989	1.907	0.241	0.96	40.28
uss	50.914	40.055	21.884	27.574	45.484	23.340	18.171	20.648	1.488	1.544	0.589	0.571	1.031	1.908	0.196	0.975	28.38
uss,bubb	49.494	36.792	21.977	28.600	43.143	20.895	14.815	17.681	1.469	1.557	0.677	0.673	1.005	1.918	0.241	0.96	39.66

Preliminary studies on the influence of ultrasounds on the heat transfer rate in a crossflow heat exchanger

Table D.4 - Values obtained for test point "13.e" ($\dot{m}_c = 1.5$ kg/min; $\dot{m}_h = 3$ kg/min)

Test reference	T_{hi} [°C]	T_{ho} [°C]	T_{ci} [°C]	T_{co} [°C]	T_{mh} [°C]	ΔT_1	ΔT_2	ΔT_{ml}	\dot{m}_c [kg/min]	\dot{m}_h [kg/min]	Q_c [kW]	Q_h [kW]	Q_c/Q_h	R	P	F	UA [W/K]
base	60.505	50.154	22.019	31.125	55.329	29.380	28.135	28.753	1.451	2.948	0.919	1.047	0.877	1.137	0.237	0.98	37.16
bubb	60.215	46.992	21.704	33.770	53.603	26.445	25.288	25.862	1.457	2.979	1.222	1.351	0.904	1.096	0.313	0.97	53.84
uss	60.497	50.517	22.122	31.401	55.507	29.096	28.395	28.744	1.460	3.075	0.942	1.054	0.894	1.076	0.242	0.98	37.41
uss,bubb	60.182	47.062	21.746	33.814	53.622	26.368	25.316	25.838	1.504	3.029	1.261	1.363	0.925	1.087	0.314	0.965	54.65

Table D.5 - Values obtained for test point "11.z10" ($\dot{m}_c = 2$ kg/min; $\dot{m}_h = 10$ kg/min)

Test reference	T_{hi} [°C]	T_{ho} [°C]	T_{ci} [°C]	T_{co} [°C]	T_{mh} [°C]	ΔT_1	ΔT_2	ΔT_{ml}	\dot{m}_c [kg/min]	\dot{m}_h [kg/min]	Q_c [kW]	Q_h [kW]	Q_c/Q_h	R	P	F	UA [W/K]
base	60.267	55.157	22.100	33.052	57.712	27.215	33.056	30.041	2.035	9.923	1.548	1.744	0.888	0.467	0.287	1	58.04
bubb	60.016	52.986	22.062	37.417	56.501	22.598	30.924	26.544	2.020	10.102	2.153	2.440	0.883	0.458	0.405	0.98	93.80

Table D.6 - Values obtained for test point "11.z10" ($\dot{m}_c = 2$ kg/min; $\dot{m}_h = 12.5$ kg/min)

Test reference	T_{hi} [°C]	T_{ho} [°C]	T_{ci} [°C]	T_{co} [°C]	T_{mh} [°C]	ΔT_1	ΔT_2	ΔT_{ml}	\dot{m}_c [kg/min]	\dot{m}_h [kg/min]	Q_c [kW]	Q_h [kW]	Q_c/Q_h	R	P	F	UA [W/K]
base	60.264	56.074	21.892	33.937	58.169	26.327	34.182	30.084	2.023	12.488	1.693	1.800	0.940	0.348	0.314	1	59.83
bubb	59.735	53.763	21.726	38.082	56.749	21.652	32.038	26.507	2.023	12.534	2.298	2.572	0.893	0.365	0.430	0.99	98.02

E. Appendix E – Calibration of the mass flow meter for the LiBr solution

The process of calibration used for the lithium bromide solution was similar to the one used for the water as the hot fluid (Appendix B.2). To weight the solution in a separate container, it was necessary to close part of the hot fluid circuit once more the same way it was done when calibrating for water. First, the solution was heated in the white bucket using the electrical resistances, then by being pumped by the pump, the LiBr aqueous solution will go through the flow meter C_2 and the gate valve to finally reach the container.

The LiBr aqueous solution was heated up to 50 °C and then while varying the flow rate with the gate valve, several operating points were taken. The “DASYLab” software would measure and register both the temperature T_3 and the voltage picked up by C_2 . The mass of the solution was weighed for each different point with the weighting scale previously calibrated for the container used and the time was timed with a cellphone.

After calculating the mass flow rate, in kg/min, for each point by dividing the mass with the time, the correlation between the voltage and the LiBr solution obtained are the ones observed in figure E.1 and equation E.1.

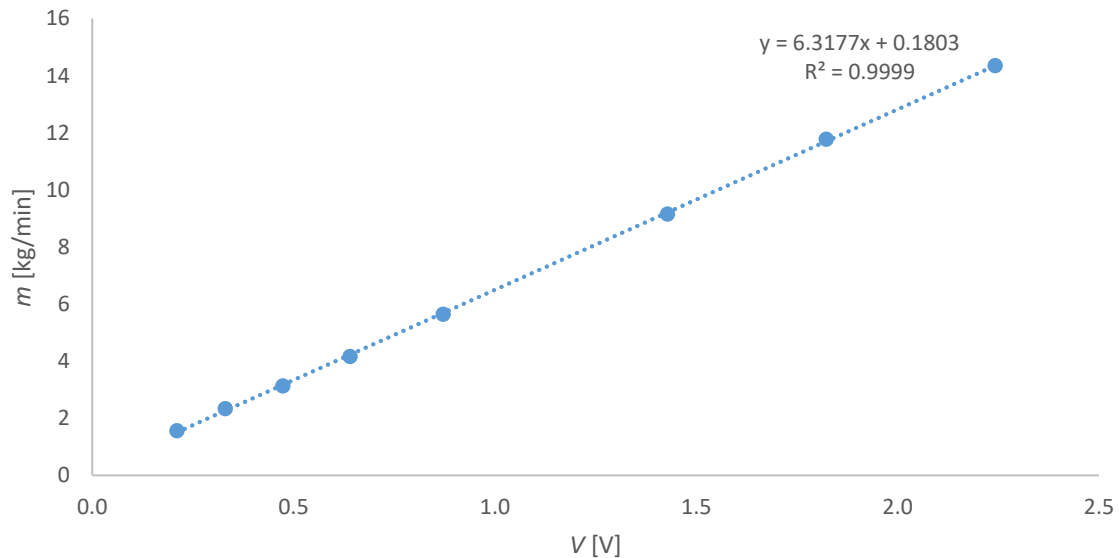


Figure E.1 – Trend line obtained through the LiBr solution calibration process.

$$\dot{m} = 6.3177V + 0.1803 \quad (\text{E.1})$$

With equation E.1, the level of uncertainty is almost null, so no other physical property is needed in the correlation. Equation E.1 was then implemented in the “DASYLab” worksheet for the forthcoming LiBr tests. Perhaps now the adopted approach was rather simplistic as no deep analysis was carried out to evaluate the importance of the liquid specific gravity upon the calibration results. Because the experiments for the LiBr aqueous solution were carried out in the final available time

Preliminary studies on the influence of ultrasounds on the heat transfer rate in a crossflow heat exchanger

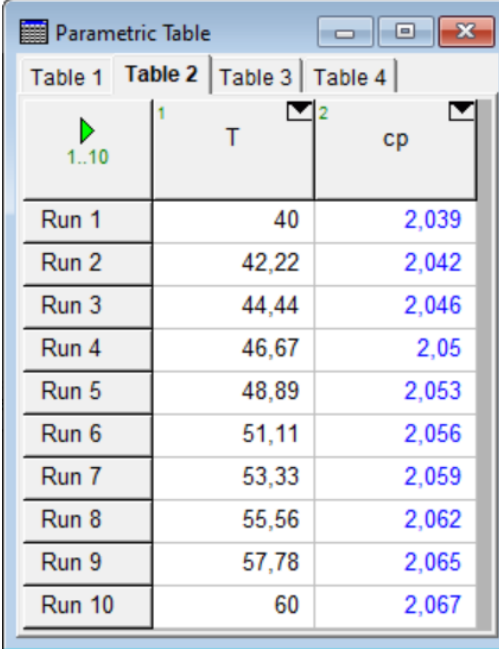
of the experimental period, this calibration line was enough for the purposed experiments as they are in fact a preliminary approach to be enhanced in further studies.

F. Appendix F – Obtaining of the LiBr solution physical properties

Physical properties of the LiBr aqueous solution like the dynamic viscosity, density, thermal conductivity, etc. are important to know as they will be used in multiple occasions for data analysis. The provided LiBr aqueous solution has 55% concentration. To attain its physical properties, the concentration of the solution should be taken into account.

Even though there are some articles concerning the physical properties of a LiBr solution depending on temperature and concentration values [25,26], the method used to obtain them was by means of the EES program (Engineering Equation Solver).

The EES is an equation-solver program that has a wide database of thermodynamic properties. To access an external library to retrieve a property of the LiBr solution, an EES routine is used, for example “ $k = \text{LiBrSSCCond}(T_c, X)$ ” is used to obtain the thermal conductivity of a LiBr solution given a temperature “ T_c ” in °C and a mass fraction “ X ”. The routines used were developed by the University of Maryland [27]. Using these routines for the desired properties and with the mass fraction being constant for all of them, $X = 0.55$, it is possible to create tables in the EES in which varying the temperature, it reveals the resulting values of the introduced routine, exemplified in figure F.1 for the specific heat.



	1	2
	T	cp
Run 1	40	2,039
Run 2	42,22	2,042
Run 3	44,44	2,046
Run 4	46,67	2,05
Run 5	48,89	2,053
Run 6	51,11	2,056
Run 7	53,33	2,059
Run 8	55,56	2,062
Run 9	57,78	2,065
Run 10	60	2,067

Figure F.1 – Variation of the specific heat with the temperature in an EES Table.

Doing this process for the μ , k , c and ν , and transporting the tables to the Excel, it was possible to achieve correlations for all the needed properties, as a function of temperature in °C. Therefore, the trend lines obtained for the thermal properties are as shown in the following equations. The density (equation F.2) was calculated by doing the inverse of the specific volume ν . The thermal properties calculated with these equations are in SI units.

$$c = 1.4T + 1982.6 \quad (\text{F.1})$$

$$\rho = -0.5797T + 1634.3 \quad (\text{F.2})$$

$$k = 0.0009T + 0.4082 \quad (\text{F.3})$$

$$\mu = -0.0000577T + 0.0060127 \quad (\text{F.4})$$

